BULK GAN GROWTH AND CHARACTERIZATION

A Dissertation

Presented to the Faculty of the Graduate School

of Cornell University

In Partial Fulfillment of the Requirements for the Degree of

Doctor of Philosophy

by

P. Phanikumar Konkapaka

August 2005

BULK GAN GROWTH AND CHARACTERIZATION

P.Phanikumar Konkapaka, Ph. D.

Cornell University 2005

GaN is a wide bandgap semiconductor material that is used for fabrication of laser diodes, light emitting diodes, and high power, high frequency electronic devices. Due to the absence of free standing GaN substrates, these devices are fabricated on foreign substrates such as SiC, Sapphire, $LiGaO_2$ or $LiGaO_3$. Performance of these devices is reduced due to high dislocation densities resulting from lattice mismatch and thermal expansion coefficient mismatch between the GaN and substrate. In order to improve the performance of devices, homoepitaxial device layers grown on high quality free standing GaN substrates are needed.

Bulk GaN crystals of dimensions 8.5 mm x 8.5 mm were grown at growth rates greater than 200μm/hr using gallium oxide vapor transport technique. Commercially available GaN powder and ammonia were used as the precursors for growing bulk GaN. Nitrogen was used as the carrier gas to transport the gallium containing species that was obtained from the decomposition of GaN powder. These experiments were performed in a flow over configuration where the nitrogen carrier gas was flowing over the powder transporting the growth species. Using this process, it was possible to achieve growth rates of above 200 μm /hr. The GaN layers thus obtained were characterized using X-Ray diffraction, scanning electron microscopy, and atomic force microscopy. X-ray diffraction patterns showed that the grown GaN layers are single crystals oriented along c direction. AFM studies indicated that the dominant growth mode was dislocation mediated spiral growth. Hall mobility measurements indicated a mobility of 550 $cm^2/V.s$ and a carrier concentration of 6.67 x $10^{18}/cm^3$.

It was found that kinetics of decomposition of pure GaN powder without oxygen resulted in incongruent evaporation leading to the formation of the liquid gallium in the powder. A flow through configuration was also used because of its high collection efficiency of growth species. A mixture of Ga_2O_3 and carbon powder as well as commercial GaN powder was used as precursors of gallium suboxide in this configuration. This configuration also demonstrated growth rates that are comparable to flow over configuration.

BIOGRAPHICAL SKETCH

Phanikumar Konkapaka was born and raised in Katravulapalli, Andhra Pradesh, India. He completed his high school studies there and moved to Kakinada, a small town 20 miles from there. In 1996, he started bachelor of technology program in Metallurgical Engineering at the Indian Institute of Technology, Madras. At the end of undergraduate studies, he joined Cornell University for graduate studies in Materials Science and Engineering and was attracted by the ongoing research in Dr. Michael Spencer's group in the department of Electrical and Computer Engineering on compound semiconductors. It is where he started working towards his Ph. D with the main focus being bulk GaN growth and characterization. Fascinated by the world of semiconductors, he changed his major to the department of Electrical and Computer Engineering to learn more about semiconductors and to pursue a career in the same. His internship at Micron Technology, Inc., Boise only strengthened his penchant towards semiconductor nanotechnology. He is presently working in the Strategic Research & Development Group at Micron Technology, Boise working on the latest advances in semiconductor memory technologies. He is a member of the Materials Research Society.

To my foster parents,

P.Suryanarayana Murthy and P.Gouri.

Without the encouragement they have given me, I would not have come this far.

ACKNOWLEDGEMENTS

I am grateful to Dr. Mike Spencer for giving me this opportunity to work under his guidance. His constant encouragement, inspiration helped me immensely while I was working on the project. The numerous discussions I had with him and his hands-on approach helped my learning curve. He was a source of constant motivation and never seemed to be lacking new ideas to solve any kind of problem that we had faced. His vast knowledge in variety of research fields made it easier for applying some concepts in one research are to the other. But, one thing that never stopped amazing me was his ingenuity in exploiting the existing knowledge in the research area to apply to the problem in context. I would also like to thank my minor committee members Prof. Lester Eastman and Prof. George Malliaras for serving on my committee and genuine support. Even though it was only a few discussions, with his way of explaining the complex semiconductor phenomena, Dr. Eastman kindled my interest in the field of compound semiconductors. The nature of project being more of a materials science oriented, having George in the committee made me feel like I always have an expert in materials science that I could talk to if there were any unsolvable issues that are completely materials oriented.

I would also like to acknowledge Dr. M. S. Ramachandra Rao at the Materials Science Research Center at IIT Madras. He introduced me to the wonderful world of materials science in my undergraduation even as I was mostly learning metallurgical engineering as a part of my undergraduate curriculum.

My groupmates, Chris Thomas, Ho-Young Cha, Huaqiang Wu, Mvs Chandrashekhar, Young-chul Choi, Lori Lepak, Xingqun Jiang, Zhitao Yang, Tadahiro Kaburaki, provided me with their help, support, and encouragement. I would like to thank Ho-Young, Chandra and Lori for helping me with my research. Barry Butterfield as the lab manager played an important role in getting me acquainted with

the tools, the growth systems, and made a valuable contribution to my practical knowledge. Chris and Barry made life at the lab an enjoyable experience by creating a friendly atmosphere. I had the pleasure of working with Huaqiang during the initial stages of the project. One ex-groupmate that I would like to acknowledge is Goutam Koley. Even after leaving Cornell following graduation, he was always available whenever I needed any guidance in any matter. Since he was a fellow ex-IITian and a senior graduate student in the field of semiconductors working in the same group, I had much to learn from him.

I would like to thank Udayan Ganguly, who has been my classmate and good friend from the years of undergrad till the end of my grad studies at Cornell. He helped me through some difficult situations both academically and personally countless number of times. I would also like to thank Shankar Radhakrishnan and Rajesh Duggirala for making my transition from Materials Science to Electrical Engineering smooth. Shankar was especially very helpful in explaining the concepts of electrical engineering. Without these people and many other friends that I can not possibly list due to space constraints, my stay at Cornell would not have been a fun filled experience.

I also would like to acknowledge the collaboration and help I received from Dr. Subhash Mahajan (ASU), Dr. Balaji Raghothamachar (SUNY, Stony Brook), Dr. Maura Weathers at the X-Ray Lab and Dr. John Hunt at the SEM lab. The help and support provided by Dorothy Palladino, Cheryl Francis, Sue Bulkley and Scott Coldren, in all administrative issues is also gratefully acknowledged. I would further like to thank MURI program for the financial support I received during my Ph. D.

I would like to thank my parents, sister and my aunt for their support. Finally I want to thank my fiancée, Soumya, for her understanding nature and continuous moral support through out.

TABLE OF CONTENTS

LIST OF FIGURES

LIST OF TABLES

Chapter 1

Introduction

1.1 Background:

The III-Nitrides are promising candidates for semiconductor device applications in blue and ultraviolet wavelength regions in a similar way the III-As and P based counterparts are used in red, infrared and yellow wavelengths in the electromagnetic spectrum. GaN, AlN and InN with bandgaps of 1.9 eV, 3.4 eV and 6.2 eV respectively form a continuous alloy system that covers wavelengths ranging from green into the ultraviolet regions (1). Due to their direct and wide bandgap they could be used for fabricating violet, green and blue light emitting diodes. This enables fabrication of semiconductor devices that could emit or detect light in blue or ultraviolet regions and hence opens up a wide range of possibilities in imaging and graphics applications. Nitride based green and blue LEDs that are already commercially available exhibit high efficiency, brightness and longevity. These LEDs have applications in traffic lights, indicator lights and medicine for diagnosis and treatment. Due to their high efficiency compared to the conventional lighting, these LEDs could potentially save energy and hence could replace conventional lighting.

Ultraviolet and blue lasers based on InGaN/GaN/AlGaN system have been demonstrated and they have reached continuous wave operation at room temperature (2). GaN lasers are of importance in the areas of optical storage and printing. Performance of both these technologies depends on the resolution of the laser spot size. They require lasers that are of short wavelength since the spotsize is limited to the square of the wavelength due to diffraction. The storage densities of a compact

disc could potentially reach 40Gb when blue lasers are used. Semiconductor diodes based on AlGaN/GaN system could be used as ultraviolet photodetectors that could be used in areas such as solar blind detectors, missile launching detection, flame detectors and sensors in combustion industry. Photovoltaic detectors with response times of the order of ns have been realized (2).

The high saturation electron velocity of GaN is suitable for applications in high power and high frequency applications. The large band discontinuity present in GaN/AlGaN system induces 2D electron gas larger than 10^{12} cm^{-2} forming the basis for nitride high-power electronic devices (2). Higher physical stability of GaN will make it possible to fabricate devices that can be used in harsh environments.

The efforts to synthesize GaN dates all the way back to 1932 by converting metal Gallium to GaN by passing a stream of ammonia over it (3). The advent of GaN epitaxial layer on sapphire grown by hydride vapor phase epitaxy then made it possible to initiate research on device applications based on GaN (4). However, obtaining p-type GaN proved extremely difficult. Later on, in 1985, an organometallic vapor phase epitaxy [OMVPE] method for the nitride growth was developed by A. Amano and K. Hiramatsu. A low temperature buffer layer of AlN introduced lowered the background carrier concentrations from 10^{19}-10^{20} cm^{-3} to about 10^{17} cm^{-3}. This reduction in carrier concentration brought an improvement in crystal quality (5). The problem of p- type doping was approached in different ways by different researchers. In one approach, the GaN sample was subjected to Low Energy Electron Beam Irradiation [LEEBI] to activate Mg dopants (6). This treatment essentially drives out the hydrogen that passivates the dopants from the sample. Another approach involved thermal annealing of GaN (7) and this enabled commercialization of LEDs in 1993 (8). Nakamura et al. reported pulsed room temperature of an AlGaN/GaN/InGaN based injection laser (9).

1.2 The need for substrates

Despite these advantages, state of the art GaN devices suffer from the defects originated by the heteroepitaxy involved in the fabrication of GaN based devices. Due to the lack of availability of bulk GaN substrates, device structures are grown on foreign substrates such as SiC, sapphire, $LiGaO_2$ or $LiGaO_3$ (10-13). The heteroepitaxial growths lead to high densities of threading dislocations (TD) in device structures. Also, the interface roughness in group III-nitrides is of considerable importance as it could severely affect the mobility of two-dimensional electron gas in AlGaN/GaN based high electron mobility transistors (14, 15). In addition, several defects such as stacking faults, inversion domain boundaries, and nanopipes are observed in GaN epitaxial layers (16). Threading dislocations were observed and were reported to be the origin of the so-called V-defects. It has been shown that the V-defects in InGaN/GaN MQW are sources of leakage current in GaN based LEDs (15). The best way to successfully eliminate all the defects that originate from heteroepitaxy is to find a commercially viable process to manufacture freestanding lattice matched substrate. No other material provides a better lattice match to the GaN epitaxial layers than bulk GaN single crystal. It has already been shown that the performance of devices fabricated on GaN substrate is much superior to those fabricated heteroepitaxially (17) proving the indispensability of GaN substrates in improving the performance of GaN-based devices.

1.3 Overview of the thesis

This thesis deals with the growth and characterization of bulk GaN single crystals. The chapters in the thesis have been organized such that a person that is new to the field can also understand the objective and scope of the current work. Since this work deals

with bulk GaN growth by sublimation or more appropriately vapor transport, the thorough understanding of thermodynamics and kinetics of GaN system is essential for successful growth and processing of the same. Chapter 2 is dedicated to acquaint the reader with the previous studies on thermodynamics and kinetics of GaN. It also provides us with the necessary background on the phase diagram of GaN that determines the phase stability of various phases involved in GaN system. A brief discussion on the decomposition of ammonia is also included at the end of the chapter because ammonia is the most commonly used nitrogen precursor for growth of GaN in most of the vapor phase crystal growth technologies.

Chapter 3 introduces the reader to the crystal structure of GaN, its physical properties, its lattice mismatch to the various substrates under consideration and discusses the different growth techniques of GaN that are being used to grow bulk GaN single crystals and their respective advantages and disadvantages.

A detailed discussion of sublimation growth of GaN and the research work that has been done till date is outlined in chapter 4. It also substantiates our motive towards sublimation process as opposed to the other processes to develop a commercially viable bulk GaN growth technology. Detailed description of the crystal growth setup and the gas handling system that have been used in our experiments are also included in this chapter.

Chapters 5-8 describe the various designs, approaches, experimental procedures, crystal growth and characterization results from our experiments and evolution of designs from one generation to another generation to solve the problems encountered in the growth experiments. Each of these chapters is further backed up by the simulation results performed by Dr. Yuri Makarov at STR, Inc. to explain the experimental results.

Chapter 5 describes the basic sublimation sandwich design used to grow GaN with the seed crystal directly above the source material to perform crystal growth. However, as we will see in this chapter, this design is faced with the problem of crust formation in the powder boat.

Chapter 6 describes a second-generation experimental design to solve the problem of crust formation. The concepts that laid the foundation to evolve into a much better second generation experimental design in terms of prevention of crust formation by isolating the source carry over to the next generation designs as well. Experimental procedure, growth results, characterization results & discussion and the modeling results performed by Dr. Yuri Makarov follow the description of the design.

Chapter 7 deals with the problems faced in the previous experiments in terms of gallium transport and hence the source materials, carrier gases. It also talks about the various approaches we have employed to solve them and their consequences and provides a logical transition to chapter 8. A third generation experimental setup is described in chapter 8 that not only includes the benefits from design 2, but also tries to solve some problems described in chapters 6&7. This again is followed up by the experimental results, characterization results, and summary.

Chapter 9 is dedicated to the discussion of V-defects and their growth kinetics. This discussion is unavoidable in the context of obtaining defect free, large, single crystal bulk GaN.

Chapter 10 is the concluding chapter summarizing the present experimental results, characterization results, challenges, and some possible directions for future work.

Chapter 2

Thermodynamics and kinetics

2.1 Thermodynamics

Unlike other III-V systems, the III-N systems are characterized by the presence of thermodynamic and kinetic barriers. As a result, synthesis of III-nitrides differs from that of other III-V compounds by a large extent. Growth and processing of these III-nitrides requires a thorough understanding of thermodynamics and kinetics involved. This chapter is divided into four sections. First section is an introduction to the thermochemistry and phase diagram of GaN. Second and third sections deal with the thermodynamics and kinetics of decomposition and synthesis of GaN respectively. Section 4 discusses the decomposition of ammonia that is used as the nitrogen precursor for the growth of GaN.

2.1.1 Thermochemistry:

Thermodynamic and kinetic barriers constitute the basic energy barriers for a reaction to occur. The difference in Gibbs free energy of products and reactants is the thermodynamic barrier for the reaction to occur. This free energy difference has to be negative for the reaction to be spontaneous. For a given material system and ambient it is the thermodynamics that determine the stability of a particular phase. However, it is not thermodynamic barriers but kinetic barriers that determine the rate of the reaction. Unlike thermodynamic barriers, kinetic barriers depend on the presence of a catalyst and the reaction path. In the case of a reaction involving molecular nitrogen, the

kinetic barrier generally tends to stem from the breaking of the triple bond present in the nitrogen molecule.

Stability regions for different phases in a reaction could be obtained by from the free energy of reactants and products. In GaN system, for the following binary reactions, 2.1 & 2.2 the regions of stability could be found by finding out the free energy difference between the products and reactants as a function of temperature and pressure according to the following equations 2.3 & 2.4.

$$Ga(l) + N_2(g) \Leftrightarrow GaN(s) \quad (2.1)$$

$$Ga(l) + NH_3(g) \Leftrightarrow GaN(s) + \frac{3}{2}H_2 \quad (2.2)$$

$$\Delta G_{P,T} = G^{GaN}{}_{P,T}(s) - G^{Ga}{}_{P,T}(l) - G^{N_2}(g) \quad (2.3)$$

$$\Delta G_{P,T} \Leftrightarrow G_{GaN(s)} \quad (2.4)$$

Under equilibrium, the free energy change of the reaction is zero at constant pressure and temperature. One could graphically represent the stability regions of a substance as a function of composition, temperature and pressure using a phase diagram. The phase rule (18) determines the number of degrees of freedom for the reaction at equilibrium depending on the number of phases and components. It is given by the following equation 2.5.

$$P + F = C + 2 \quad (2.5)$$

where P=no of phases, C=no of components and F =no of phases.

Both the reactions 2.1 and 2.2 have one degree of freedom calculated by the phase rule. This essentially means that if one of the variables, pressure or temperature is fixed, it automatically determines the other variable at equilibrium. Figures 2.1 and 2.2

show the regions of stability for the phases that are involved in equations 2.1 & 2.2 (19).

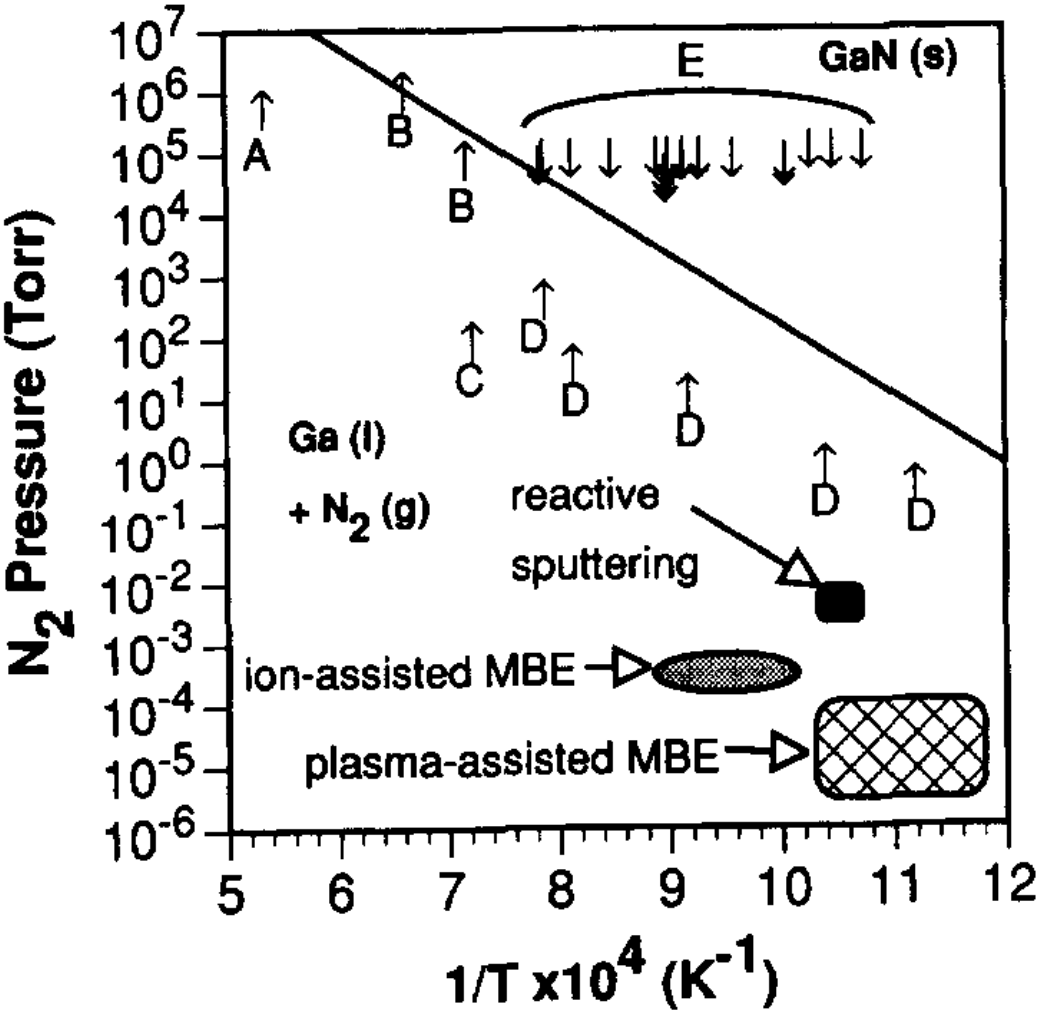

Figure 2.1. Phase diagram for the reaction 2.1. from Ref. [11]

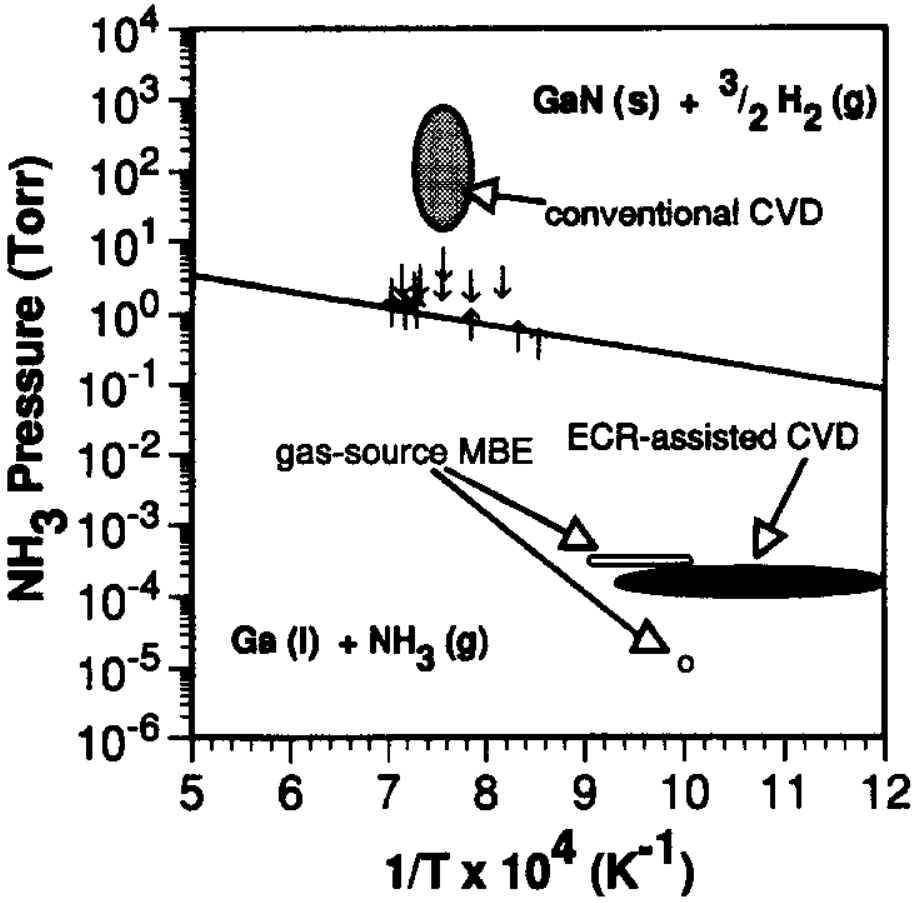

Figure 2.2. Phase diagram for the reaction 2.2. from Ref. (19, 20).

The same regions of stability could be represented using a free energy-temperature diagram. A thermodynamic statistical partition function known as equilibrium constant could be used to determine the thermodynamic properties of the reaction equilibrium as well as the concentrations of the species involved in the reaction (21). In general, it is the activity that replaces the concentration of the species in the mathematical analysis of reaction equilibria especially when the species involved are not ideal (22, 23). The activity of pure liquids and pure solids is unity

when they are in their standard states. Activity of ideal gases is given by P/P_o where P_o is the reference pressure. By convention, this reference pressure is generally taken as 1 bar (18, 22, 23). Equations 2.3 & 2.4 can be used to obtain the free energy change at arbitrary temperature and pressure. Due to the presence of a triple bond in molecular nitrogen it is essentially inert at the temperatures used for GaN growth. Hence, other precursors of atomic nitrogen such as hydrazine, excited molecular nitrogen, and ionized molecular nitrogen were used by various research groups to synthesize III-N compounds (20, 24-34).

2.1.2 Phase diagram

Since the understanding of thermodynamic properties of GaN is indispensable for its processing, precise determination of boundaries of phase stability is extremely important. Thermodynamics play a very important role especially in semiconductor device processing where the fabrication procedure involves subsequent processing steps at various temperatures, the material could either sublime or decompose at high temperatures. Hence a consistent thermodynamic model for Ga-N binary system that includes all the thermodynamic parameters and that could be extrapolated to estimate the thermodynamic properties at various other temperatures, pressures and compositions. However, due to the extremely high equilibrium pressures of nitrogen and high melting point of GaN involved in Ga-N system, it is extremely difficult to determine Ga-N phase diagram experimentally. Hence, efforts to theoretically calculate Ga-N binary phase diagram utilizing a procedure named CALPHAD (35, 36). This involves calculation of entropy from the heat capacitance data obtained from experiments and calculation of fugacity of nitrogen as a function of pressure. Since nitrogen is a real gas and its fugacity differs significantly from the pressure at high pressures, it is important to determine fugacity as a function of pressure for nitrogen in

Ga-N system. The thermodynamic model thus developed has a good agreement with the observed experimental data. (35). The temperature-composition phase diagram calculated using the above procedure at a pressure of 1 bar is shown in Fig 2.3

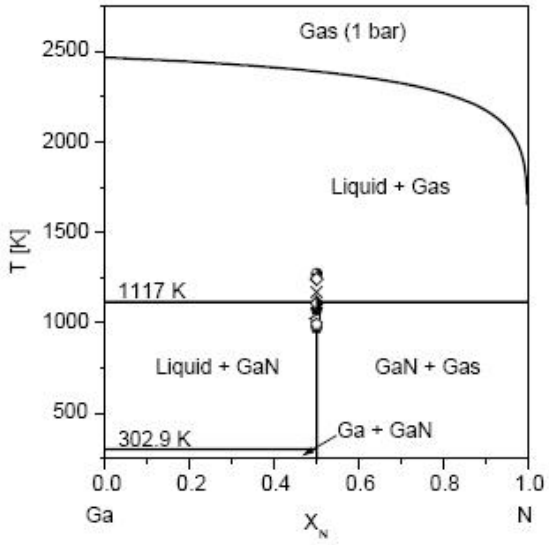

Figure 2.3. Phase diagram of Ga-N system –Reproduced from Ref. (35)

2.2 Decomposition reaction:

As mentioned earlier, unlike other material systems, the evaporation kinetics of III-nitride compounds differ from that predicted by thermodynamic data indicating a kinetic barrier for the decomposition reaction. Thermodynamic barrier sets an upper limit to the reaction rate through the following expression known as the Hertz-Langmuir relationship (23, 37-39).

$$J_{eq} = \frac{P_{eq}}{\sqrt{2\pi RT}} \tag{2.6}$$

where J_{eq} is equilibrium flux,

P_{eq} is the equilibrium pressure,

M is the mass of the gaseous species,

and T is the temperature expressed in Kelvin.

The ratio of actual evaporation rate to that of thermodynamically predicted rate is given by a factor α, called the evaporation coefficient (37-39). So, the actual evaporation rate could be given by the modified Hertz-Langmuir equation as

$$J_{eq} = \frac{\alpha P_{eq}}{\sqrt{2\pi RT}} \qquad (2.7)$$

The physical origin of the evaporation coefficient lies in the bond strength between the metal atoms and the nitrogen atoms at the surface. This reduction in evaporation rate compared to that calculated by equilibrium thermodynamic data was observed in other III-nitride systems as well (40-44) and was attributed to the strong III-N bond strength. However it was also shown in other systems (23) that the bond strength alone is not the sufficient condition for the material system to have a low evaporation coefficient. This low evaporation coefficient has significant implications on the decomposition of GaN in vacuum. Instead of evaporating incongruently in vacuum as predicted by thermodynamics, GaN evaporates congruently because the experimentally observed evaporation rate of GaN falls below that of the evaporation rate of Ga(v) from the surface (43). However, later work (43, 45) confirmed using mass spectrometry the presence of Gallium containing species and nitrogen. Contradictory to this observation, Groh et al. (44) reported that a mass spectrometer detected only nitrogen containing species and a metallic Gallium deposit on the colder portion of the vacuum-annealing furnace. Further, it was also reported from the same authors that gallium droplets were observed on top of the GaN surface. Groh et al. also found that the activation energy of the decomposition reaction to be less than that of the bond strength of Ga-N bond indicating that the decomposition reaction involves surface

interactions with the species in the gas phase rather than breaking Ga-N bond alone. The discrepancies between the observations in GaN decomposition studies by Groh et al. and Searcy et al. could be attributed to the following factors. The samples used in both the studies are highly doped polycrystalline samples and were different. Further, as explained by Averyanova et al. (46), the langmuir free evaporation is different from the Knudsen cell evaporation where, the effective orifice area of the Knudsen effusion cell could be different in both the studies. From Fig. 2.4 it could be seen that if the decomposition reaction occurs in conditions equivalent to langmuir free evaporation, i.e. in a Knudsen cell with orifice area equal to the evaporating are of the crystal, then GaN evaporates congruently.

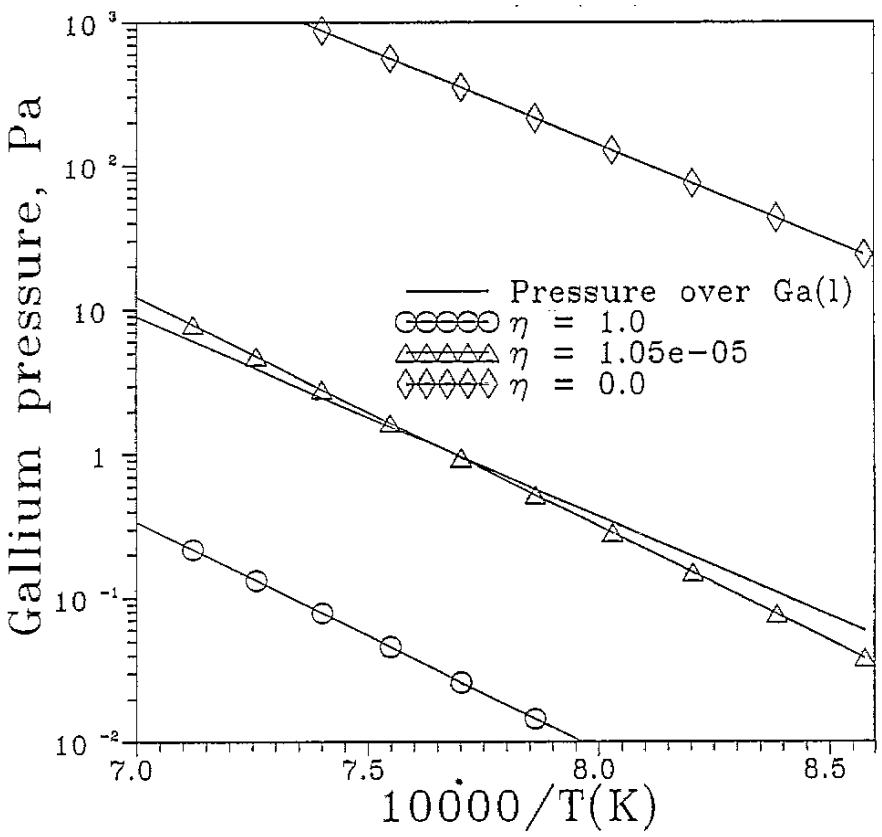

Figure 2.4. Calculated Gallium vapor pressure for evaporation under Knudsen evaporation conditions. From Ref. (46).

As the figure 2.4 shows the ratio of the orifice area to that of the evaporation area (η) determines liquid formation on the surface by determining if the vapor pressure of gallium over GaN is above the vapor pressure of gallium over liquid gallium at that temperature. Studies by researchers (47) established stability regions for GaN under vacuum as well as OMVPE pressures over wide range of temperatures. The very small the rate of decomposition of GaN at atmospheric pressure of nitrogen (48, 49) could be attributed to the higher activity of nitrogen at near atmospheric pressures (23). Further, evaporation rates are further reduced due to a higher probability of gas scattering thus redirecting Ga [g] species towards substrate and hence maintaining higher gallium vapor pressure near the surface (50). GaN decomposition could be influenced by the presence of hydrogen, liquid Gallium and Indium, impurities and dislocations present in the material, and the crystal face that is undergoing decomposition. Initial studies on GaN decomposition in hydrogen atmosphere (43, 49) tried to explain the decomposition mechanism by the reduction in surface free energy by comparing it with Munir and Searcy's work. However, due to the difference in crystalline qualities involved in the studies, a concrete conclusion could not be made. This problem was addressed in a later study by Koleske et al. (51, 52). GaN decomposition rate was found to be enhanced when it was annealed in pressures greater than 100 torr. The mechanism of GaN decomposition in hydrogen atmosphere was proposed to be dissociation of hydrogen on GaN surface, reaction of dissociated hydrogen with GaN to form ammonia and the desorption of ammonia from the surface.

Liquid gallium and Indium were found to enhance GaN decomposition rate by acting as catalysts (53). These metals form Ga-N or In-N bonds on the top atomic layer across the solid-liquid interface and thus reduce the bond strength of solid Ga-N

bonds. The decomposition process is completed by the dissolution of GaN in the liquid and evaporation of nitrogen molecule from the liquid.

The dependence of GaN decomposition rate on the type of crystal facet was studied by various researchers by studying decomposition of GaN grown on different substrates. It was found that the decomposition rate strongly depends on the facet that is undergoing decomposition. In a study by Sun et al. (49) the GaN layers grown on different substrates were annealed in a hydrogen atmosphere at 900 ^{0}C. The films that were deposited on sapphire decomposed completely leaving gallium droplets on the wafer. However, GaN layers grown on Si faced 6H:SiC did not significant decomposition in a similar environment. Sun et al. also reported that in hydrogen atmosphere at 900 ^{0} C, (11-20) films deposited on (01-12) sapphire have a higher decomposition rate than the (0001) GaN films deposited on (0001) Sapphire. The authors concluded from these experiments that the N terminated (0001) GaN is more stable than that of (11-20) GaN surface that in turn is more stable than Ga terminated (0001) face. One should however keep in mind while comparing the GaN decomposition rates of different crystal facets that these samples were fabricated on different substrates. This could lead to a difference in dislocation density in the grown layers. Since the dependency of GaN decomposition on the dislocation density and impurities was proven, (41, 42) it should be noted that the layers grown on various substrates will have different dislocation densities and might affect the conclusions drawn from the above study on crystal facets by Sun et al.

2.3 GaN growth from thermodynamic perspective:

2.3.1 MBE

Device quality single crystal thin films of III-V semiconductors were grown using molecular beam epitaxy (MBE). As mentioned earlier, it was demonstrated that GaN

could be grown under non-equilibrium conditions using MBE. MBE offers several advantages over the conventional thin film growth techniques. These include much better control over the thickness and composition of the films that could be attributed to the layer by layer growth at the atomic level (54, 55). Further, it was shown that the quality of the grown material is independent of the growth conditions (55). A study by Newman extends the growth principles from other systems to III-N system (19). In the MBE growth of other nitride systems, kinetic barriers play a very important role. However, it was demonstrated that in GaN system, due to the strong bonding present in Ga-N and nitrogen molecule these kinetic barriers are required for the growth using MBE (20). Since the conditions of MBE growth of GaN are not thermodynamically favorable, the reaction occurs via meta-stable growth mode. Earlier studies on MBE growth of III-V compounds (55) mention that thermodynamically favorable conditions are necessary in order to successfully grow thin films using MBE. However, this study does not address the influence of kinetic barriers in adatom diffusion and incorporation into the lattice. From the phase diagram in Fig.2.1 & Fig. 2.2, one could see that the conditions under which most of the thin film GaN growths were reported were not thermodynamically favorable. Despite this thermodynamic barrier growth of GaN occurs due to an unusually large barrier for GaN decomposition (31). The reaction boils down to a competition between the forward reaction and the decomposition reaction. As long as the rate of the forward reaction to form GaN is higher compared to the rate of decomposition reaction, it is possible to grow GaN. However, it should be noted that the reacting species should be activated in order to provide sufficient energy for the GaN formation reaction. The reverse reaction of GaN decomposition could be enhanced by the presence of liquid gallium metal on the surface (53). So, excessively gallium rich conditions and high temperatures are generally avoided in MBE growth of GaN even though gallium rich conditions favor

the growth. The kinetic energy of the activated species plays an important role in determining the quality of the films. However, if this energy is too high, it could cause damage to the growing film and also enhances the reverse decomposition rate (56).

2.3.2 CVD:

Even though it is the industry standard to produce thin films for all other III-V devices, and despite its advantages such as uniformity, high yield and high throughput, the development of CVD GaN was delayed due to the amount of time it has taken to develop exotic precursors, reduce the rate of competing reactions and to precisely control transients involved in multiplayer growth (57, 58). The basic principle of CVD is to maintain a supersaturation of reactants in the gas phase so that they can diffuse through the boundary layer on top of the substrate towards to the growing crystal. However, the diffusion of reactants through the boundary layer establishes an upper limit to the rate of the growth reaction that is only a fraction of the growth rate predicted by thermodynamics (59). Maruska and Tietjen (4) successfully demonstrated the CVD of GaN by using a chloride vapor transport technique. As opposed to MBE of GaN, the chemical vapor deposition of GaN takes place under the conditions that are thermodynamically favorable. This leads to a higher quality material compared to the material grown by other techniques.

The CVD growth of GaN using chloride vapor transport was modeled by studies by Ban et al. (60) and Liu et al. (61). These studies include thermodynamic and kinetic aspects involved in chloride vapor transport of GaN.

2.4 Ammonia decomposition:

Ammonia, as the nitrogen source plays a very important role in the CVD growth of GaN. Even though the reaction involving ammonia in CVD of GaN seems to be trivial, in reality it is not so. Ammonia is thermodynamically unstable in the operating conditions of CVD growth. This generates molecular nitrogen N_2 that is inert at CVD temperatures (60, 61).

$$NH_3 \Leftrightarrow \frac{1}{2}N_2 + \frac{3}{2}H_2 \qquad (2.8)$$

Thermodynamically, during the conditions encountered in CVD reactions [0.1-1 bar and 1000-1100 C] the decomposition reaction should be 99.99% complete (19, 20). However, fortunately, there exists a kinetic barrier to N-H bond breaking that considerably slows down the rate of decomposition of ammonia. It was found that even though the extent of ammonia decomposition increases with temperature, catalysts have a significant effect on the efficiency of decomposition (60-62). Platinum, Tungsten and Iron (63), and graphite were reported as catalysts for ammonia decomposition (61, 62) reaction. Even though the mixture of Ga (l) and GaN(s) acts as a catalyst for ammonia decomposition (61), these conditions are not favorable for the growth of GaN since Ga (l) alone acts as a catalyst for GaN(s) decomposition.

Chapter 3

Bulk growth techniques of GaN

3.1 Crystal structure

GaN crystallizes in three crystal structures: wurtzite, zinc-blende and rock-salt. Thermodynamically wurtzite structure is the stable one at room temperature and atmospheric pressure. However at higher pressures, a phase transition to rocksalt structure (64) occurs. The zinc blende/cubic structure is a metastable phase and is stable when grown heteroepitaxially on substrates that sustain this particular phase. The chemical bond between Ga atom and nitrogen atom is covalent with each Ga atom tetrahedrally bonded to four nitrogen atoms through covalent bonds and vice versa.

The wurtzite structure could be thought of as a two overlapping hexagonal close packed structures and shifted from each other by 3/8 c along the c axis as shown in Fig 3.1. The two axes c and a satisfy the relation c/a = $\sqrt{8/3}$) = 1.633. The chemical bond between Ga atom and nitrogen atom is covalent with each Ga atom tetrahedrally bonded to four nitrogen atoms through covalent bonds and vice versa. So, the coordination number for the wurtzite structure is four. Symmetry of wurtzite structure belongs to space group $P6_3mc$ with two inequivalent atom positions at (1/3, 2/3,0) and (1/3, 2/3, u) where 'u' is the dimensionless cell internal structure parameter. Even though the ideal wurtzite structure has the same length for four tetrahedral bonds, it is

not the case for actual nitrides. In reality, due to the deviation of axial ratios from the ideal 1.633 value, two bonds differ from the other two (65).

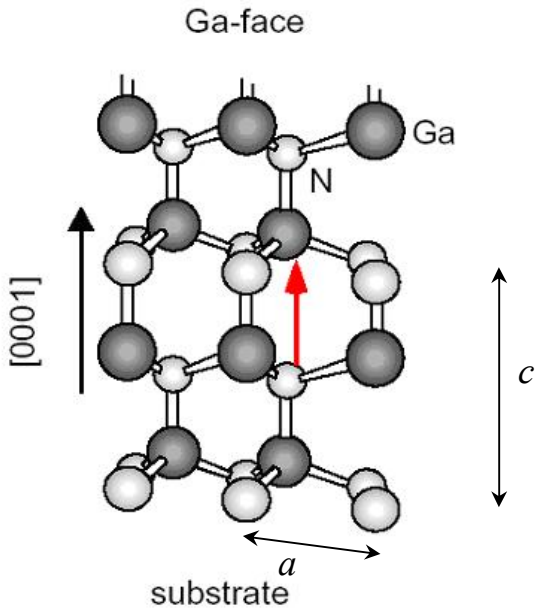

Figure 3.1 Crystal structure of GaN. From Ref. [64]

Physical properties of GaN are summarized in Table 3.1.

3.2 Lattice mismatch

GaN based devices proved to be an exception in exclusive commercialization of semiconductors by implementing heteroepitaxy in device fabrication owing to the lack of substrates of GaN. Even though the LEDs based on heteroepitaxy of GaN demonstrated high luminescence efficiencies despite the high dislocation densities (67) GaN substrates are indispensable in improving the performance of the GaN based devices. Since state-of-the-art GaN based devices are fabricated on foreign substrates such as sapphire, SiC, $MgAl_2O_4$, MgO (66),the lattice mismatch and the coefficient of thermal expansion mismatch leads to a high dislocation density in the heteroepitaxially

Table. 3.1 Properties of GaN from Ref. [66]

Property		**Value**
Energy band gap (eV) (300 K)		3.44
Maximum electron mobility (cm^2/V s)	300 K	1350
	77 K	19200
Maximum hole mobility (300 K) (cm2/V s)		13
Controlled doping range (cm^{-3})	n-type	10^{16} to 4 x 10^{20}
	p-type	10^{16} to 6 x 10^{18}
Melting point (K)		>2573 (at 60 kbar)
Lattice constants (300 K)	a (nm)	0.318843
	c (nm)	0.518524
Percentage change in lattice constants (300–1400 K)		Δa/a=0 0.5749, Δc/c0 0.5032
Thermal conductivity (300 K) (W/cm K)		2.1
Heat capacity (300 K) (J/mol K)		35.3
Modulus of elasticity (GPa)		210 ± 23
Hardness (nanoindentation, 300 K) (GPa)		15.5 ± 0.9
Hardness (Knoop, 300 K) (GPa)		10.8
Yield strength (1000 K) (MPa)		100

grown GaN layers. Figure 3.2 shows a graph of energy bandgap vs. lattice parameters of various materials that are used as substrates for GaN devices. As can be seen from the plot, sapphire has a lattice mismatch of ~13% with GaN and this results in a very high dislocation density of the order of 10^{8}-10^{11}/cm^{2}. Table 3.2 shows the lattice parameters, coefficient of thermal expansion mismatch and the lattice parameter mismatches of various substrates with GaN (2).

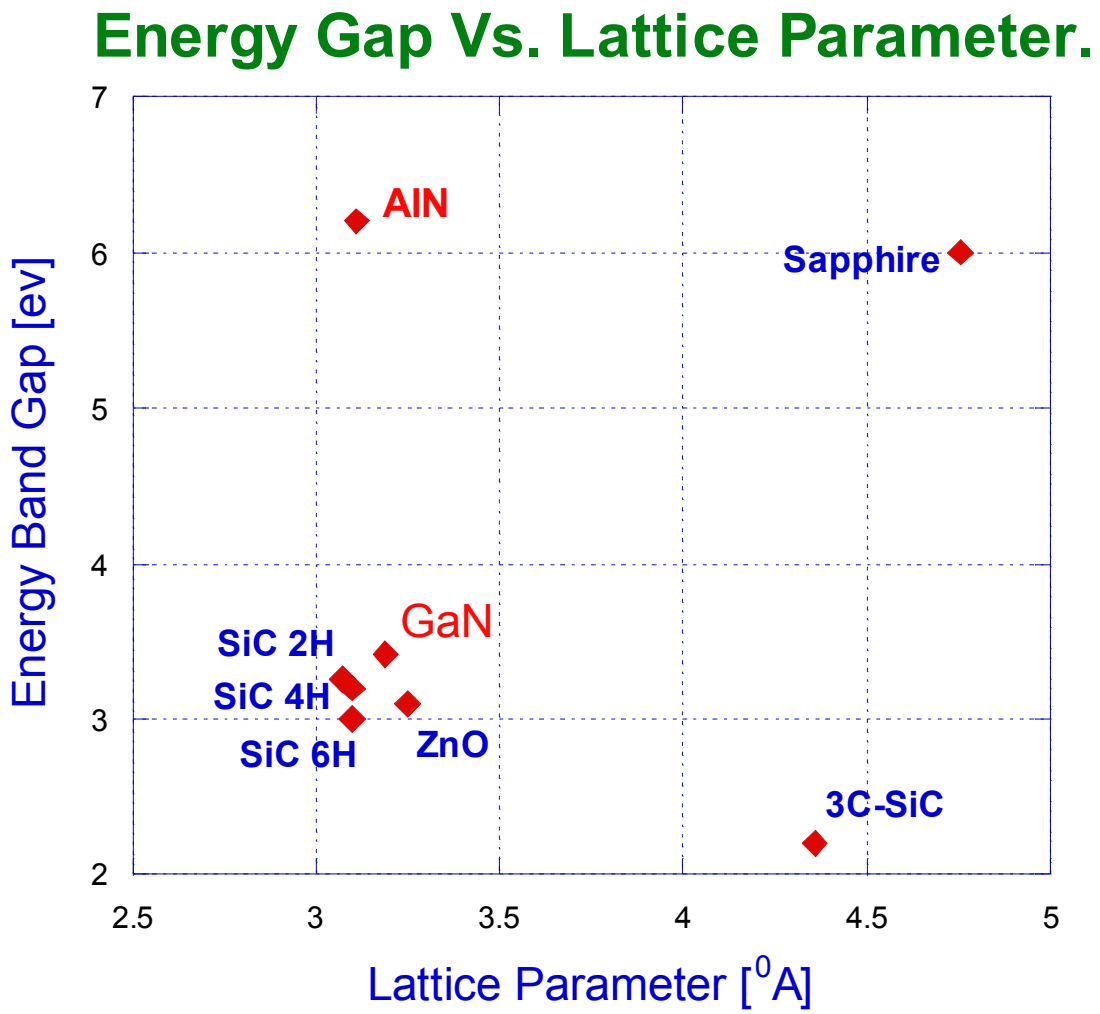

Figure 3.2. Energy Bandgap Vs. Lattice Parameter

3.3 Bulk growth techniques of GaN

3.3.1 HVPE:

The first report of HVPE growth of GaN was by Tietjen (4) in 1969. This method of growing was used to grow epitaxial layers of GaN till early 1980s. However, due to high density of native nitrogen vacancy defect concentrations that was thought to be due to the high deposition temperatures involved in the process (68), researchers stopped using this method to produce GaN layers. Despite the experimental evidence that HVPE GaN layers could be grown with non-degenerate carrier concentrations, (69) the inability to achieve p-type doping was thought to be due to the nitrogen vacancies. HVPE essentially involves a reactor with two different temperature zones. First zone is usually the low temperature one that is kept at ~800-900^0 C and contains a boat consisting of gallium. HCl is made to react with gallium in the low temperature zone and transported to the high temperature zone using a carrier gas such as H_2, N_2 or He (70). In the high temperature zone, it is made to react with ammonia to form GaN on the substrate held on a rotational platform. The temperature of this high temperature zone is kept at 1000-1100^0 C. The reactions that occur in the two zones are given below.

Low temperature zone:

$$Ga(l) + HCl(g) \Leftrightarrow GaCl(g) + H_2(g) \qquad (3.1)$$

$$GaCl(g) + 2HCl \Leftrightarrow GaCl_3(g) + H_2(g) \qquad (3.2)$$

The efficiency of the above reaction (3.1) was reported to be highly dependent on the temperature of the reaction. Higher the temperature, higher the efficiency of the conversion reaction (60, 61). Reaction (3.2) is a parasitic reaction that reduces the partial pressure of GaCl (g) in the gas phase. GaCl (g) formed in the above reaction is

transported to the high temperature zone of the reactor where it is reacted with NH_3 according to the following reaction.

High Temperature Zone

$$GaCl(g) + NH_3(g) \Leftrightarrow GaN(s) + HCl(g) + H_2(g) \qquad (3.3)$$

The extent of ammonia decomposition at these temperatures determines the amount of atomic nitrogen available for the GaN formation reaction. Ammonia is thermodynamically unstable at reaction temperature. However, the kinetic barrier to the decomposition of ammonia restricts the extent of ammonia decomposition. Taking into account the mole fraction of ammonia decomposed (α) as shown in the reaction below.

$$NH_3 \Leftrightarrow (1-\alpha)NH_3 + \alpha/2\, N_2 + 3/2\, H_2 \qquad (3.4)$$

The efficiency of the above reaction (3.4) was found to be dependent on the type of carrier gas (60). It was found that He is a more conducive environment for GaN growth.

One of the disadvantages of HVPE is the gas phase reaction leading to the formation of GaN in the gas phase and on the walls since GaN formation reaction is thermodynamically favorable under growth conditions. These parasitic reactions have a deleterious effect on the growth rate as well as leading to particle formation in the gas phase that might get incorporated into the growing crystal thus contributing to the defects. Further, HCl is corrosive and could contribute to the degradation of the reactor equipment (68). In order to avoid this, $GaCl_3$ was used by several researchers as a source of gallium instead of GaCl (71-73). As stated above, $GaCl_3$ could form

when GaCl reacts with HCl. $GaCl_3$ tends to react with NH_3 and condense thus reducing the amount of gallium available for the crystal growth reaction (74). Despite these limitations, HVPE is still being used to grow epitaxial layers of GaN and as a technique for growing bulk GaN due to its high growth rates as high as 60 microns per minute (75-77). Film morphology in subsequent studies was using modifications such as sputtered AlN/ZnO low temperature buffer layers GaCl pretreated substrate, and epitaxial layer overgrowth (72, 75, 78).

3.3.2 Solution growth:

Various solution growth methods were used to grow GaN. A low pressure, low temperature pulling method from a gallium containing solution was reported (79) to result in polycrystalline GaN with grain sizes of the order of a few mm (80). The growth rate achieved in this method was 1-2 mm. Even though crystals of 25mm diameter and 12mm length were grown, as mentioned earlier, they were polycrystalline. Another way of growing GaN single crystals was developed using high pressure solution growth method in Poland, Warsaw (81, 82). In this method, high quality GaN crystals were grown from solutions of atomic nitrogen in liquid gallium using high pressures of nitrogen. It was known that gallium metal catalyses the dissociation of molecular nitrogen (81). However, there exists a potential barrier for the molecular nitrogen to reach the metal surface. This barrier was overcome by high pressure and high temperatures used in this particular form of solution growth technique. Nitrogen atoms efficiently undergo chemisorption under these growth conditions. The number of nitrogen atoms that could be dissolved in the solution is limited by the solubility limit (83). If this number of nitrogen atoms in the solution is high enough, in other words, if the pressure of atomic nitrogen in the solution is high enough, it could form GaN in the solution. This equilibrium was studied previously by

Karpinski (84). Fig. 3.3 (a) and 3.3(b) shows the phase diagram of p-T curve for GaN system and solubility curve for Ga-N_2 system respectively (85).

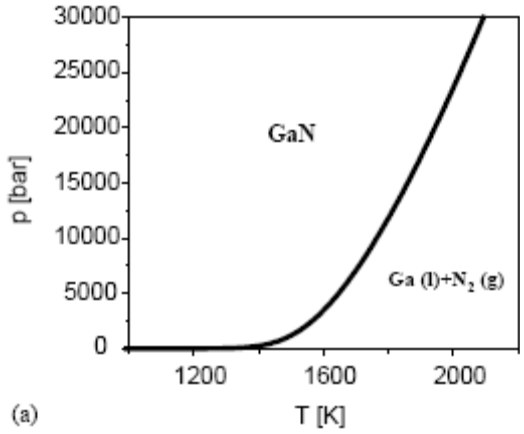

Figure 3.3(a) Phase Diagram of GaN. From Ref. (85)

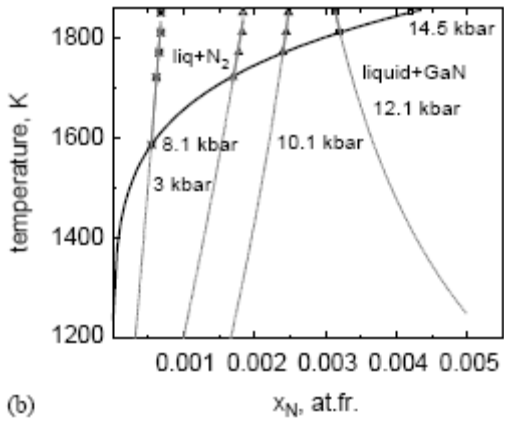

Figure 3.3(b) Solubility curve for Ga-N_2 system. From Ref. (85)

Since the solubility of nitrogen in the solution is an increasing function of temperature, crystal growth in this technique was achieved by maintaining a temperature gradient. In the higher temperature portion of the solution, there is a higher amount of dissolved nitrogen in the solution and vice versa. This dissolved nitrogen was transported from high temperature region to low temperature region due to the presence of a concentration gradient of nitrogen in the solution as well as convection currents. This leads to a supersaturation in the low temperature region of

the melt thus giving rise to crystal growth. Even though this method resulted in higher quality crystals compared to that of low temperature-low pressure solution grown crystals, it still has some disadvantages. Crystals grown using this method are generally platelets of relatively small size i.e. of the order of 1 cm^2. Higher degree of anisotropy, difficulty in controlling the nucleation sites on polar surface (0001), and lack of control over mass transport in solution are the main drawbacks of solution growth technique. Further, the slow growth rates encountered in this technique are unsuitable for industrial production environment (85).

A variation of the above mentioned solution growth method was developed by Inoue et al. (86). This method is called pressure controlled solution growth and addresses some of the problems involved in the conventional solution growth. Conventional solution growth involves maintaining relatively high temperature gradients over short distances. Conventional solution growth also leaves behind major portion of solvent where as this is not the case in PC-SG. This technique also amends the dropping growth rate problem observed in the conventional technique. PC-SG is based on increasing the over pressure of the solute at constant temperature as opposed to the constant over pressure of the solute in the conventional SG method. This eliminates the temperature gradient problem and also addresses the decreasing growth rate problems encountered in CSG. Furthermore, it doesn't leave any solvent behind. From this study, it was observed that the lower rate of pressure increase gives rise to better crystalline quality.

3.3.3 Flux method:

Even though the solution growth method offers a way to grow GaN single crystals, the pressures required in this process are extremely high (81, 82). It was found that the addition of Na to the gallium increases the solubility of nitrogen in the melt and hence makes possible the single crystal growth at lower pressures. This method was developed by Yamane et al. (87). This flux method is a variation of high pressure solution growth method except that the flux method utilizes a mixture of gallium and sodium instead of pure gallium to increase the solubility of nitrogen and hence bring down the operating pressures. In order to have a good understanding of flux growth technique, a thorough understanding of high-pressure solution growth [HPSG] technique is essential. A detailed analysis of HPSG and Na flux based growth technique was performed by Kawamura et al. (88). Since a congruent melt of GaN could not be formed at the operating conditions of HPSG, the technique should be regarded as growth in gallium self flux. Solution growth techniques described previously (84, 85, 86, 89) make use of only increasing solubility with increasing pressure or maintaining a temperature gradient Figures 3.3 & 3.4. The self explanatory Figure 3.4 describes how maintaining a higher pressure than equilibrium pressure can lead to crystal growth. From Fig. 3.4, it could also be seen that the solubility of nitrogen in the melt increases dramatically with the addition of sodium. This makes the solution growth of GaN possible at much lower pressures compared to the solution growth of GaN in pure gallium melt.

The mechanism of GaN crystal growth by sodium additions was described by Kawamura et al. (88) as follows. Addition of sodium to the melt ionizes the nitrogen molecules at the gas-liquid interface above 900 K. These ionized nitrogen species are easily dissolved in the Ga-Na melt system.

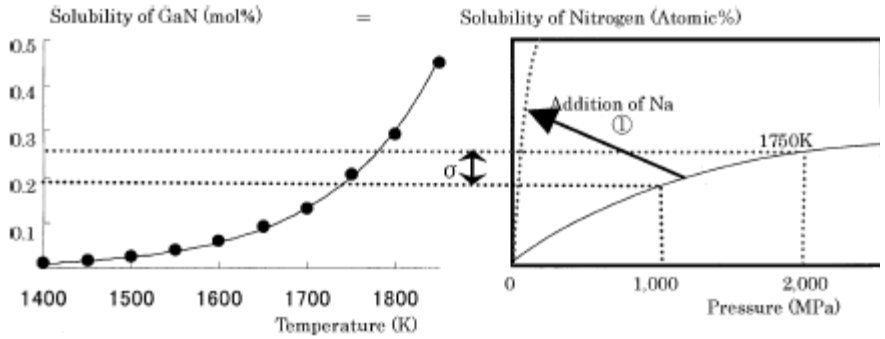

Figure 3.4. Solubility curve of GaN in gallium melt and the effect of addition of sodium on the solubility of nitrogen in GaN. From Ref. (88)

Application of pressure enhances the dissolution of ionized nitrogen in the melt and when the nitrogen concentration exceeds the solubility of GaN, crystal growth initiates. Aoki et al. (90) demonstrated single crystal GaN growth at a pressure of 1-5 Mpa at low temperatures [650-900^0 C] using high pure Na flux based method as opposed to the high pressure method where the operating pressures are of the order of GPa. In this study, crystal growth experiments were carried out at the temperatures of 750-800 °C, N_2 pressures of 3-5 MPa and sodium mole fractions of 0.36- 0.60 for 150-450 h. Single crystals of size 5 mm were prepared using this method. The effect of other additives such as lithium or calcium was also discussed by Kawamura et al. Even though the addition of sodium depends on its power to ionize, lithium and calcium were not found to act in the same manner. Li and Ca have high binding energies and form nitrides even at high temperature and hence they decrease the activity of the melt. The yield of the GaN crystal growth process was found to increase with increasing Li or Ca concentration up to a certain point after which any more of the additives tend to decrease the yield. This decrease in yield was thought to be due to the decrease in the reduction power of the melt after a certain additive concentration.

As could be seen from these results, the growth rates involved in this method are extremely low (~mm/day) and not suitable for growing large size bulk GaN crystals.

3.3.4 Ammonothermal process:

Dwilinski et al. (91) reported the synthesis of GaN using ammonothermal process for the first time. This process involved the reaction of gallium with supercritical ammonia in a nickel-alloy autoclave at a temperature of 550^0 C and at a pressure of 5kbar. In order to expedite the chemical reactions, mineralizers such as lithium, potassium, or lithium amide compounds were added to the autoclave and the reaction was carried out for 3-21 days. The alkali metals or their amides react with ammonia solution forming imides that dissociate into RNH^- and H^+ ions where R represents an alkali metal. The higher the concentration of these alkali imides, the more is the GaN formation along with other Ga-NH_2 complexes. The GaN thus formed was in the form of powder, highly pure and has high crystalline quality as proven by the PL. The position of the peaks in the PL spectrum was sample independent and hence indicated stress free samples. The crystalline size was of the order of few microns. Another approach of growing bulk GaN single crystals using GaN feed stock was developed by Ketchum et al. (92). This method is similar to hydrothermal growth of quartz where a feedstock of SiO_2 was dissolved by a OH^- mineralizer (93). In the approach by Ketchum et al., amide was used as the mineralizer. The purpose of the mineralizer is to dissolve the feedstock forming a soluble species that can be transported to the crystal growth site. In order to achieve supersaturation, a temperature gradient was maintained. The following reaction explains the processes involved in the ammonothermal growth of GaN.

$GaN + NH_2^- + 3NH_3$

→ soluble Ga-imide complex

→ GaN crystals + $NH_2^- + 3NH_3$ (3.5)

Using this process, single crystals of 0.5 x 0.2 x 0.1 mm^3 size were synthesized.

Next chapter focuses on sublimation growth of GaN and discusses the reasons behind our approach to grow bulk GaN crystals. It also gives a description of the growth system and the gas handling system used in our experiments.

Chapter 4

Sublimation growth

4.1 History of sublimation growth

Sublimation technique has proven to be a successful technique to grow bulk AlN crystals (94). AlN undergoes congruent evaporation at high temperatures providing Al and N_2 in the gas phase the necessary species for the growth of AlN. The over pressure of these species is sufficient enough to grow AlN in the temperature range of 1950-2250 ^{0}C (95). Using this technique, AlN bulk crystals of area 10mm x 10mm and thickness of 1mm were produced. However, in contrast to AlN, as explained in section 2.2, GaN undergoes congruent evaporation only under langmuir free evaporation conditions (43, 96). At higher pressures, GaN undergoes incongruent evaporation forming liquid gallium and N_2. However, since the N_2 is extremely unreactive with liquid gallium at atmospheric pressure, it is not possible to drive the GaN formation reaction in the forward direction. So, one has to use a different source of nitrogen such as ammonia.

Sublimation sandwich technique growth of GaN was attempted by Wetzel et al. (97). They placed a series of growth cells each consisting of a gallium boat and a SiC seed placed directly above it. By passing ammonia gas through the gap at flow rates of 25-50l/min, they were able to obtain epitaxial layers of GaN at growth rates of 300 μm/hr. The characterization results showed that the epitaxial layers were highly crystalline with FWHM of the X-ray rocking curves ~ 6 arc min. The grown layers

were found to be n-type with electron mobilities ranging from 30-80cm^2/Vs. Fisher et al. (98) reported the growth of GaN layers grown at high temperatures in the range near and above 1200^0C. The growth rates obtained using this high temperature vapor phase epitaxy were 40-80 μm/hr. However, the FWHM of the rocking curves ranged from 420-1000 arcsec for the layers deposited on 6H-SiC substrates and 1000-1250 arcsec for the films that were grown on sapphire. However, the flow rates of ammonia were of the order of 20 sccm in HTVPE as opposed to 25-50 l/min by Wetzel et al. Baranov et al. reported the growth of GaN by sublimation sandwich technique at growth rates greater than 1mm/hr in detail. They found that even though liquid gallium source resulted in higher growth rates, its special and temporal stability was inferior compared to that of the GaN powder source. However, it was found that the pure GaN powder decomposed incongruently to give rise to liquid gallium in the powder. A mixture of liquid gallium and GaN powder was used as the source material in these experiments. Using this process, GaN crystals of size 0.5 mm x 15mm x 15mm were obtained at growth rates ranging from 0.1-1.1 mm/hr. However, the best quality crystals were obtained when growth rate ranged from 0.2 to 0.4 mm/hr. Numerical simulation based on the Navier-Stokes equation, conservation of momentum, mass and energy and including the heterogeneous reactions at the source and the substrate were performed assuming NH_3, N_2, H_2, Ga as the transporting species, and neglecting the homogeneous reactions between the transporting species. These simulation results indicated that the hydrogen concentrations inside the growth cell exceeded 93%. This high concentration of H_2 is predicted to hinder the supply of ammonia to the growing surface and result in lateral non-uniformity in the III-V ratio. Further, the simulated growth rates were much lower compared with the experimentally observed growth rates. The gallium transport rates were calculated considering three different mechanisms, i) gas convection in the growth cell enhanced

by hydrogen generation at the surface of the source due to NH_3cracking, ii) multiple channel desorption of Ga (via gaseous compounds with hydrogen and other possible species), and iii) generation of Ga droplets at the surface of the source followed by their transport to the substrate. However, these mechanisms were not able to substantiate the high gallium transport rates experimentally observed. A growth process window was found as a function of substrate temperature (T) and the temperature gradient (ΔT) between the source and the seed. At higher ΔT and/or T, gallium droplets were observed on the surface resulting in numerous material defects. At low substrate temperatures, polycrystalline growth was observed where as at lower ΔT, the re-evaporation rate at the seed was higher resulting in island formation. X-Ray rocking curve FWHM of the GaN crystals grown on SiC substrates was found to vary from 2.5-6.5 arcmin where as it was in the range of 6-9 arcmin for the crystals grown on sapphire. A serious issue encountered in this process was that of bending of grown GaN layers because of the lattice mismatch and thermal coefficient mismatch between the substrate and the grown layers. The dislocation densities calculated using X-ray diffraction technique were found out to be ~1-2 x $10^{10}/cm^2$. Even though the growth rates achieved were high, the simulation results suggested further optimization of the process conditions to achieve better uniformity. Later studies on sublimation growth of GaN using crystalline GaN powder containing few hundred micron size crystals resulted in single crystal GaN layers (99). Even though high growth rates were not reported using this process, it was reported that the process was more stable resulting in a higher quality of grown layers. A direct synthesis method [DSM] similar to sublimation sandwich technique was reported by Nishino et al. (100) where liquid gallium and ammonia were used as the precursors and resulted in growth rates ~70μ/hr. Crystalline quality and the surface morphology were found to improve

significantly when seeds of sapphire with GaN epitaxial layer were used instead of sapphire.

The extensive research that has been done over the years to grow bulk GaN has been described in this section as well as in section 3.3. From the literature, it was clear that sublimation technique produced good quality GaN crystals at high growth rates. We tried to improve the growth rate of GaN by using a carrier gas to transport the gallium containing vapor species that is obtained from the decomposition of GaN powder. The advantage of this approach is that the growth system is relatively inexpensive as opposed to the high pressure solution growth where pressure vessels that can tolerate upto 10,000 bar pressures are needed. Further, the growth rates obtained in sublimation technique are way more than those obtained in HPSG, ammonothermal, and flux based growth techniques. High growth rates provide the advantage of commercializing the bulk GaN growth technology because of higher throughput. The following section describes the growth system as well as the gas handling system that was used in the growth experiments. Since the growth setups used to perform the experiments were modified over time, they are described chronologically in the later chapters to maintain a continuous flow of GaN growth technology development.

4.2 System description

This section describes the crystal growth system that is used in our experiments (101). The growth system comprises of a 1400^0 C furnace mounted vertically on a steel base plate. In order to provide high-pressure capabilities, the furnace is surrounded by a pressure vessel. A tube steel frame supports the base plate as well as the power module meant for power distribution to the furnace elements. Attached to the steel tube frame is an electric winch that is used to lift the pressure

vessel cover up for furnace maintenance. A combination of steel and molybdenum rod serves as the puller rod and is operated by a linear motion mechanism mounted above the vessel. This rod can be attached to a motor that can be used to rotate the rod to employ seed crystal rotation during the crystal growth process. The puller rod goes through a double seal assembly in the top pressure vessel and holds the seed holder at the bottom by means of a 10-32 threaded hole.

The pressure vessel has a water jacket and a water cooling loop in the top vessel cover. Water enters the bottom side of the water jacket and exits at the topside of the jacket. The side water jacket and the top water cooling loop are connected in series. The water that exits from the side jacket enters the water cooling loop at the top and exits at the top of the cover. A flow switch interfaces the furnace power supply to the water flow. This switch turns the power to the elements off when the water is below a certain flow rate.

The top side of the pressure vessel is covered by an adapter flange that has five ports out of which three ports were used for gas flows, one for a thermocouple and one for a pressure transducer. On top of the adapter flange, there is another flange that could be lifted by a slider mechanism that is attached to the steel tube frame. This slide mechanism has an electrically operated break switch that can be used to load and unload the growth assembly. The vessel is sealed on both top and bottom sides by means of stainless steel bolts. A torque wrench is used to tighten the bolts in three steps [20ft-lbs, 40 ft-lbs and 60 ft-lbs]. For sealing the bottom side, a circular pattern was implemented while tightening the bolts. In order to accommodate for the gasket compression, this tightening has to be repeated one more time around the bolt circle at the 60 ft-lb level. However, for tightening the top cover and the two flange assembly on the topside of the vessel, a cross pattern is used instead of the circular pattern.

Again, a three-step torque level similar to the bottom side sealing procedure is implemented.

The system is turned on by turning on the circuit breakers first. Then the system reset toggle should be actuated. The water flow through the cooling water jacket should keep the flow switch turned on to allow electrical power to the molybdenum furnace elements. The current to the molybdenum elements is limited by employing phase angle fired SCR's with current limiting. The over temperature display should read ambient. One must note that the over temperature display indicates an out of range condition at room temperature because B type thermocouples are employed to read the temperature of the furnace.

An alarm circuit causes the power contactors to drop out and the power to the furnace is turned off if the water flow stops. This circuit also rings an alarm to warn about the insufficient water supply through the water jacket. However, this alarm could be silenced by toggling a switch

The vessel base plate has several ports to connect the system to gas or vacuum equipment. There are two vacuum ports that are connected to the front side of a roughing pump and a turbo pump respectively. The backsides of these pumps are connected together via a foreline. A pirani gauge monitors the pressure in the foreline as shown in the schematic.

The entire system can be controlled by a PC based ADAPT program.

A schematic of the growth system that was used to perform the experiments is as shown in figure 4.1. The graphite boat that shown is suspended by three molybdenum rods that are held by three stainless steel rods by means of set screws. These three stainless steel rods are screwed in to the top flange. The suspension rods are not shown in the schematic. Two quartz tubes that serve as gas inlets shown in the figure are employed to provide the N_2/ H_2/ NH_3 gas flows as shown. These two quartz

tubes are held by two cajon fitting that is welded to the top flange. A thermocouple is inserted into the boat to measure graphite boat temperature. The whole assembly is enclosed in a graphite/quartz ampoule that is attached to the top flange. This graphite ampoule isolates the experimental set up from the rest of the furnace tank. This ensures the safety of the filaments, as they are not in direct contact with the process gases.

The gas flow inputs comprises a seed flow that is directed towards the seed and a ampoule flow that is into the ampoule ambient. This flow is used to deliver the carrier gas such as nitrogen in the later designs. Exhaust line from the ampoule is divided into two lines that are connected to a turbo pump and a roughing pump separately. A foreline connects these two pumps as shown in the schematic. These two pumps are used to pump down on the tank as well the ampoule. The tank and the ampoule are connected to two different pressure transducers via a throttle butterfly valve and to two exhaust valve controllers [not shown] to control the pressures in the tank and the ampoule independently. A leak valve on the foreline was used for the purpose of leak checking the system.

The gas handling system for the growth system is shown in Figure 4.2. Nitrogen gas passes through the regulator and is divided into two lines as shown by two mass flow controllers [MFC 1 & 2]. MFC3 and MFC4 are used to flow hydrogen and ammonia respectively. A rotameter is also used to pass hydrogen gas due to the malfunction of MFC3. A separate line for argon is established to backfill the tank. After passing through the MFCs, the gases are mixed as shown to give rise to seed flow and ampoule flow that could possibly consist of $N_2/NH_3/H_2$ and N_2/H_2 respectively.

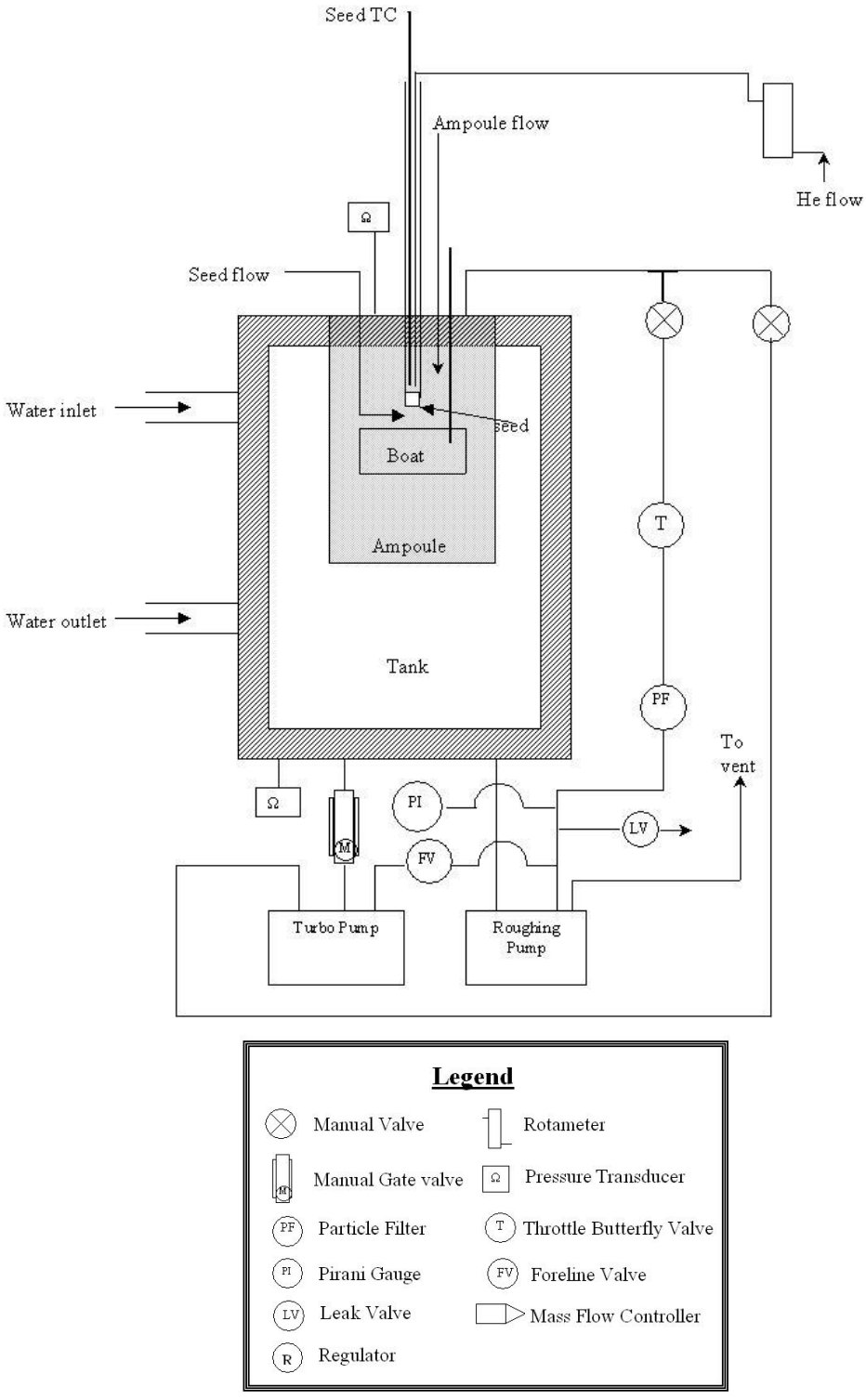

Figure 4.1 Schematic of the growth system

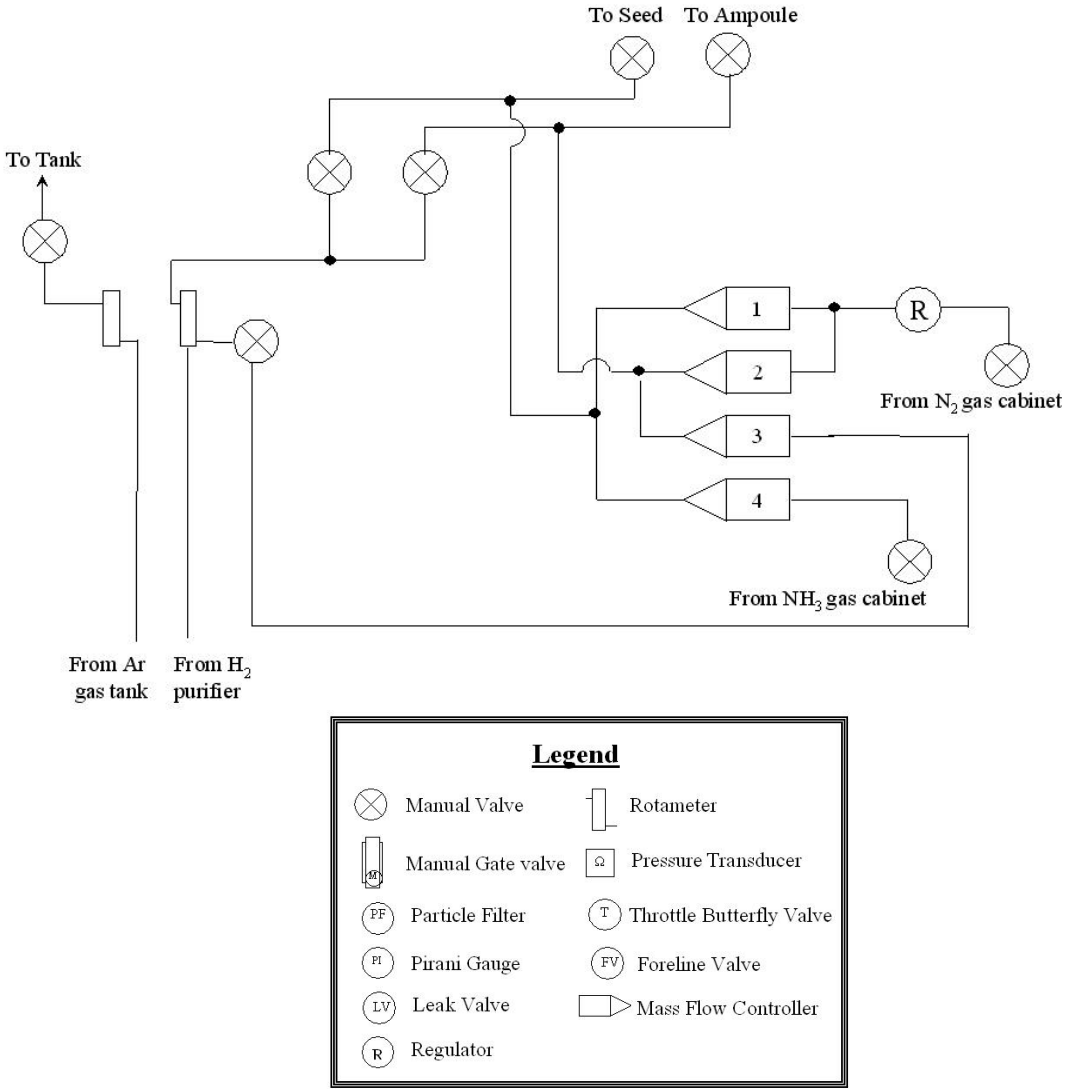

Figure 4.2. Schematic of the gas handling system.

Chapter 5

GaN Growth using commercial GaN powder – Sublimation sandwich.

5.1 GaN decomposition experiments:

In chapter 4, we discussed sublimation and a detailed description of growth system and gas handling system. This chapter focuses on the experimental results that were obtained from the first generation growth setup. The choice of GaN powder as the source gallium in bulk growth of GaN was made based on the fact that powder will have more surface area compared to a crystal of the same weight. If GaN powder is used instead of a wafer of the same weight, number of Ga atoms produced per second from the powder will be a factor of $4t(1-\rho)/r$ more than that of wafer decomposition due to higher surface area of the powder. ρ is the porosity of the powder, t is the thickness of the wafer and r is the radius of the GaN granule respectively in the above expression. This principle was used to increase the incoming flux of gallium containing species and hence increase the growth rate of GaN. In order to make sure that GaN powder acts as a stable source of Ga vapor for crystal growth experiments, we have performed GaN powder decomposition experiments at different temperatures. GaN powder decomposition experiments were performed in order to measure gallium transport rates. Commercially available GaN powder [Alfa Aesar, 99.99% pure metals

basis] was used as the source in the decomposition experiments. Weight loss of the powder was measured as the difference between the initial weight and the weight after the experiment. A schematic of the experimental setup that was used to perform the decomposition experiments is as shown in Figure 5.1.

5.1.1 Design - I

This configuration consists of a graphite boat that is suspended by three molybdenum rods that are held by three stainless steel rods by means of set screws. These three stainless steel rods are screwed in to the top flange. The suspension rods were not shown in the schematic. Two quartz tubes that serve as gas inlets shown in figure 5.1 were employed to provide the sees/ampoule gas flows as shown. These two quartz tubes were held by two cajon fittings that is welded to the top flange. A thermocouple was inserted into the boat to measure graphite boat temperature. The whole assembly was enclosed in a graphite ampoule that is attached to the top flange.

5.1.2 Experimental procedure:

This involved loading the graphite boat with commercial GaN powder and pumping down the system to a foreline pressure below 10^{-2} torr. Once pumped down, the ampoule was backfilled with nitrogen through the two gas inlets and the tank with argon. The temperature was then ramped from room temperature to 800 ^{0}C and stabilized for an hour at this temperature. After the stabilization period, the temperature was ramped to the decomposition temperature set point as read by the thermocouple. Once the decomposition temperature was reached, the gas flows were set to the required composition through the right side quartz tube in the schematic. The left side tube was used only to flow nitrogen. Once the decomposition time was over, the power to the filaments was turned off.

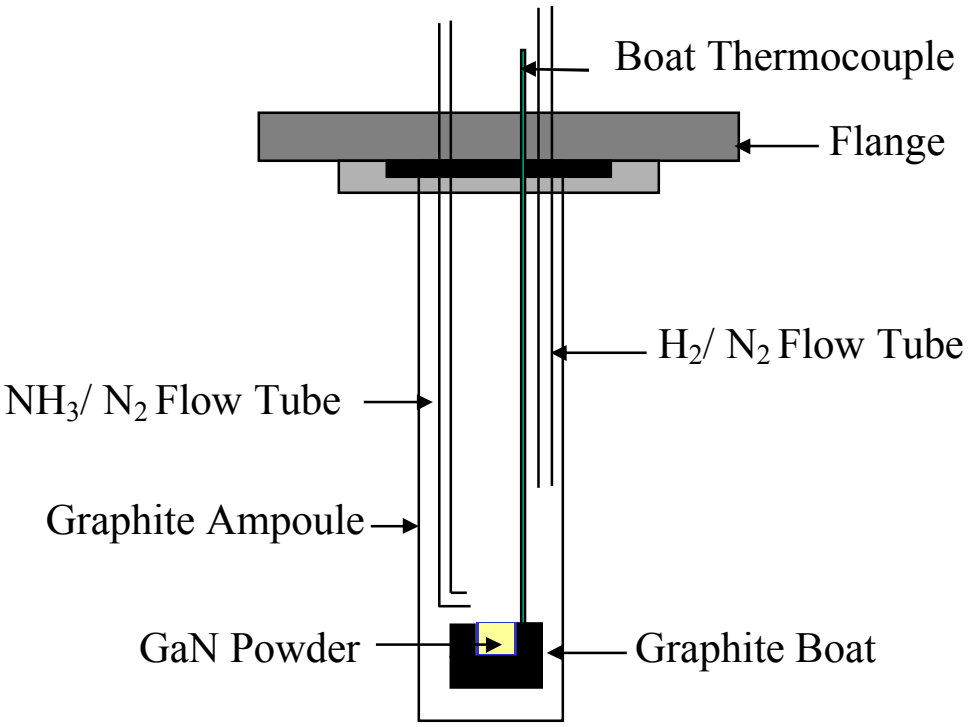

Figure 5.1. Experimental setup for GaN powder decomposition experiments

5.1.3 Experimental results and discussion:

Figure 5.2 summarizes the weight loss variation with respect to temperature. These experiments were performed for 1 hr at a pressure of 100 torr under an atmosphere of 50 % nitrogen and 50% hydrogen. An exponential increase in weight loss was observed with an increase in temperature. Figure 5.3 shows the variation of weight loss with respect to time. These decomposition experiments were performed at a boat temperature of 1000 ^{0}C, 100 torr pressure and an atmosphere that contains 50 % nitrogen and 50% hydrogen. A non-linear variation of weight loss with time could be observed from the plot. At longer times, the rate of weight loss was observed to have slowed down indicating depletion of source material.

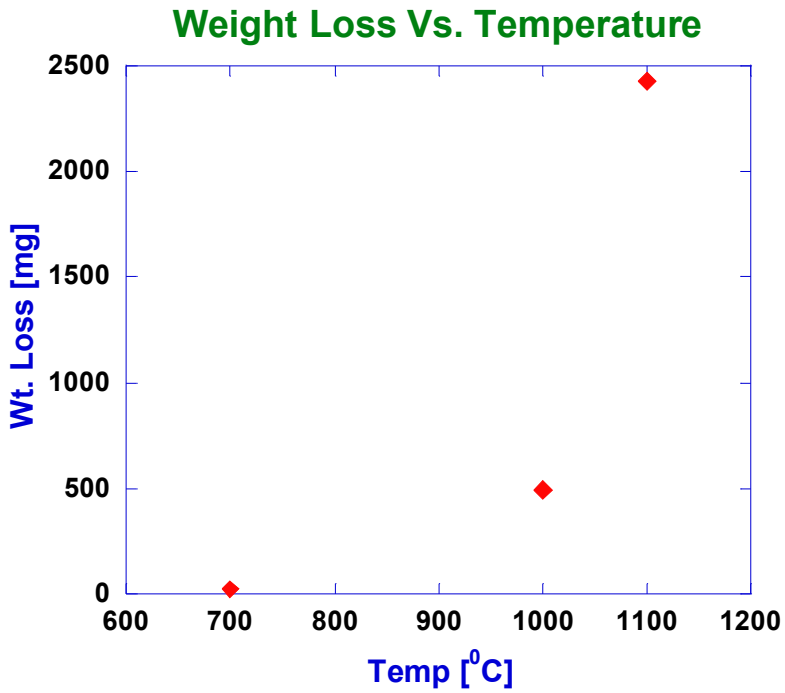

Figure 5.2 Weightloss of GaN with temperature

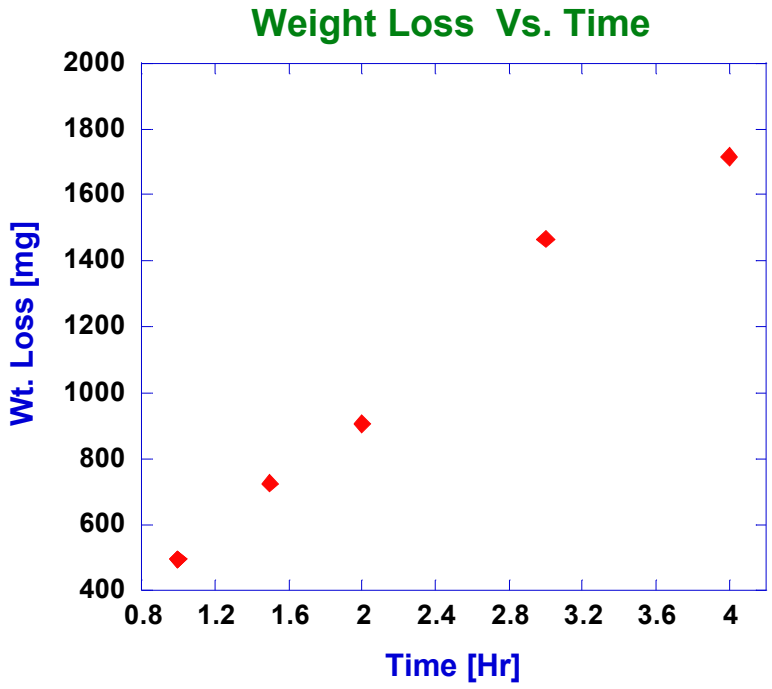

Figure 5.3. Weightloss of GaN with time.

The effect of hydrogen on GaN decomposition was also studied by varying the concentration of hydrogen in the right side gas inlet. Figure 5.4 shows the effect of hydrogen on GaN decomposition. It can be clearly seen from the graph that the presence of hydrogen enhances the decomposition of GaN through reaction 5.1

$$GaN(s) + \tfrac{3}{2} H_2(g) \rightarrow Ga(g) + NH_3(g) \qquad (5.1)$$

These decomposition experiments were carried out at a total pressure of 100 torr and a temperature of 1000^0 C. These results were in direct agreement with the previous work by Koleske et al. (51, 52).

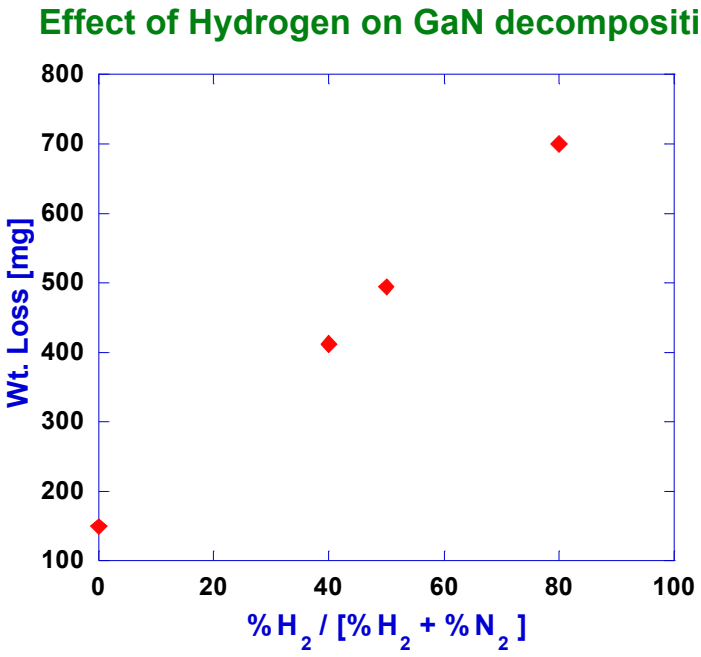

Figure 5.4. Effect of hydrogen on decomposition of GaN.

5.1.4 Simulations:

Theoretical modeling of GaN powder sublimation in the present experimental setup was performed by Dr. Yuri Makarov at Semiconductor Technology Research, Inc (102). A code developed in STR, Inc. was used to simulate axisymmetric steady-state heat transfer in the growth chamber. Special attention is given to the effect of powder thermal conductivity, powder charge weight, as well as the effect of powder granule size on the temperature distribution in the source zone. A model of heat transfer in granular powder suggested earlier in STR, Inc. for SiC powder was extended to GaN powder. This model has the ability to calculate heat transfer in porous media with porosity and the grain size of the powder particles as parameters. Using this model, thermal conductivity of the powder was calculated as a function of distance from the walls both radially and longitudinally inside the boat that contains the GaN powder. It was found that the thermal conductivity of the powder was two orders lower than that of GaN crystal. It was further reported that bigger the granule size, the better the temperature uniformity is through out the powder. Moreover the thermal conductivity of the powder was found to be relatively independent of the ambient pressure. The porosity of the powder creates noticeable temperature gradients across the powder as the powder weight increased from 1g to 5g inside the boat.

Mass transport of species in the powder source and in the gas phase between the source and the seed was studied using a one-dimensional model. GaN powder was treated as a heterogeneous medium consisting of GaN granules and a multicomponent vapor consisting of N_2, H_2, NH_3, and Ga filling the porous space. In the computations, both the convective and diffusive mechanisms of the species transport are taken into account together along with the heterogeneous chemical processes occurring on the granule. An appropriate set of heterogeneous reactions was employed which accounts

for the coexistence of *GaN(s)* and *Ga(l)* and the fast sublimation of the granules for the GaN decomposition reaction.

The mathematical formulation performed (102) involves a set of Mass Transport Equations (MTE) written for every species and coupled with the ideal gas state equation. These equations derived for the powder charge and the gap include a source term accounting for the interphase mass exchange between the multicomponent vapor in the porous space and the granule surface and the mass exchange between the growth cell and the ambient. The state equation for the gas mixture in the powder charge accounts for the reduced gas volume in the porous medium. Therefore, the equations used for modeling were,

In the charge bulk:

$$\frac{d}{dz}\left(\rho C_i U - \rho D_i \frac{dC_i}{dz}\right) = S_i \qquad i = N_2, H_2, NH_3, Ga \qquad (5.2)$$

$$\varepsilon \cdot p = \rho R^* T \sum_{i=1}^{4} \frac{C_i}{\mu_i} \qquad (5.3)$$

In the gaseous gap:

$$\frac{d}{dz}\left(\rho C_i U - \rho D_i \frac{dC_i}{dz}\right) = Q_i \qquad i = N_2, H_2, NH_3, Ga \qquad (5.4)$$

$$p = \rho R^* T \sum_{i=1}^{4} \frac{C_i}{\mu_i}. \qquad (5.5)$$

Here C_i is the i-th species mass fraction, U is the mixture velocity, ρ is the mixture density, D_i is the i-th species effective diffusion coefficient, S_i is the source term, μ_i is

the molar mass of the *i*-th species, and R^* is the universal gas constant. The source terms S_i is written as

$$S_i = \frac{4}{d_{gr}} \varepsilon \cdot (1-\varepsilon) \cdot G_i \qquad (5.6)$$

where G_i is the mass flux of the *i*-th species per unit granule area.

$$G_i = \alpha_i \cdot \beta_i \cdot m_i \cdot (p_i - p_i^0), \qquad (5.7)$$

where α_i is the *i*-th species sticking coefficient, β_i is the *i*-th species Hertz-Knudsen factor, m_i is the mass of the *i*-th species molecule, p_i and p_i^0 are the *i*-th species partial and thermodynamic pressures, respectively.

The concept of diffusion resistance was employed to derive an expression for the source term Q_i in the gas gap

$$Q_i = \rho D_i \frac{c_i^e - c_i}{R} \qquad (5.8)$$

Here R is the powder source radius.

In order to account for the non-equilibrium processes that go on at the granule surface, a quasi-thermodynamic approach was developed (103-105) based on the following assumptions.

The atoms in the adsorption layer are almost in thermodynamic equilibrium with the granule. This means that the rate of atomic incorporation into the crystal from the adsorption layer and the rate of the reverse process are much higher than their net difference equal to the growth rate of the crystal.

The introduction of sticking/evaporation coefficients was used to account for the kinetic effects at the stage of adsorption-desorption of individual species. In general, these coefficients are functions of temperature and partial pressures of the species.

The one-dimensional model of the species mass transport shows a reasonable agreement between the predicted and measured sublimation rates. Both experimental observations and theoretical predictions show high powder sublimation rates in the H_2-

N_2 ambient, due to the GaN decomposition in the charge bulk. The enrichment of the ambient gas with hydrogen provides a further increase of the sublimation rate.

5.2 Crystal growth experiments

Crystal growth experiments were performed using a seed holder that is held above the boat by means of a seed holder rod that enters through the top flange as shown in the figure 5.5. This seed holder rod is equipped with a rotary mechanism to enable the rotation of the seed. A seed thermocouple that goes through the seed holder rod is used to measure seed holder's temperature as shown. Experimental procedure is the same as that used in the decomposition experiments for the most part except that in case of growth experiments, ammonia is used as the source of nitrogen to grow GaN.

5.2.1 Experimental procedure:

GaN epi on Sapphire seeds of 8.5 mm x 8.5 mm size were diced from 2" GaN epi on sapphire wafers purchased from TDI Inc. The GaN epi layer is 3-6 μ thick and unintentionally doped to a level of 1 x 10^{16} – 1 x 10^{17} cm^{-3}. Samples were cleaned with acetone, and methanol and blown dry with a nitrogen gun before they were loaded. Experimental procedure involved loading the graphite boat with commercial GaN powder and pumping down he system to a foreline pressure below 10^{-2} torr. Once pumped down, the ampoule was backfilled with nitrogen through the two gas inlets and the tank with argon. The temperature was then ramped from room temperature to 800 ^{0}C and stabilized for an hour at this temperature. After the stabilization period, the temperature was ramped to the growth temperature set point as read by both the seed and the source thermocouples. Once the growth temperature was reached, the gas flows were set to the required composition through the right side quartz tube in the schematic. The power to the filaments was turned off at the end of growth time. But, the ammonia flow was retained till the seed temperature was below 600^{0}C to help

maintain the ammonia overpressure on the grown crystal to prevent it from decomposing during the ramp down of temperature.

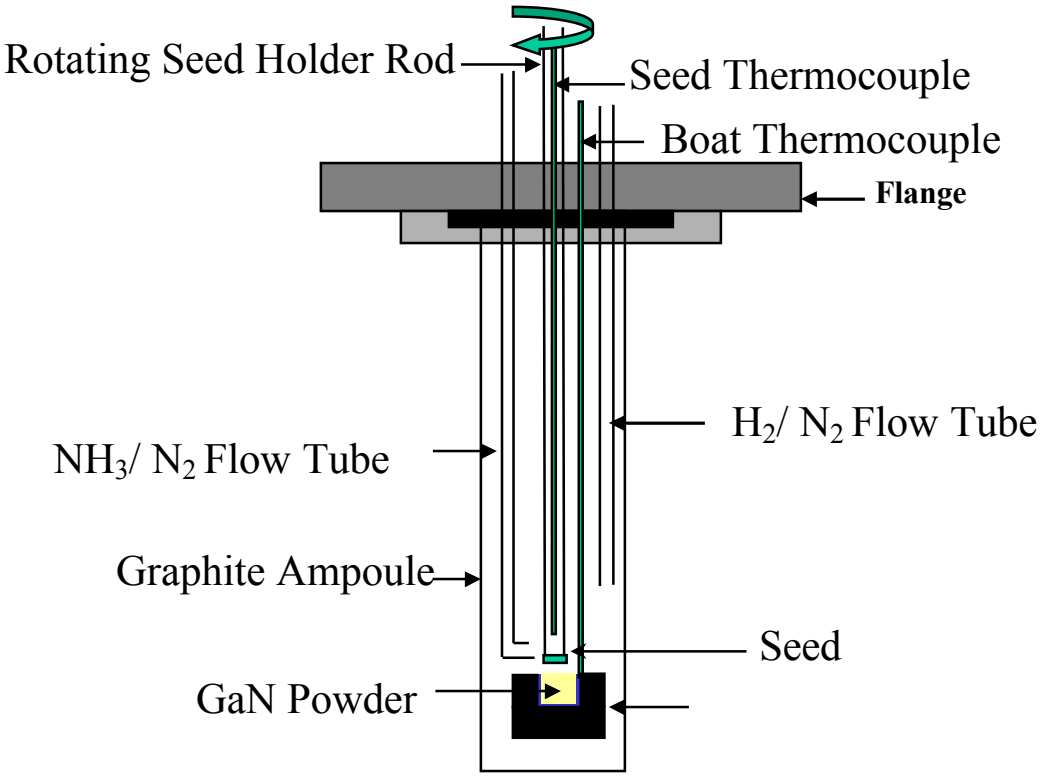

Figure 5.5. GaN crystal growth setup.

5.2.2 Growth results and discussion:

The maximum growth rate observed was 25 μ/hr at a seed temperature of 1095^0C, a boat temperature of 1165^0C with an ammonia flow of 1000 sccm and at a pressure of 600 torr. However, a crust was observed on top of the GaN powder boat

that prevented transport of growth species towards the substrate thus resulting in the observed low growth rates. This crust was observed only when there was ammonia present in the atmosphere and not in the decomposition experiments performed in nitrogen ambient. Moreover, the computations (102) predicted recrystallization of the vapor in the top domains of the source where the supersaturated vapors are deposited on the granule. The recrystallization leads to vapor deceleration near the powder/gap interface.

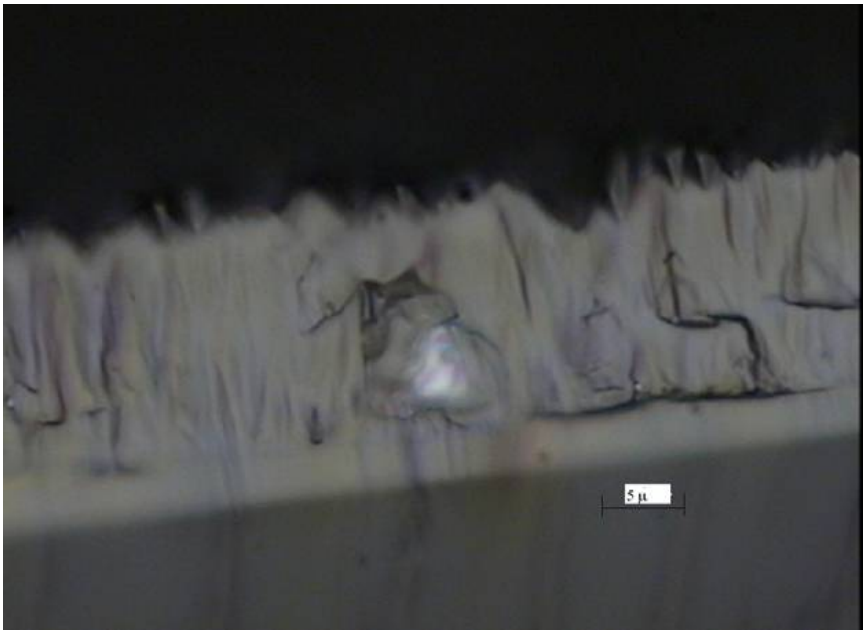

Figure 5.6. Nomarski optical photograph of the cross-section of the sample showing ~25μ/hr growth layer.

5.2.3 Characterization Results:

Figure 5.7. shows a Nomarski optical micrograph of the cross section of the sample that was grown at a seed temperature of 1095^0C, a boat temperature of 1165^0C with an ammonia flow of 1000 sccm and at a pressure of 600 torr. The sapphire substrate,

original GaN epi layer and the GaN layer grown by sublimation could be seen in the cross-section. The GaN layer grown by sublimation is ~ 25 microns thick. A top view of the graphite boat with a crust used in the growth experiments could be seen in Figure 5.7. As mentioned earlier, this crust was observed in the experiments that involved ammonia.

Figure 5.7. Top view of the graphite boat showing the crust formed after the growth experiment in ammonia environment.

Later growth setup designs eliminated the formation of crust and will be discussed in the following chapters.

Chapter 6

GaN Growth using commercial GaN powder – Flow over the powder configuration.

6.1 Design – 2: Prevention of crust formation

First design used for growth experiments, the conventional sublimation sandwich experimental setup, resulted in crust formation on top of the powder during growth experiments in the presence of ammonia as discussed in the previous chapter. So, a new experimental design was conceived to isolate ammonia from the source GaN powder to prevent the formation of the crust. A schematic of the boat and the seed holder alone is shown in Fig. 6.1. It consists of boat that contains the GaN powder and a seed holder [A & D]. The vapor of gallium containing species that is sublimed from GaN powder is transported by nitrogen carrier gas towards the seed where it reacts with ammonia gas that comes from the bottom as shown. The annular boat is made up of hot pressed Boron Nitride. The transition from graphite in the first design to that of hot pressed BN in design II took place because hot pressed BN is cheaper compared to SiC coated graphite and is easily machinable. The graphite parts used have to be SiC coated because of the presence of H_2 in the ampoule. Hydrogen can aggressively react with graphite under typical growth temperatures. A groove deep enough to hold the source material is machined into the BN boat as shown. This boat is suspended from the top of the flange by means of three stainless steel rods. The seed holder rod enters the configuration from the top and the position of the seed can be adjusted by means of a thread arrangement. Hence the distance between the source and the seed can be adjusted by adjusting the seed holder. The whole assembly is

enclosed within a graphite ampoule coated with SiC in order to protect the furnace elements from reacting with the process gases. This coating of SiC prevents etching of graphite by the hydrogen produced from the cracking of ammonia. A hole is drilled into the circumference of the BN boat to hold a thermocouple that measures the temperature of source GaN powder. The seed holder is made up of hot pressed BN and is attached to the bottom end of the Molybdenum seed holder tube. This seed holder rod is driven by a motor and has the ability to rotate up to a speed of 3000 rpm. The temperature of the seed is measured using a thermocouple that goes through the seed holder tube. From the schematic, it can be seen that there are two different flows directed towards the seed. The side flow [B] consists of Nitrogen and it carries the Ga vapor that is obtained from the decomposition of GaN powder. The second flow [C] that is a mixture of ammonia and nitrogen comes from the bottom and is directed vertically upwards towards the substrate. In order to specify the differences between this design and the previous design, in figure 6.1, only the boat portion of the experimental setup is shown instead of showing the entire growth system as in figure 5.5.

6.2 Experimental procedure:

The surfaces of the substrates were cleaned in methanol to get rid of any dust particles on the surface. Initially 5 grams of GaN powder was weighed and filled into the groove to the brim in the BN boat as shown in Fig.6.1. At the beginning of the process, the system was pumped down to < 1 mTorr and back filled to growth pressure [600 Torr] with either nitrogen or argon. Then the temperature of the system was raised slowly to 400^0C and maintained there for 30 minutes to account for any outgassing from the powder as well as the system. Once the foreline pressure was below 10^{-2} Torr, the temperature of the system was ramped up again and stabilized

once again at 800^0 C for 30 more minutes. At this point, the side nitrogen flow was introduced. This was followed by a final ramping of temperature to growth temperature [1155^0C]. Once the system reached the growth temperature, the bottom flow was introduced. At the end of growth, the power to the heating coils was turned down and the bottom flow was turned off. The distance between the seed and the source was kept at a constant value of 3 mm. The temperature of the source was varied from 1000^oC to 1155^oC. The side flow was varied from 320 sccm to 600 sccm. The ammonia flow was varied from 10 sccm to 40sccm keeping the total bottom flow was kept constant at 100 sccm. A typical growth process flow is shown in Fig. 6.2.

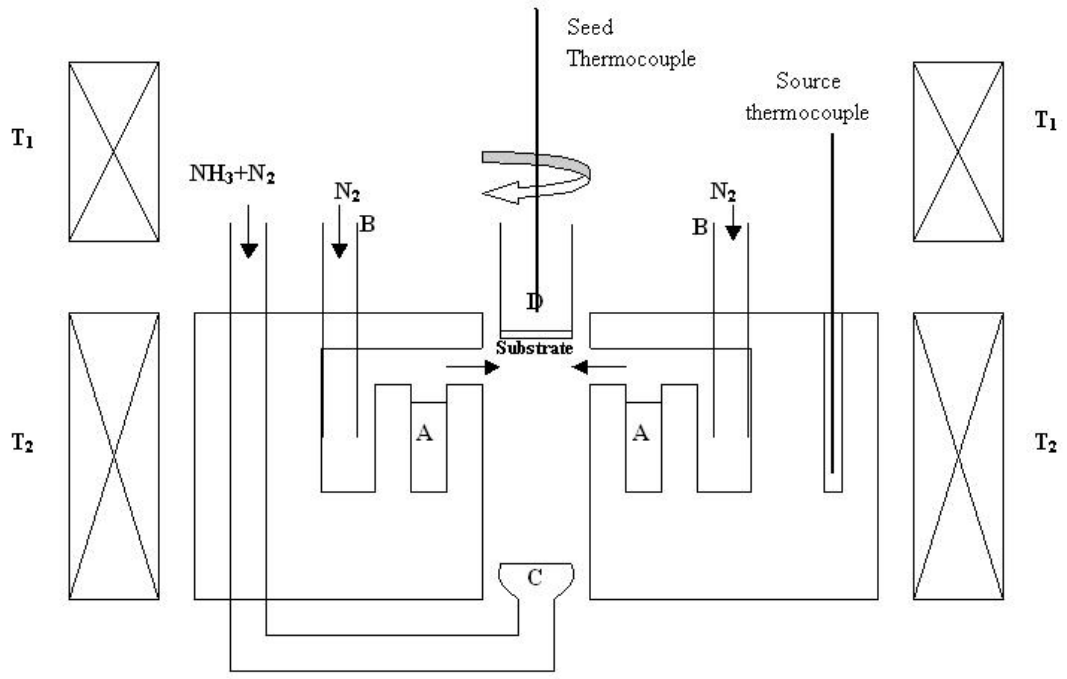

Figure 6.1. GaN growth setup-Design II

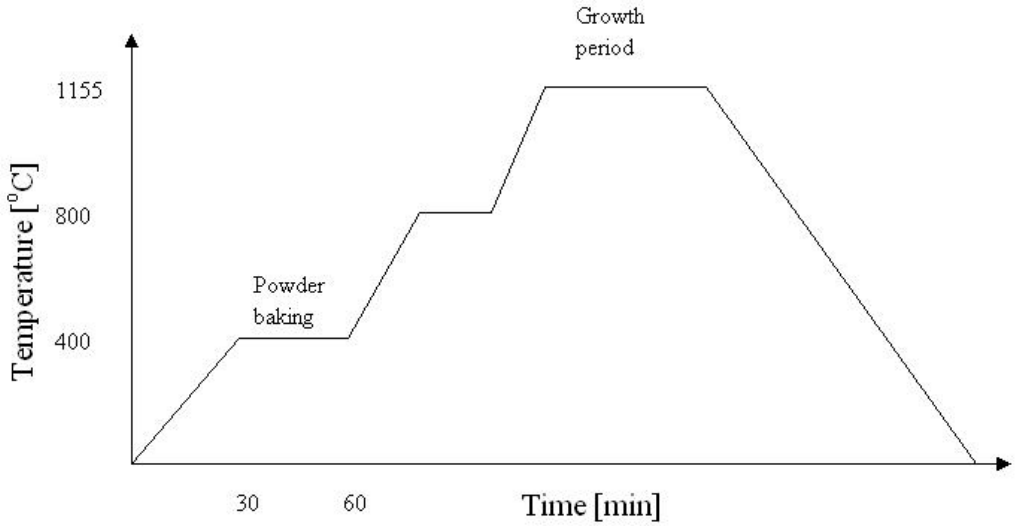

Figure. 6.2. Process flow.

6.3 Results and Discussion:

Crystal growth experiments have been performed for different time periods to obtain the variation of growth rate with respect to time. Fig. 6.3 shows the variation of weight loss from GaN powder with respect to time. These growth runs were performed at a source temperature of 1155^{o}C, seed temperature of 1185^{o}C side flow of 450 sccm [N_2] and a bottom flow of 100 sccm [90 sccm N_2 + 10 sccm NH_3]. It can be observed from the plot that weight loss increases linearly with time for shorter growth runs. But, the rate at which the source looses weight becomes slower as the time progresses. This indicates that the source GaN powder is getting depleted of gallium containing species as the growth progresses. Due to misalignment problems with the current setup, the seed holder was not rotated in the current set of experiments. This resulted in a linearly varying thickness profile of the growth layer, the layer being thicker on the portion of the seed that is closer to side nitrogen flow inlet. Average

thickness of the growth layer was defined as the algebraic mean of thicknesses measured at both ends of the substrate. Average thickness of the growth layer variation with time follows the same variation as the weight loss as shown in Fig. 6.4. From this plot, it can be seen that the differential growth rate at the beginning of the growth run exceeds 200 μ/hr. Ga deposition was observed in the colder region of the growth cell indicating a lower Ga incorporation efficiency. Conditions of growth could be further optimized to increase the growth rate.

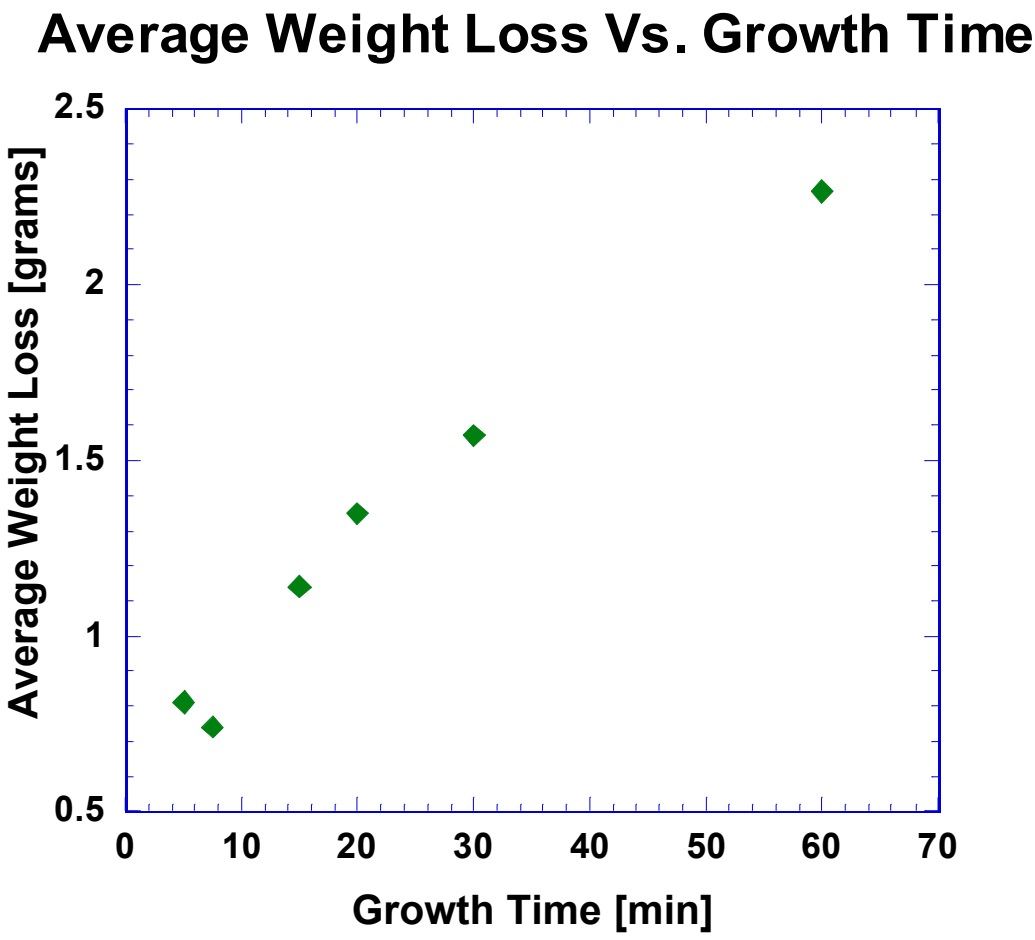

Figure 6.3. Average weight loss Vs. growth time.

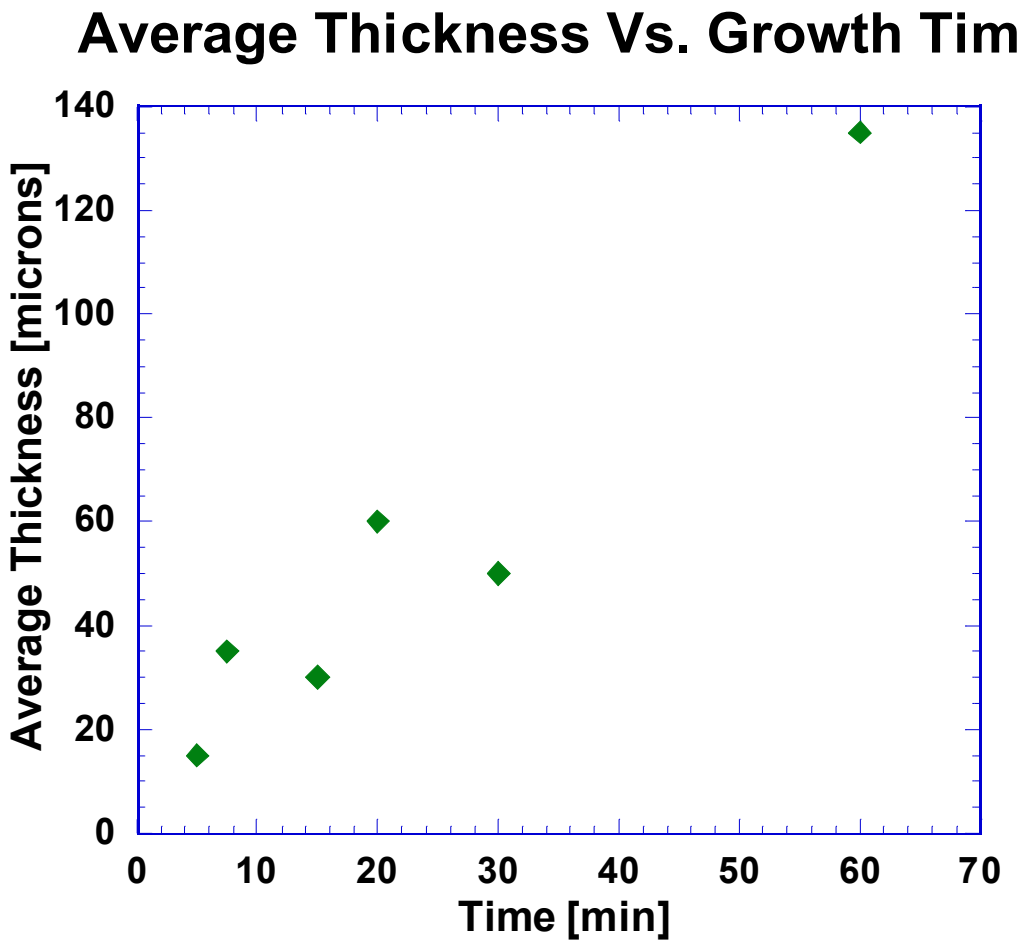

Figure 6.4. Average thickness Vs. time.

The color of the powder changed from yellow before the experiment to dark grayish after the experiment. However, there was no evidence of liquid gallium in the powder after the experiment suggesting congruent evaporation of commercial GaN powder.

6.4 Characterization

A Nomarski optical microscope image of a typical growth sample is shown in Fig. 6.5. Each division in the background corresponds to 1mm. The circular deposition corresponds to the GaN layer that was grown with our experimental setup. Since the seed holder enclosed the corners of the substrate, there is no deposition on the corners of the seed crystal.

As grown GaN layers were characterized using the following apparatus

- LEICA 440 SEM.
- Scintag, Inc. Theta-Theta Diffractometer with Cu K_α ($\lambda = 1.5405$ A^o) radiation.
- Philips High Resolution Diffractometer
- Bede D1 diffractometer system using Cu $K_{\alpha 1}$ radiation .
- ThermoMicroscopes AFM
- Hall effect measurements
- HP 4145 Semiconductor paramter analyzer.
- Stony Brook Synchrotron Topography Station, Beamline X-19C, at the National Synchrotron Light Source, Brookhaven National Laboratory

6.4.1 Structural characterization

Fig. 6.6(a) and Fig. 6.6(b) show the surface view and the cross section view of the layer that was grown at a seed temperature of 1185^{o}C,a source temperature of 1155 ^{o}C with a sideflow of 450 sccm and a bottom flow of 100sccm that is comprised of 10 sccm of ammonia and 90 sccm of nitrogen. Surface view shows number of hexagonal V-defects (15, 106-108) as well as and particles on the surface in some cases.

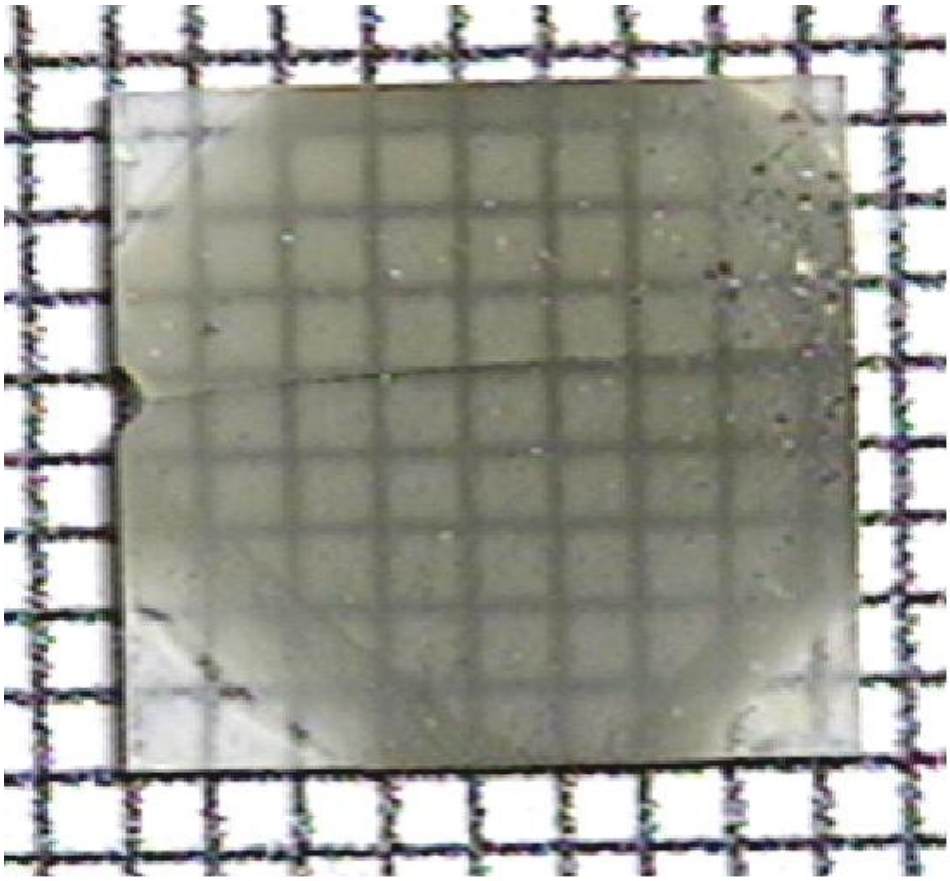

Figure 6.5. Optical microscope image of a typical growth sample

The cross section shows the substrate, the original GaN epi layer and the sublimation grown layer. This layer was 35 μm thick and was grown in 15 minutes was grown at a seed temperature of 1185^{o}C,a source temperature of 1155 ^{o}C with a sideflow of 450 sccm and a bottom flow of 100sccm that is comprised of 10 sccm of ammonia and 90 sccm of nitrogen.

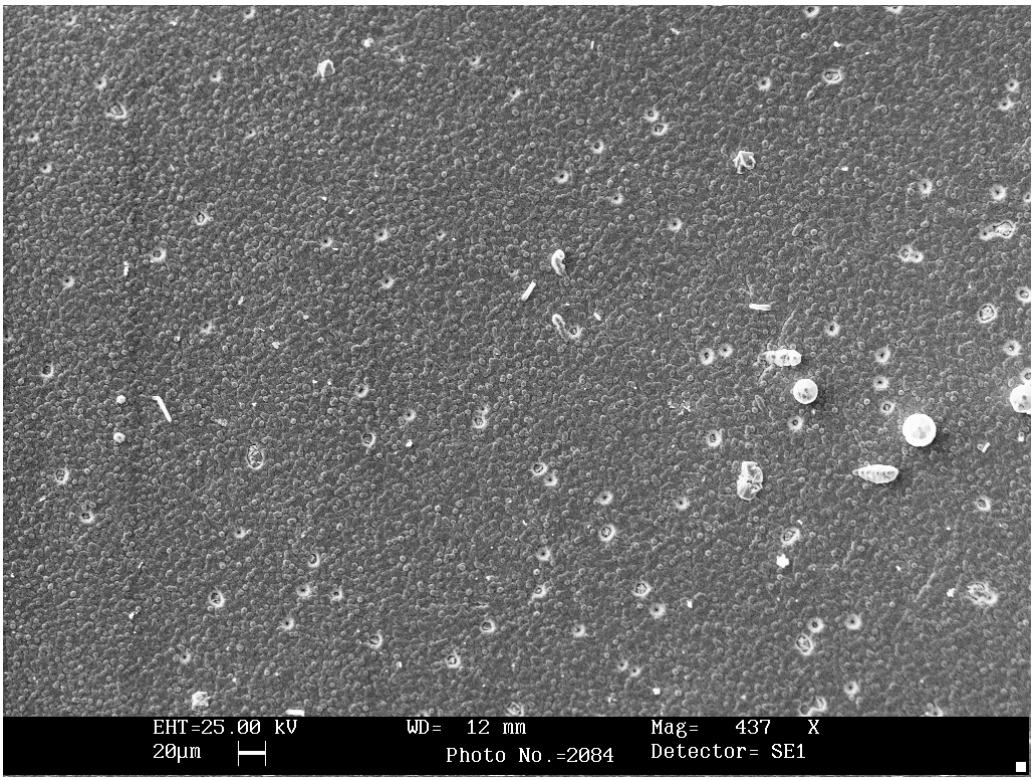

Figure 6.6(a). SEM image of the surface view respectively of a GaN sample grown at ST=1185^{o}C, BT=1155 ^{o}C with a sideflow of 450 sccm and a bottom flow of 100sccm [10%NH_3]

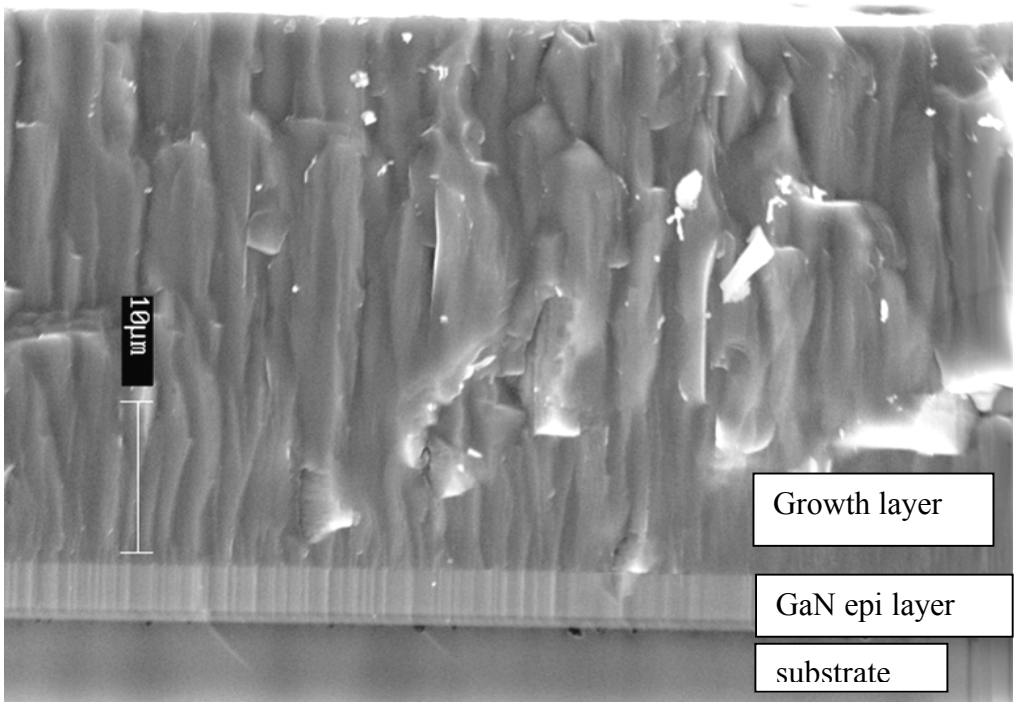

Figure 6.6(b). SEM image of the cross-section views respectively of a GaN sample grown at ST=1185^{o}C, BT=1155 ^{o}C with a sideflow of 450 sccm and a bottom flow of 100sccm [10%NH_3].

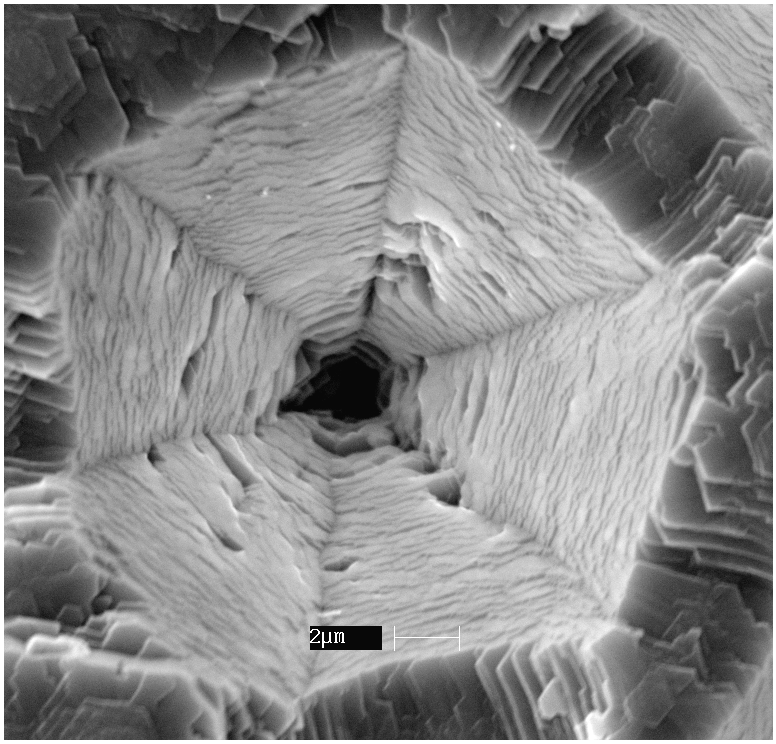

Figure 6.7. Top view of a V-defect.

The top view of a typical V-defects is shown in Fig 6.7. These V-defects are similar to those that are observed in HVPE GaN and GaN/InGaN system(109). They are concave hexagonal pyramids that are encircled by six {1-101} facets. These V-defects will be discussed separately in chapter 9. The grown GaN layers were studied with X-ray diffraction using Cu $K_{\alpha 1}$ radiation. θ–2θ scan in Fig. 6.8 proves that the grown layers are single crystal wurtzite GaN. Sharp peaks corresponding to (0002) and (0004) sets of planes are observed at 34.4^{o} and 72.75 ^{o} respectively. This particular sample was grown at a source temperature of 1155 ^{o} C at a side flow of 450 sccm and a bottom flow of 100 sccm [10sccm ammonia and 90 sccm of nitrogen]. A typical double crystal rocking curve (ω-scan) of the sample is shown in Fig. 6.9(a) and 6.9(b). The figure demonstrates the difference in the crystallographic quality of the seed and the

layer that was grown on top of the seed. Rocking curve measurements of the GaN layer reveal the full width at half-maximum (FWHM) of 5 arc min whereas it is 9 arc min for the substrate. This clearly indicates the superior quality of the bulk grown GaN layer compared to that of the substrate.

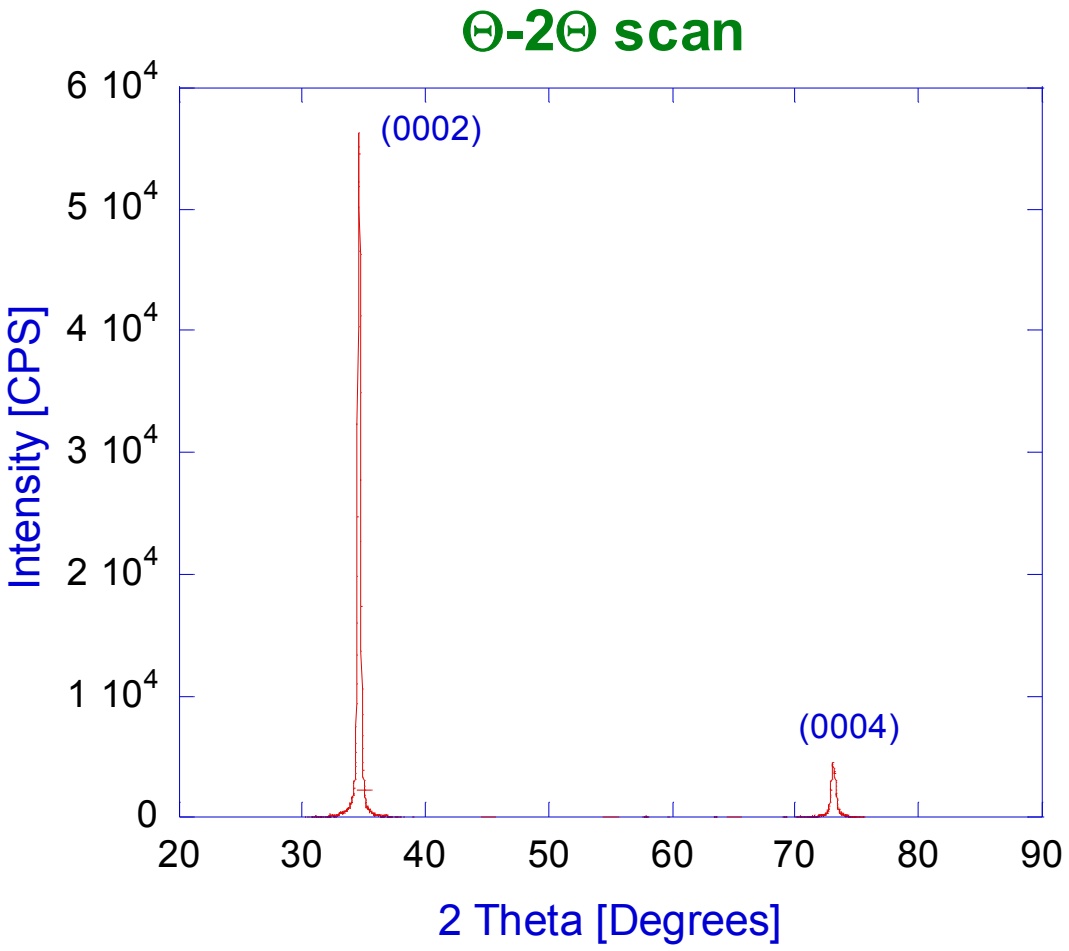

Figure 6.8. Theta-2Theta scan of a GaN layer grown at grown at a source temperature of 1155 ^{o} C at a side flow of 450 sccm and a bottom flow of 100 sccm [10% NH_3]

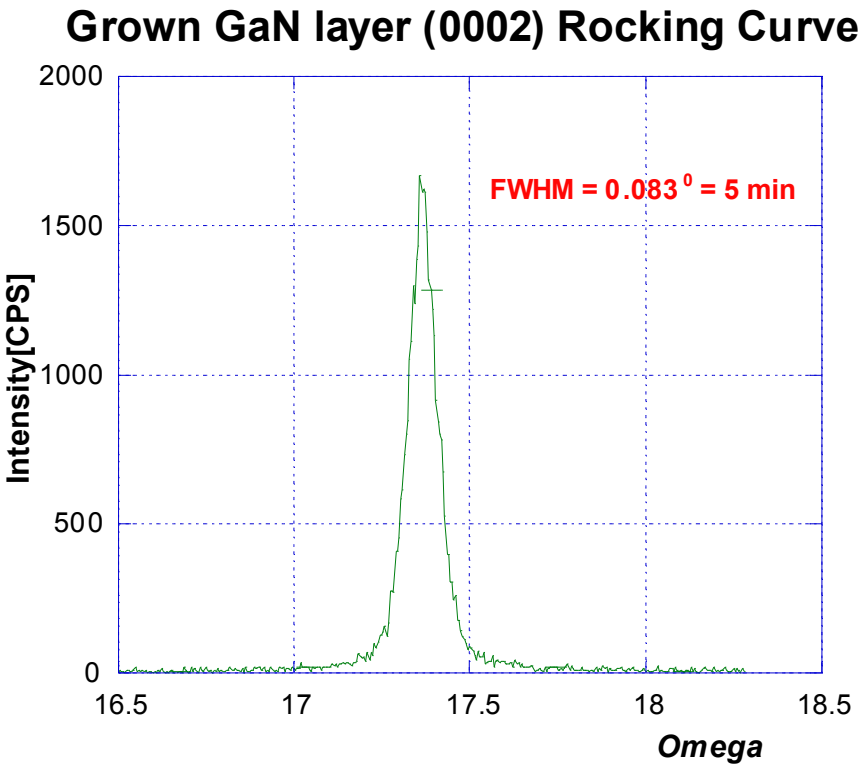

Figure 6.9(a). Double crystal rocking curve of GaN layer grown by sublimation

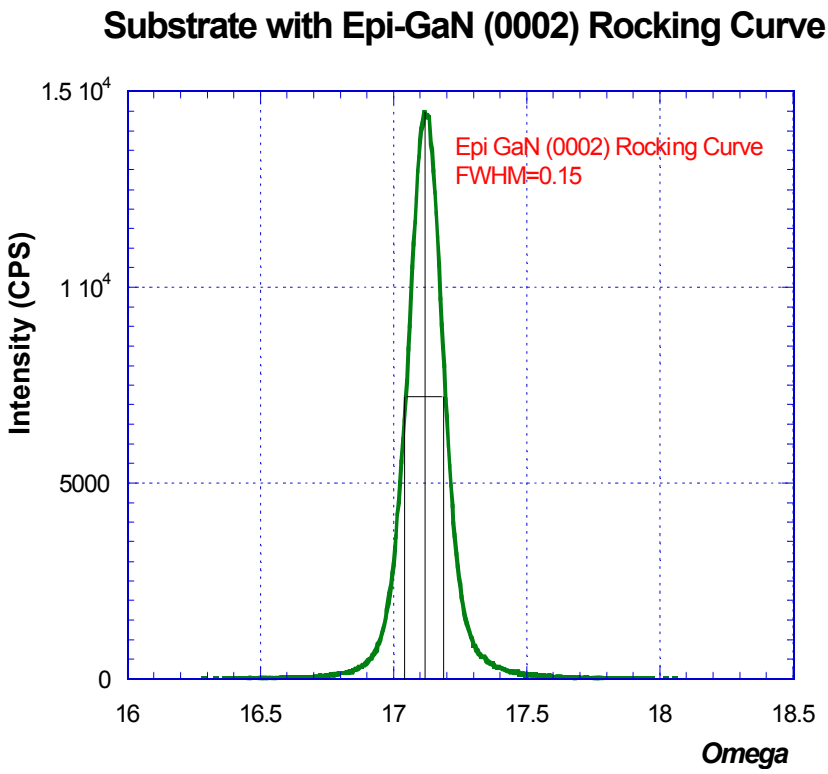

Figure 6.9(b). Double crystal rocking curve of the substrate with GaN epi layer.

Synchrotron white beam x-ray topography (SWBXT) experiments were carried out at the Stony Brook Synchrotron Topography Station, Beamline X-19C, at the National Synchrotron Light Source, Brookhaven National Laboratory by Dr. Balaji Raghothamachar. Reflection geometry was employed. Topographs were recorded on 8" × 10" Kodak Industrex SR-45-1 high-resolution x-ray film. HRTXD measurements were carried out on the highly versatile Bede D1 diffractometer system using Cu $K_{\alpha 1}$ radiation. X-ray beam size at the sample was approximately 0.5mm × 5mm. Triple crystal rocking curves and reciprocal space maps were recorded on this system. Fig.6.10. shows the reciprocal space map of the layer grown at a source temperature of

1155 ^{o} C at a side flow of 450 sccm and a bottom flow of 100 sccm [10 sccm NH_3 +90 sccm of N_2]

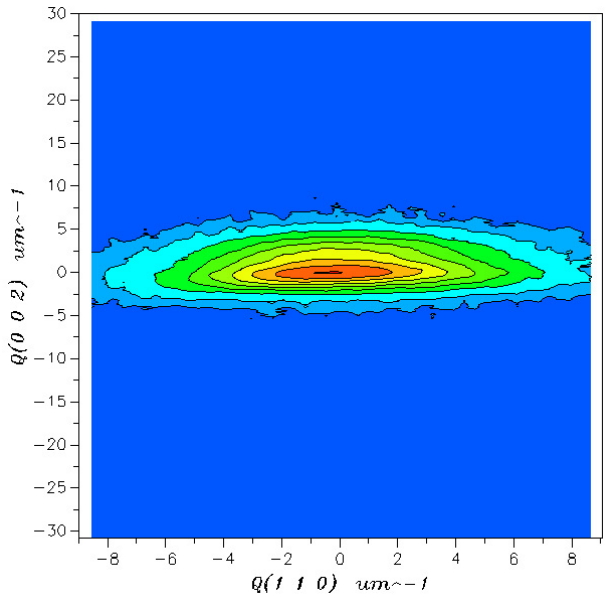

Figure 6.10. Reciprocal space map of a GaN layer grown at a source temperature of 1155 ^{o} C at a side flow of 450 sccm and a bottom flow of 100 sccm [10% NH_3]

The double crystal rocking curve width for this sample was found to be 369 arc min, the triple crystal rocking curve width is only 36" indicating that the broadening of the DCRC is chiefly due to tilts. Fig. 6.11 shows an AFM scan of the surface of the grown layer. The scan area is 3.2 x 3.2 μm. The growth spiral in the figure shows that the dominant growth mode is dislocation-mediated growth. It can be seen from the figure that the step heights do not correspond to the atomic step height indicating step bunching.

6.4.2 Electrical Characterization

Electrical properties of the grown layers were measured by Hall effect measurement technique. Electrical contacts were made using Indium metal and Hall measurements

were carried out using van der Pauw technique using Indium contacts. From the Hall effect measurement, the layer was found to be n-type with a carrier concentration of 6.67 x 10^{18} cm^{-3} and a mobility of 550 cm^2/Vs.

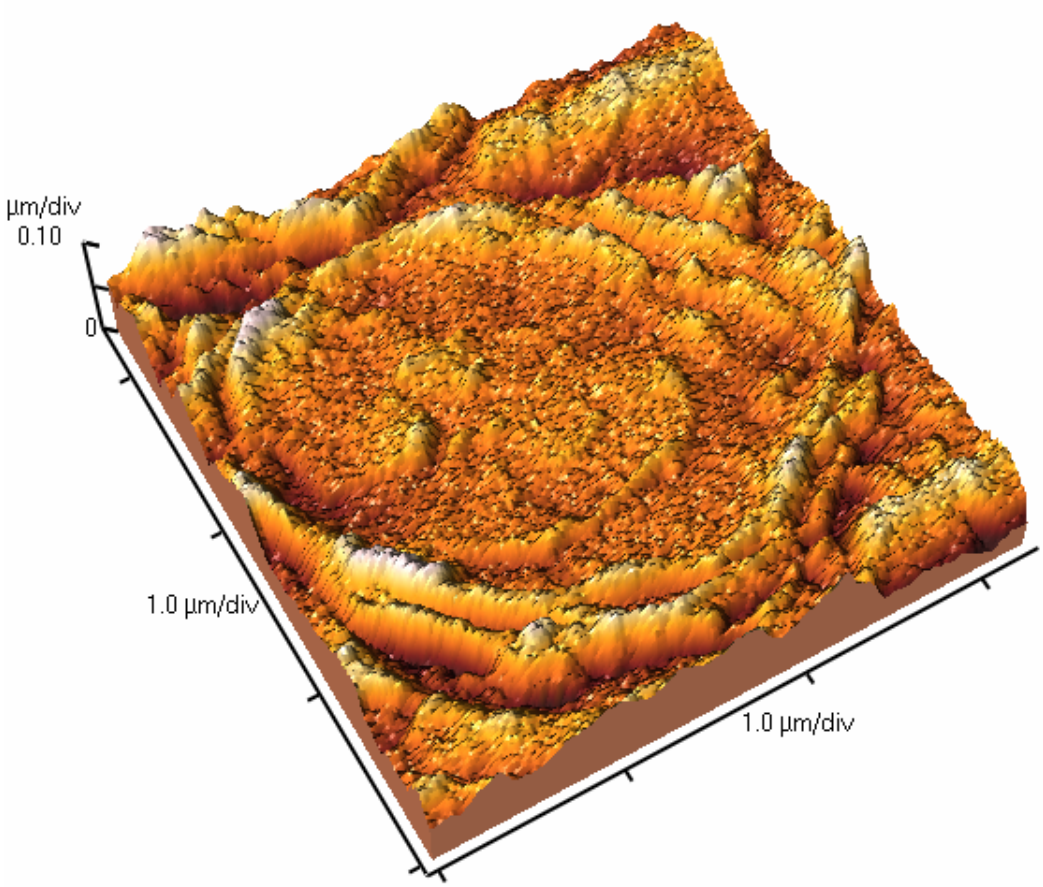

Figure 6.11. AFM scan of the growth spiral indicating the dislocation mediated growth mode.

This high carrier concentration is attributed to the presence of impurities in the source material. Glow discharge mass spectroscopy analysis of the powder [Table 6.1] and SIMS on the grown GaN layer was performed by Evans East. It was found that the C & O concentrations were beyond the measurable range in the powder [>10^{21}/cm^3] and Si concentration was at 58 ppm. The impurity profiling in the growth layer was done

by SIMS and is shown in Fig. 6.12. The impurities in the growth layer could be attributed to the impurities in the source material that is the commercially available GaN powder. Hydrogen in the growth layer was originated from the decomposition of ammonia.

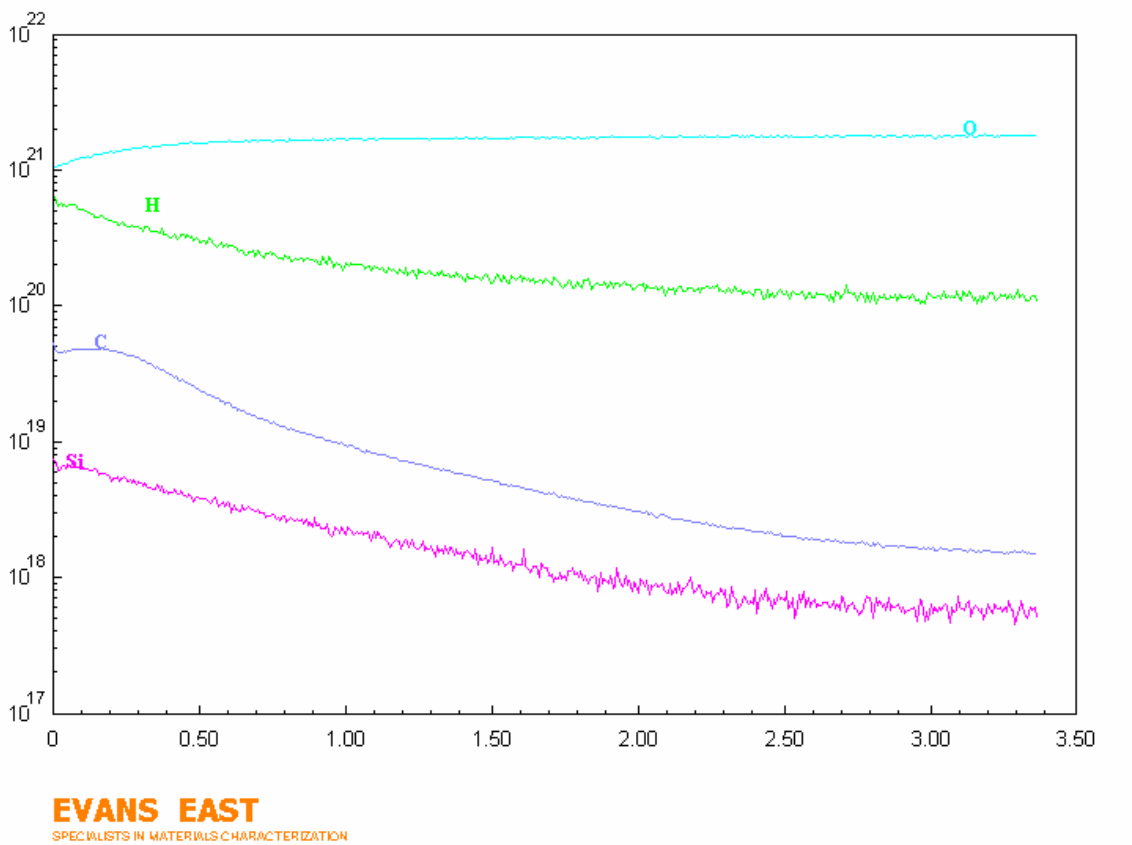

Figure 6.12. SIMS analysis of the sublimation grown GaN layer.

Table 6.1. Glow discharge mass spectroscopy analysis performed on the commercial GaN powder.

Elements	C	O	Al	Si	S	Cl	Cu	Fe	Zn
Commercial GaN Powder [ppm]	-	-	19	58	180	78	16	4.6	2.7

6.5 Simulations:

Modeling analysis of the physical and chemical processes involved in these crystal growth experiments was done by Dr. Yuri Makarov (110). Simulations on the growth setup were carried out using Navier-Stokes equations, Heat and Mass Transfer equations and heterogeneous kinetics for a 2D-asymmetric geometry. Fig. 6.13 shows the temperature and streamlines distribution for the growth setup for the experimental conditions described above. Streamlines indicate that all the gallium that is being decomposed from the source is not available at the substrate. This was experimentally verified since 100 % incorporation efficiencies would have given rise to growth rates of the order of mm/hr corresponding to a weight loss of few grams of GaN powder.
Since commercially available GaN powder has very high level of oxygen impurities, GaN powder decomposition analysis was modeled with oxides of gallium included in the analysis. Simulations were carried out with N_2, Ga, GaO and Ga_2O as the species involved, GaN(s) and Ga_2O_3 as the condensed phases, and heterogeneous chemistry.
Fig. 6.14 shows the weight loss of the source GaN powder as a function of the side nitrogen carrier gas. The three lines predict the weight losses of the source powder assuming three different evaporation mechanisms of Ga, GaO, Ga_2O. From the plot, it can be seen that the weight loss from the experimental data closely matches to the curve corresponding to Ga_2O evaporation.

Since the grown GaN layers have high level of impurities originating mostly from the source GaN powder, efforts to synthesize high purity GaN powder and using it as a source for bulk GaN growth were carried out. From experiments that were conducted later on using high purity GaN powder fabricated in our lab, it was clear that oxygen is aiding in the transport of gallium by forming volatile oxides.

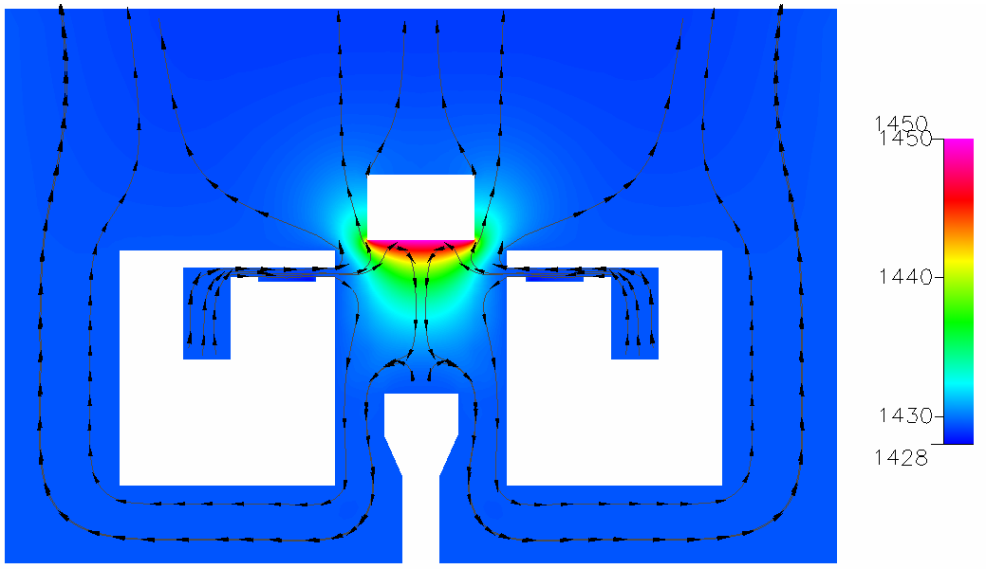

Figure 6.13. Simulated temperature and streamline distribution

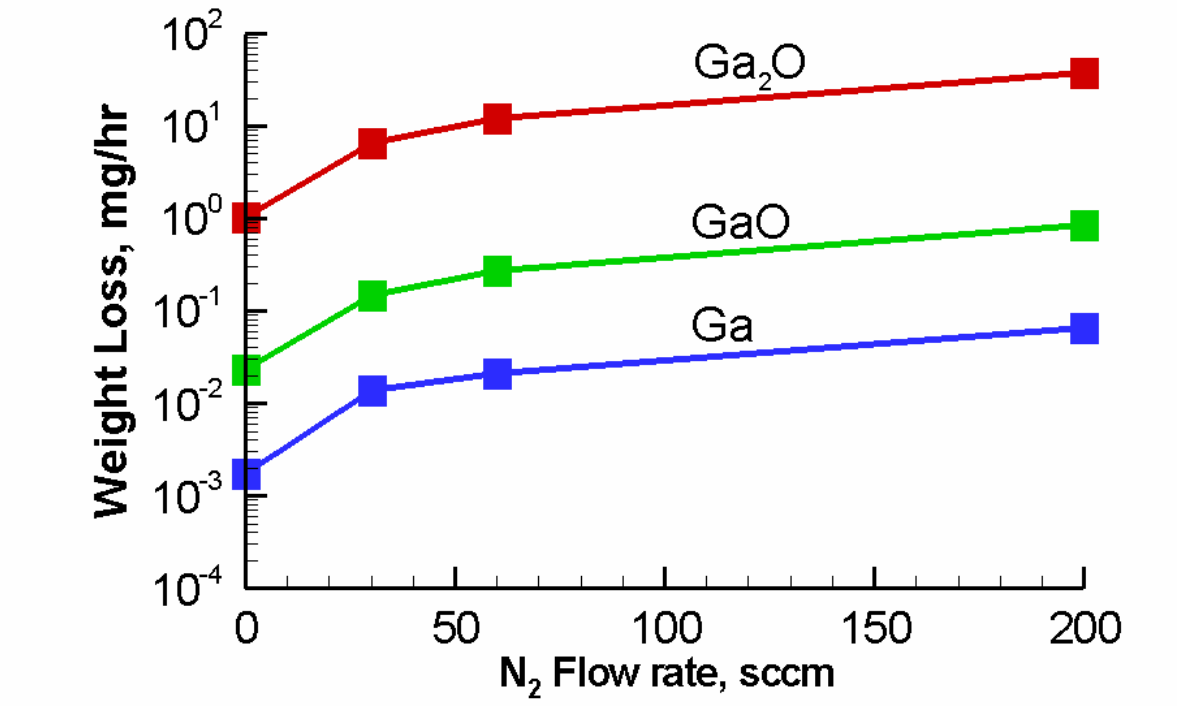

Figure 6.14. Computed evaporation rated of various species

Among the impurities that are present in the commercial GaN powder, oxygen has the ability to form oxides of Gallium that are volatile at reaction temperatures and hence assist in enhanced Gallium transport. This could explain the high Ga transport and hence the high GaN growth rate observed in the experiments performed using commercial GaN powder. This speculation was further confirmed by the simulations performed by Dr. Yuri Makarov at STR, Inc.

To summarize this chapter, a new experimental growth setup was conceived in order to solve the problem of crust formation. Good quality bulk GaN crystals of 8.5 mm x 8.5 mm were prepared by transporting Gallium containing species [presumably Ga_2O] obtained from the decomposition of GaN powder. Growth rates > 200 μm/hr were achieved using this technique. SEM characterization showed that the crosssection of the GaN growth layers to be uniform. The surfaces of the GaN crystals show V-defects and in some cases, particles. AFM scan of the growth layer shows that the growth mode is dislocation mediated spiral growth. Double crystal X-ray diffraction rocking curve FWHM of the grown layer was found to be smaller than that of the substrate indicating the higher quality of growth layers compared to the substrate. Hall Effect measurements, and SIMS show very high impurity levels that can be attributed to the highly contaminated source GaN powder. This was further supported by GDMS of the source GaN powder.

An important observation to note from these experiments is that liquid gallium was not observed in the powder after the growth experiments. The presence of high levels of oxygen in the commercially available GaN powder affects the congruent evaporation of the powder. Gallium transport may be occurring by formation of gallium suboxide [Ga_2O]. Wu et al. (111) succeeded in synthesizing high pure lab made GaN powder with low oxygen content and this powder was used in performing GaN growth experiments. These experiments will be discussed in the next chapter.

Chapter 7

GaN Growth using lab made "pure" GaN powder

7.1 Introduction

In the previous chapter, we have discussed growth of bulk GaN at growth rates higher than 200 μm/hr. But, the SIMS analysis of the growth layer and the GDMS of the commercial GaN powder indicated the presence of oxygen and other impurities at very high levels. Hall effect measurements further supported this data with high carrier concentrations. In order to obtain GaN layers with low doping densities, it was imperative that the GaN powder should contain low impurity levels. Wu(111) developed an in-house process to synthesize high pure GaN powder. This chapter deals with our efforts to grow bulk GaN using this powder as the source material instead of the commercial GaN powder. These efforts include using HCl as the carrier gas instead of nitrogen and using a high pressure process below the triple point of GaN decomposition to suppress liquid gallium formation in the powder. A brief discussion of the decomposition experiments performed by Wu (112) to determine the best source of gallium along with the simulations performed by Dr. Yuri Makarov is also included at the end.

7.2 Experiments

7.2.1 Experimental Setup:

Initial experiments using lab made pure GaN powder as the source were performed in the same experimental setup described in section 6.1 and shown in Fig.6.1. This figure is reproduced in Fig.7.1 for easy reference, this time shown without the thermocouples and the furnace zones surrounding the boat. This is a flow over design since the carrier gas flows over the powder carrying the growth species.

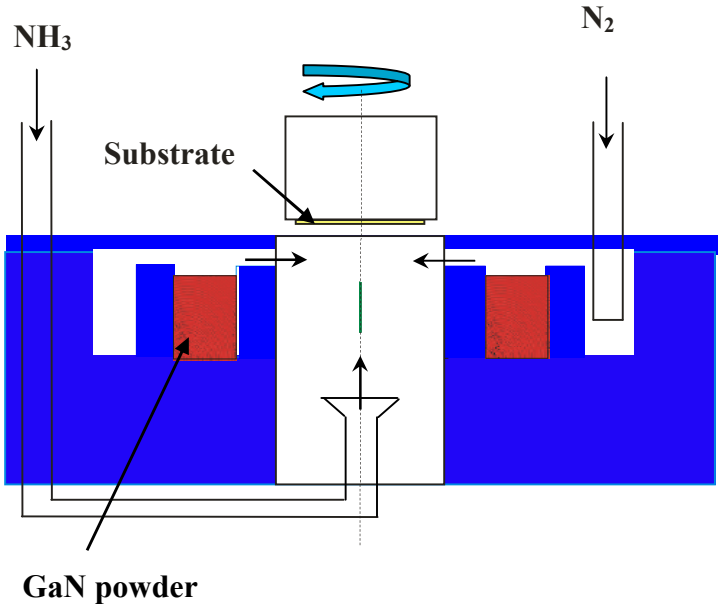

Figure 7.1. Experimental setup to perform GaN growth experiments with pure lab made GaN powder.[Flow over design]

Experimental procedure is similar to the one that was described in section 6.2.

7.2.2 Results and discussion:

Replication of the process flow with commercial GaN powder replaced by that of lab made pure GaN powder did not result in GaN growth. Despite dedicated efforts to

grow GaN using this powder source, these experiments were not successful in growing GaN. Maximum thickness of the growth layers observed was ~ 1μ. At the end of these growth runs, the powder was found to contain liquid gallium. So, at growth temperatures employed (1155^0C), pure GaN powder was undergoing incongruent evaporation leading to the formation of liquid gallium in the powder.

It was clear from these experimental results that oxygen present in the commercial GaN powder was affecting the GaN evaporation kinetics in such a way that it was evaporating congruently without any liquid gallium formation.

7.3 Suppression of liquid gallium in the powder

A study of GaN phase diagram (35) reports that, above a temperature of 844^0C [referred to as triple point temperature from here], GaN undergoes incongruent evaporation at 1 bar pressure. Further, it was also found in the same study that this temperature below which GaN undergoes congruent evaporation could be raised at higher pressures. So, in order to prevent liquid gallium formation in the powder so that gallium is available in the vapor phase for transporting towards the seed to grow bulk GaN, two approaches were followed:

(i) reducing the source temperature to below 844^0C and

(ii) increase the operating pressures so that the triple point temperature below which GaN undergoes congruent evaporation is higher.

This was done because reducing the source temperature to below 844^0C suppresses not only liquid gallium formation in the powder but also reduces the rate of GaN decomposition reaction. It should be remembered that rate of GaN decomposition is an exponential function of temperature and at low temperatures, the rate of GaN decomposition also becomes slower. The experiments performed at 600 Torr and a source temperature below the triple point did not result in growth even though the

liquid formation was suppressed possibly due to the fact that lower source temperatures could not provide enough gallium species in the vapor phase to initiate growth. Following these experiments at 600 Torr, we tried performing high pressure experiments at pressures of 1800 Torr (~2.5 bar). Even though the reactor used in the experiments is a pressure vessel rated for 5 bar, the throttle butterfly valve used in the experiments could not hold the high pressure in the chamber. So, the pressure in these experiments kept varying. Another disadvantage is that at high pressure, the transport of the reactants to the growth surface becomes diffusion limited and this has a deleterious effect on the growth rates. Hence this approach was also not successful in obtaining growth of GaN. During these experiments another modification was made to the growth setup allowing us to flow the carrier gas through the powder rather than over the powder. However, none of the above described approaches were successful in obtaining GaN growth even with the flow through approach. The advantage of flow through approach was that it has a higher collection efficiency of decomposed species as opposed to the flow over the powder configuration. This configuration shown in Fig.7.2. uses a quartz frit at the bottom of the powder.

7.4 Experiments with HCl as the carrier gas.

Another approach to suppress liquid gallium formation in the powder and to successfully transport gallium towards the substrate involved using HCl as the carrier gas. Even though this process is similar to HVPE in the sense that HCl is used as a carrier gas, it is not exactly the same as HVPE because the source used in our experiments was GaN powder and not gallium.

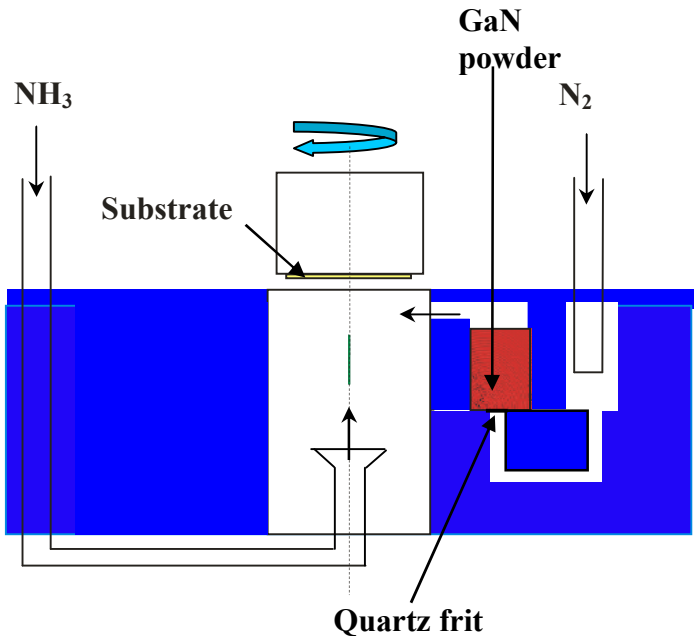

Figure 7.2. Flow through design.

7.4.1 Experimental procedure:

Experimental procedure was the same as that discussed in section 6.2. with the following two modifications.

(i) A flow through design shown in Fig.7.1 was used as opposed to the flow over design shown in Fig.7.2.

(ii) A mixture of HCl and nitrogen was used as the carrier gas instead of nitrogen alone.

For quick reference, the experimental procedure is reproduced in this section as well. The surfaces of the substrates were cleaned in methanol to get rid of any dust particles on the surface. Initially 5 grams of GaN powder is weighed and filled into the groove to the brim in the BN boat as shown in Fig.7.2. At the beginning of the process, the system was pumped down to < 1 mTorr and back filled to growth pressure [600 Torr] with either nitrogen or argon. Then the temperature of the system was raised slowly to

400^0C and maintained there for 30 minutes to account for any outgassing from the powder as well as the system. Once the foreline pressure is down below 10^{-2} Torr, the temperature of the system was ramped up again and stabilized once again at 800^0 C for 30 more minutes. At this point, the side carrier gas flow was introduced. This was followed by a final ramping of temperature to growth temperature[1150^0C]. Once the system reached the growth temperature, the bottom flow was introduced. At the end of growth, the power to the heating coils was turned down and the bottom flow was turned off. The distance between the seed and the source was kept at a constant value of 3 mm. The flow through the powder as mentioned earlier was a mixture of HCl and nitrogen [1.5%HCl]. The ammonia was kept constant at 400 sccm.

7.4.2 Results and discussion:

The use of HCl and nitrogen as the carrier gas enabled us to achieve GaN crystal growth. The thickness of the growth layer was determined to be ~ 35 microns from the depth of focus measurement in the optical microscope. This sample was grown in 1 hr. However, there was a peeling off problem associated with the growth layer. The layer was peeled off during the characterization. Even though most of the layer was peeled off, there was a small area of the growth layer that was still attached to the substrate that enabled us to characterize using SEM. Fig.7.3 shows the SEM image of the surface of the GaN layer grown at the conditions described in the experimental procedure. From the SEM pictures, it could be readily seen that the dominant growth mode again is dislocation mediated spiral growth. Despite the success in growing GaN, there were some disadvantages with this process such as the adhesion between the growth layer and the substrate, and low growth rates compared to that obtained with commercial GaN powder.

7.5 Decomposition experiments:

Simultaneously, a set of decomposition experiments were carried out by Wu(112) in a U shaped quartz tube with commercial GaN powder and lab made GaN powder with nitrogen as the carrier gas. The results of these decomposition experiments are summarized here.

Main experimental observations:

(a) Lab made GaN powder

(i) Weight loss is constant with changing N_2 flow rate.Weight loss increases with temperature. The lab-made powder has only about 1/3 weight loss of commercial powder at the same temperature.

(iii) Weight loss increase is about 5-10 times high compared to that of pure GaN powder. Further, it increases with increasing HCl concentration

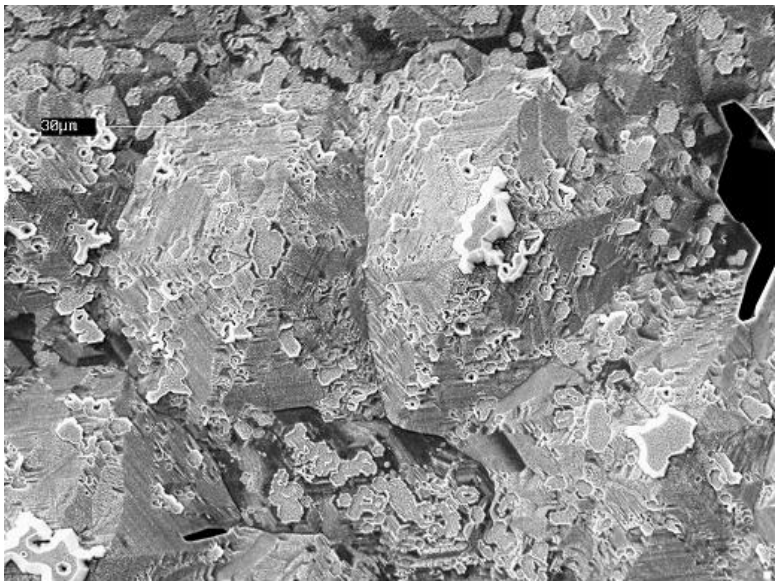

Figure 7.3. SEM image of the GaN layer grown using a mixture of HCl and nitrogen as the carrier gas.

(b) Commercial GaN powder

(i) Weight loss increases with the N_2 flow rate.

(ii) Weight loss increase with temperature.

7.6 Simulations

7.6.1 Simulations of U-tube experiments with nitrogen carrier gas

Modeling of these decomposition experiments was performed by Dr. Yuri Makarov at STR, Inc (113). The underlying assumptions in the modeling the involved species and heterogeneous reaction chemistry for the decomposition experiments and the condensed phases are tabulated in Table 7.1. Based on these assumptions, the simulations have been carried out. The summary of the simulations from the report has been reproduced here.

(i) The total weight loss of the Lab-made powder is weakly dependent on the N_2 flow rate.

(ii) Gallium weight loss of the Lab-made powder is predicted to be proportional to the N_2 flow rate.

(iii) Presence of oxygen in the commercial powder results in increase of the sublimation rate

(iv) Evaporation rates of oxygen-containing species Ga_2O and GaO in commercial powder is much higher than the rate of gallium evaporation in lab made powder

The total weight loss of the commercial powder is visibly dependent on the nitrogen flow rate due to the contribution from Ga_2O species.

7.6.2 Simulation of U-tube experiments using HCl as the carrier gas

Again, modeling of these decomposition experiments was performed by Dr. Yuri Makarov at STR, Inc (113). The underlying assumptions in the modeling the involved

species and heterogeneous reaction chemistry for the decomposition experiments and the condensed phases are tabulated in Table 7.2. Based on these assumptions, the simulations have been carried out. The main points of the report are as follows.

(i) HCl is quickly absorbed in the powder

(ii) If nitrogen gas is mixed with HCl, then the surface of GaN grains is depleted of gallium and the GaN decomposition is suppressed

Table 7.1. Physical and chemical processes included in the modeling of U-tube experiments with N_2 as the carrier gas.

	Lab made powder	Commercial Powder
Species	N_2, Ga	N_2, Ga, GaO, Ga_2O
Condensed phases	GaN (s)	GaN(s) Ga_2O_3(s)
Heterogeneous chemistry	$2Ga+N_2 = 2GaN(s)$	$2Ga+N_2 = 2GaN(s)$ $3GaO = Ga_2O_3(s)+Ga$ $3Ga_2O = 4Ga_2O_3(s)+Ga$

Table 7.2. Physical and chemical processes included in the modeling of U-tube experiments with HCl +N_2 as the carrier gas.

	Lab made powder	Commercial Powder
Species	N_2, GaCl, HCl, H_2	N_2, $GaCl_3$, HCl, H_2
Condensed phases	GaN(s)	GaN(s)
Heterogeneous chemistry	$2GaCl+N_2+H_2 = 2GaN(s)+2HCl$	$2GaN(s)+6HCl=2GaCl_3+N_2+3H_2$

GaN experiments were performed with lab made pure GaN powder and commercial GaN powder as the source material using N_2 & N_2+HCl as the carrier gases, involving various configurations, i.e. flow through and flow over configurations. From these experimental results, it was obvious that oxygen aids in the transport of gallium. The growth rates have dramatically dropped from >200μ/hr to almost zero when lab made GaN powder was used instead of the commercial GaN powder. Even though HCl can act as a transporting agent of gallium, the growth rates

obtained were not as high as in the case of growth experiments involving commercial GaN powder. So, use of oxygen as the transporting agent seems inevitable to enhance the growth rate. However, one has to ensure that the incorporation efficiencies of oxygen into the growth layer are low enough to keep the doping densities at tolerable levels. The next chapter deals with a new experimental setup that emulates the U-tube used in the decomposition experiments and a flow through configuration. A different source material that can produce oxides of gallium for GaN growth also will be discussed as well as the efforts to keep the oxygen concentrations at tolerable levels.

Chapter 8

GaN growth by oxide transport: Flow through powder

8.1. Introduction

In the previous chapter, we discussed the role played by oxygen in gallium transport and its affects on the congruent evaporation of GaN powder by forming oxides of gallium that have high vapor pressure. Since high amount of oxygen can increase the doping levels of the growth layers, one must try to obtain a control over the level of oxygen concentration so that it does not go above the solubility limit of oxygen in GaN and form a precipitate (114). Formation of these oxide precipitates could be deleterious to the crystalline quality. Further, there is a class of thought that connects high concentration of oxygen to the V-defects in the growth layers (115).

Previous studies on using Ga_2O_3 as the source material for growing GaN nanowires (116). Nam et al. (116) used Ga_2O_3 as the source of Ga_2O and then transporting it to make it react with ammonia to form GaN nanowires. Ga_2O transport was used to grow other III-V compound such as GaP and GaAs (117, 118). Since Ga_2O_3 is much cheaper compared to the commercially available GaN powder, the possibility of Ga_2O_3 as the source for the growth of bulk GaN by conventional sublimation technique has already been investigated previously (119). However, the growth rates achieved in this technique were quite low [5 μm/hr]. In the present work, we tried to grow GaN by transporting gallium containing vapor species that were obtained from decomposing oxygen contaminated GaN powder to the seed. In the present discussion,

we present a technique to grow bulk GaN single crystals with growth rates as high as 240 μm/hr.

A new growth setup that employs a flow through configuration was used in the experiments described in this chapter. A mixture of carbon and Ga_2O_3 was used as the source material to produce the required Ga_2O. Later experiments also made use of the commercial GaN powder that was proven to generate Ga_2O as discussed in the previous chapter.

8.2 Experimental setup & procedure

GaN epi on Sapphire seeds of 8.5 mm x 8.5 mm size were diced from 2" wafers purchased from TDI Inc. Bulk GaN samples of 8.5 mm x 8.5 mm size were grown in a 4 zone vertical resistive heating furnace. These GaN epi [3-6 μ thick] on Sapphire wafers were unintentionally doped to a level of 1 x 10^{16} – 1 x 10^{17} cm^{-3}.

The experiments with Ga_2O_3 powder as the source were performed in the setup shown below in Fig. 8.1. It was deigned to increase the growth rate by increasing the Ga_2O transport efficiency to the growing crystal surface and by flowing carrier gas through the source powder as opposed to flowing it over the powder in the previous design. Ga_2O_3 powder that is commercially available [99.999% metals basis] was purchased from Alfa Aesar and mixed with graphite powder in molar ratios ranging from 1:3 to 1:20 as the source of Ga_2O. This mixture was placed at the bottom of the triple legged quartz tube as shown. Similar to the previous growth setups described in section 6.1, two thermocouples were employed to measure temperatures of the powder and the seed. At typical growth temperatures involved in this process, Ga_2O_3 reacts with carbon according to the following reaction to produce Ga_2O (120).

$$Ga_2O_3 + 3C \rightarrow Ga_2O + 3CO \qquad (8.1)$$

The temperature of this assembly was raised to a predetermined seed temperature while nitrogen was injected into the right side inlet of the setup shown. The Ga_2O thus generated was transported by nitrogen towards the substrate where it reacts with the ammonia that is coming from the left side inlet as shown in Fig.8 1 according to the following equation.

$$Ga_2O + 2NH_3 \rightarrow 2GaN + H_2O + H_2 \qquad (8.2)$$

Left side tube from now on is referred to as the ammonia tube whereas the one on the right side as the nitrogen tube. In the experiments performed, the temperature of the seed was varied from 1100°C to 1200°C and the source temperature from 1050^0 C to 1130^0C. The side flow was varied from 200 sccm to 600 sccm. The ammonia flow was varied from 10 sccm to 50sccm keeping the total bottom flow constant at 100 sccm. At the beginning of the process, the system was pumped down to < 1 mTorr and back filled to growth pressure [600 Torr] with either nitrogen or argon. Once the foreline pressure was below 10^{-2} Torr, the temperature of the system was ramped up. During the temperature ramping, nitrogen flow through the powder was maintained at 80 sccm. Once the temperature reaches the growth temperature, nitrogen flow through the powder was brought up to the preset growth flow of nitrogen and the total flow through the ammonia tube was set at 100 sccm. At the end of growth, the power to the heating coils was turned down and the bottom flow was turned off.

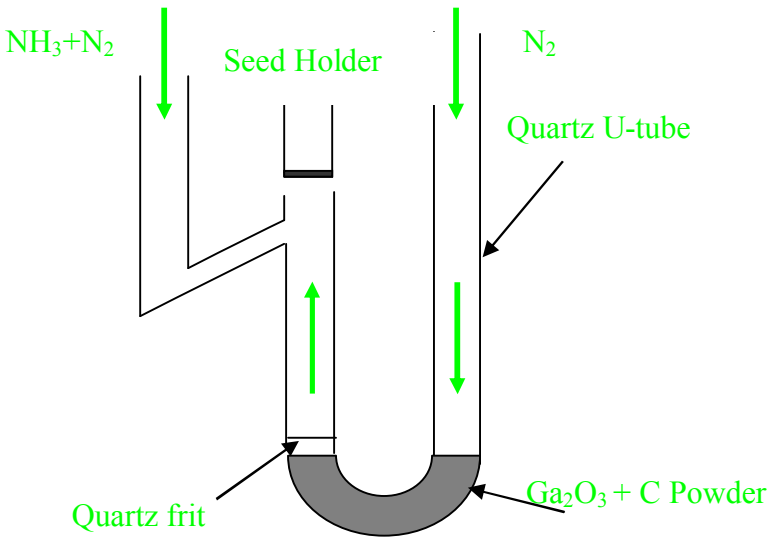

Figure 8.1. Experimental setup.

Other methods of producing Ga_2O species in the vapor phase such as flowing hydrogen or a mixture of hydrogen and nitrogen through the Ga_2O_3 powder could also be used in these experiments. However since hydrogen enhances the decomposition of GaN, using hydrogen to produce Ga_2O could have a deleterious effect on the growth rate of GaN.

The advantages of this design compared to the previous design in section 6.1 are as follows.

- Higher collection efficiency of growth species from the source by carrier gas compared to flow over configuration
- More efficient transport of growth species towards the substrate
- Better control of temperature gradient between source and the seed
- Quartz frit prevents any particles from entering the growth region

A reverse temperature gradient was maintained in the experiments to prevent gas phase nucleation of GaN as the upward traveling stream of Ga_2O mixes with ammonia

before it meets the substrate. Even though no particles were observed after the experiment to augment this argument, no growth was observed in the runs that have both the seed and the source at the same temperature.

8.3 Results & Discussion

GaN layers thus grown were characterized using LEICA 440 SEM, Scintag, Inc. Theta-Theta Diffractometer with Cu K_α ($\lambda = 1.5405$ A^o) radiation and Philips High Resolution Diffractometer. Synchrotron white beam x-ray topography (SWBXT) experiments were carried out at the Stony Brook Synchrotron Topography Station, Beamline X-19C, at the National Synchrotron Light Source, Brookhaven National Laboratory. Reflection geometry was employed. Topographs were recorded on 8" × 10" Kodak Industrex SR-45-1 high-resolution x-ray film. HRTXD measurements were carried out on the highly versatile Bede D1 diffractometer system using Cu $K_{\alpha 1}$ radiation. X-ray beam size at the sample was approximately 0.5mm × 5mm. Triple crystal rocking curves and reciprocal space maps were recorded on this system. Fig. 8.2 shows the cross section view of the layer that was grown at a seed temperature of 1175^{o}C, a source temperature of 1050 ^{o}C with a flow of 400 sccm through the powder and an ammonia tube flow of 100sccm that is comprised of 50 sccm of ammonia and 50 sccm of nitrogen.

Using this technique, it was possible to achieve single crystal GaN with growth rates of ~ 50 μm /hr. Growth experiments performed at a higher seed temperature [1200^{0}C] and higher source temperature [1130^{0}C] resulted in higher growth rates with thickest portions of the sample indicating a growth rate of 100 μm /hr. The grown GaN layers were studied with Scintag, Inc. Theta-Theta Diffractometer using Cu $K_{\alpha 1}$ radiation. θ–2θ scan showed that the grown layers are single crystal wurtzite GaN. This particular sample was grown at a seed temperature of 1155 ^{o} C at a side flow of 400

sccm and a ammonia tube flow of 100 sccm [50sccm ammonia and 50 sccm of nitrogen]. Maximum growth rate observed was ~ 240 mm/hr for a source temperature of 1210 ^{0} C and a seed temperature of 1175 ^{0} C with the same flows as described above.

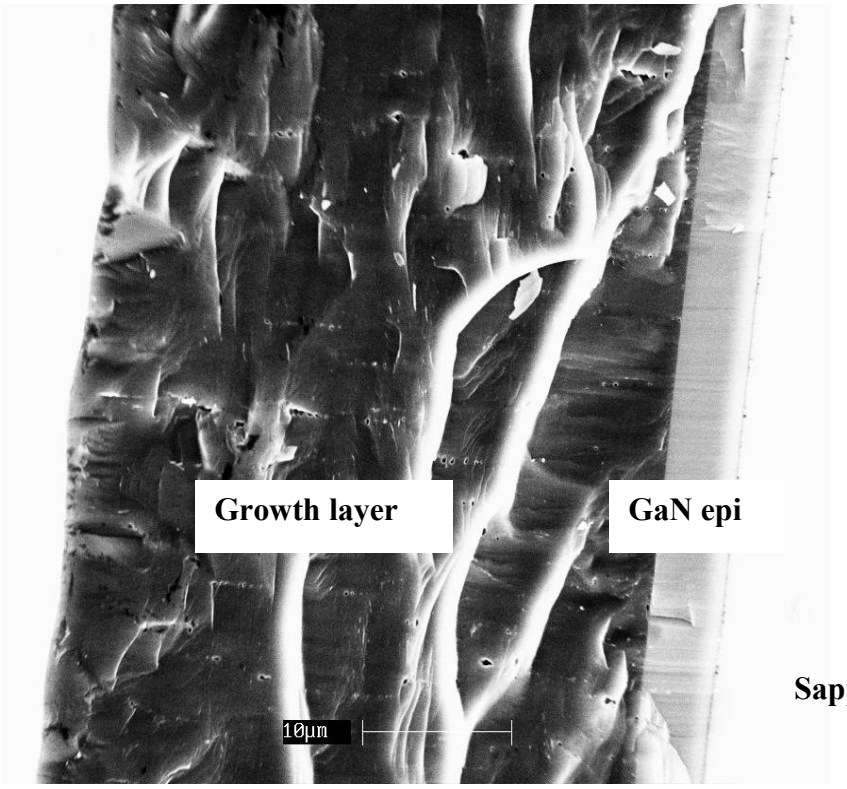

Figure 8.2. SEM image showing cross-section of the sample grown in 15 minutes.

Sample morphologies improved when the source material was changed from the mixture of Ga_2O_3 and carbon to commercial GaN powder as shown in Fig. 8.3(a) & 8.3(b) respectively. Fig. 8.3(a) shows the top view of the sample that contains numerous V-defects. The GaN layer grown using commercial GaN powder shows the dislocation-mediated spirals as the dominant growth mode. Further, the morphologies in both cases were better on the area that is closer to the ammonia inlet. From this observation, one could assume that the ammonia is not distributed uniformly over the

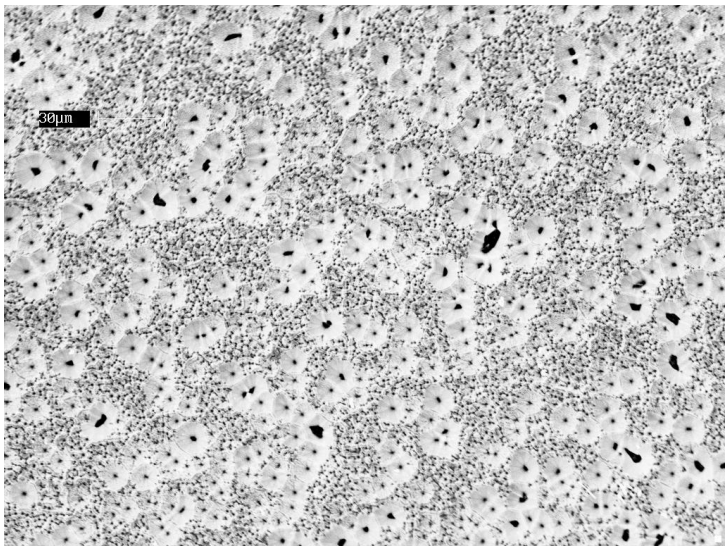

Figure 8.3(a). Surface morphology of the GaN sample grown using a mixture of Ga_2O_3 + C powder as the source at a Seed T=1175^{0}C, Source T=1080^{0}C, side flow=400 sccm & ammonia tube flow =100sccm [50% NH_3]

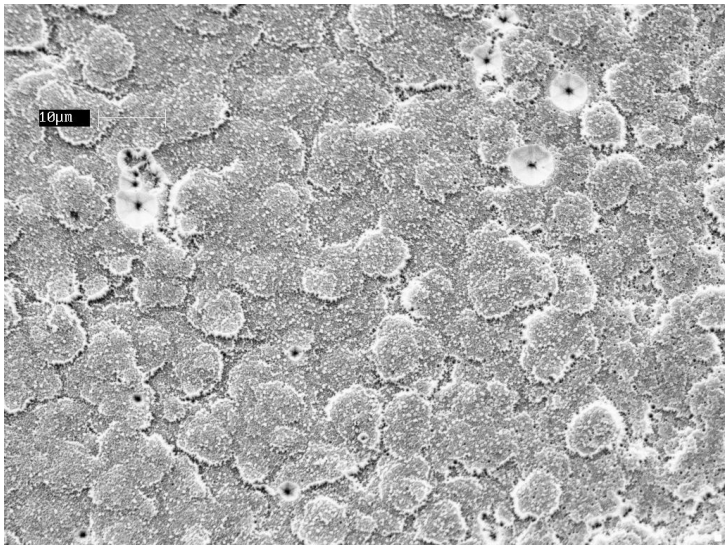

Figure 8.3(b). Surface morphology of the GaN sample grown using commercial GaN powder as the source at a Seed T=1175^{0}C, Source T=1080^{0}C, side flow=400 sccm & ammonia tube flow =100sccm [50% NH_3]

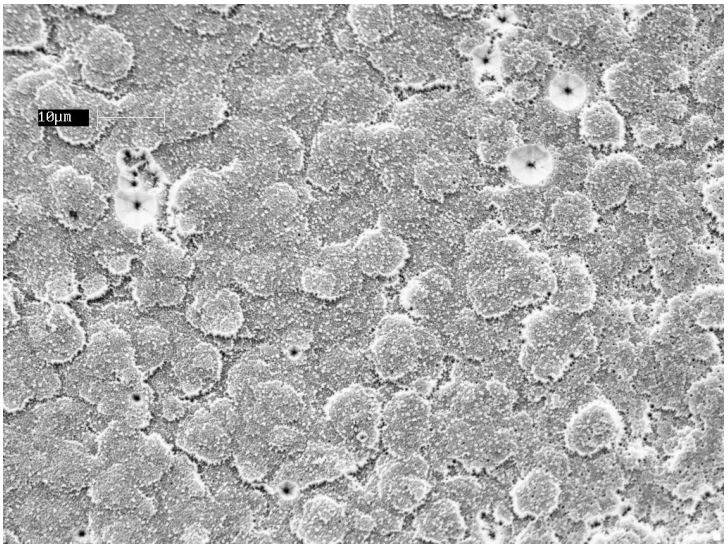

Figure 8.4(a). Surface morphology of the GaN sample grown using commercial GaN powder as the source at a Seed T=1175^{0}C, Source T=1080^{0}C, side flow=400 sccm & ammonia tube flow =100sccm [50% NH_3]

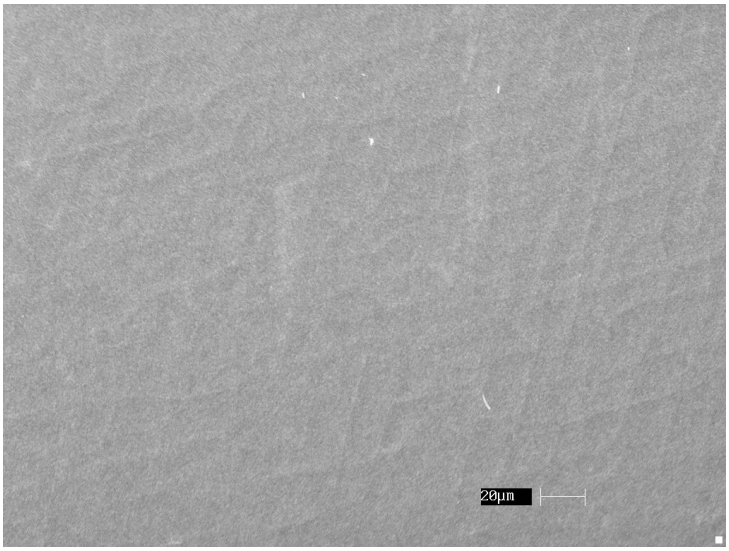

Figure 8.4(b). Surface morphology of the GaN sample grown using commercial GaN powder as the source at a Seed T=1175^{0}C, Source T=1080^{0}C, side flow=200 sccm & ammonia tube flow =100sccm [50% NH_3]

entire surface of the sample during growth process. The regions closer to ammonia inlet appear to have better surface morphologies. This argument was further supported when a region free of V-defects was obtained on the surface of the sample grown at a side flow of 200 sccm as opposed to the sample grown with 400 sccm sideflow.of nitrogen. In both these cases, commercial GaN powder was used as the source material. These experiments were performed at a seed temperature of 1175^0C, source temperature of 1080^0C and total ammonia tube flow of 100 sccm out of which 50 sccm was ammonia. This comparison is shown in Fig. 8.4(a) & 8.4(b).

X-ray topographs recorded in the reflection geometry from the GaN layers are shown in Figure 8.5. Images indicate absence of long range strains and the only distortion is purely geometric caused by recording in the reflection geometry. The topograph images are slightly blurred possibly due to slight tilt between the GaN epilayers and sublimation grown layers that is confirmed from the reciprocal space map. Contrast observed suggests a heterogeneous distribution of dislocations where they are aligned to form dense cellular networks. Overall defect density is higher than $10^6/cm^2$. The reciprocal space map (Figure 8.6) recorded shows two distinct reciprocal lattice spots corresponding to the epilayer and sublimation grown layer. Separation of the two spots both along the vertical (ω-2θ scan) and the horizontal axis (ω scan) indicate the layers are both tilted as well as characterized by different (0002) lattice plane spacings. The average tilt is estimated at about 720" while the lattice parameters differ on an average by about 1.085%. Note that the lattice spacing in the sublimation grown layer is lower than that in the epilayer. The epilayer is likely to be strained due to the mismatch with the sapphire substrate and probably has a larger lattice parameter than bulk GaN (since a(Sapphire) > a(GaN)). The shape of the sublimation layer spot suggests an increasing tilt with increasing deviation from the epilayer lattice plane spacing. This suggests a gradient lattice spacing distribution where the initial sublimation layers are likely to be

aligned with the epilayer (but with different (0002) lattice plane spacing) with increasing tilt as the subsequent sublimation layers relax to the bulk GaN value.

SIMS analysis on the grown GaN layers that were grown at two different temperature profiles was performed by Evans East. The SIMS profiles showed very high concentrations of oxygen, hydrogen, carbon and Silicon. An oxygen concentration of 6×10^{20} /cm^2 was observed in the sample that was grown at a seed temperature of 1150^0C and a source temperature of 1050^0C where as higher oxygen concentration of 3.3×10^{21}/cm^2 was measured on the sample that was grown at a seed temperature of 1200^0C and a source temperature of 1110^0C. These concentrations were measured at a depth of 3μm from the surface. High carbon and hydrogen concentrations in the growth layer could be due to the carbon in the source powder mixture (Ga_2O_3 + C) and ammonia respectively. The source of aluminum possibly is the powder or the quartz experimental set up that we were using. However, the source of aluminum is not precisely determined. Table 8.1. shows the concentrations of impurities in the sample that was grown at a seed temperature of 1150^0C and a source temperature of 1050^0C.

Table 8.1. SIMS analysis of the GaN layer grown at seed temperature = 1150^0C and source temperature = 1050^0C.

Impurity	Oxygen	Silicon	Carbon	Hydrogen	Aluminum
Concentration [/cm^3]	6×10^{20}	2.2×10^{19}	1.45×10^{18}	1.3×10^{19}	2.4×10^{19}

4

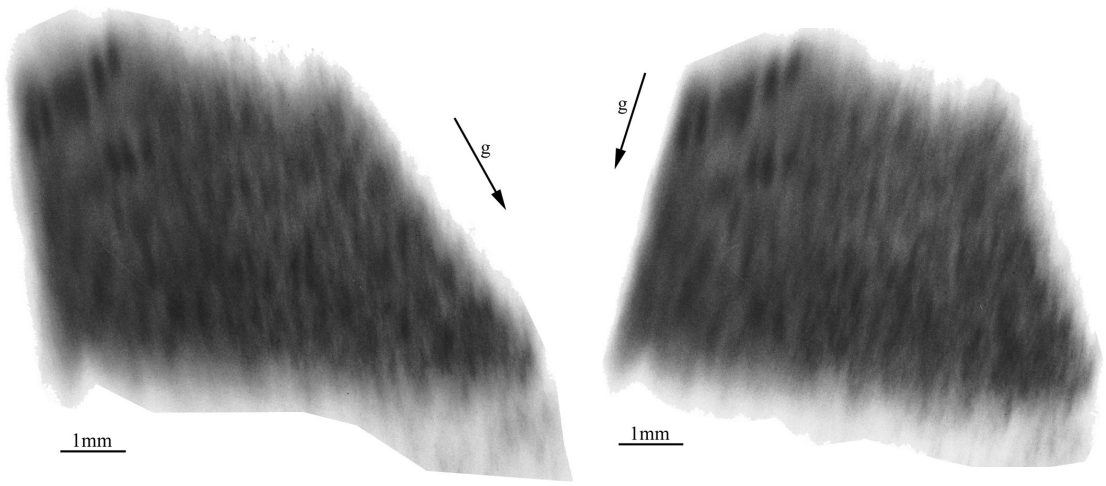

Figure 8.5. Reflection topographs (a) g = $01\bar{1}5$, λ = 0.74Å; (b) g = $10\bar{1}5$, λ = 0.74Å recorded from the sublimation grown and epi grown GaN layers. Slight blurring is possibly due to tilt between the two types of layers.

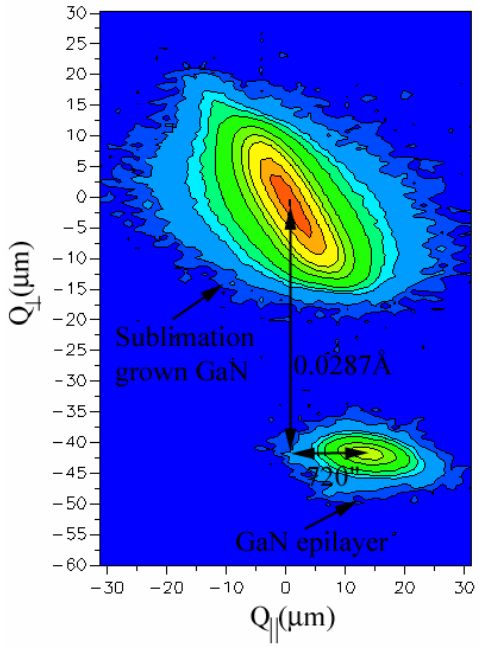

Figure 8.6. 0002 reciprocal space map recorded showing lattice spots corresponding to the epilayer and sublimation grown layer.

Good quality bulk GaN crystals of dimensions 8.5 mm x 8.5 mm x 25 μm were prepared by transporting Ga_2O vapor obtained from a mixture of commercially

available Ga_2O_3 and graphite powder. Commercial GaN powder was also used as the source material in later experiments. Growth rates approaching 240 μm /hr were achieved using this technique. Surface morphologies were observed to be better when commercial GaN powder was used as the source instead of the mixture of Ga_2O_3 + C powder. The regions on the sample that are closer to the ammonia inlet exhibited better morphologies indicating that ammonia was not being distributed all over the sample surface uniformly and proved the necessity of availability of ammonia to obtain good morphologies. Double crystal X-ray diffraction proved that the grown layers were single crystal wurtzite GaN. Reciprocal space map analysis of the layer showed that the double crystal rocking curves of ~342" and a triple crystal rocking curve with of 142". SIMS analysis performed on these samples showed that the oxygen incorporation was higher at high growth temperatures.

From the FWHM of double crystal rocking curve widths, it could be seen that the crystalline quality of these GaN layers is comparable to that of the GaN layers grown using the design in section 6.1. Moreover, this design also demonstrated growth of GaN layers that do not have any V-defects. Also, this design demonstrated growth rates that are more than those demonstrated by the previous design. The various parameters could be optimized further to improve crystalline quality and completely eliminate V-defects on the growth layer simultaneously achieving high growth rates. The next chapter deals with the V-defects observed on the GaN growth layers grown in flow over configuration [Fig. 6.1]. These V-defects are of important concern because they reduce the effective area available for fabricating devices.

Chapter 9

Effect of growth time on the size of V-defects

9.1 Introduction:

This chapter is dedicated to the study of V-defects observed in GaN layers grown by oxide vapor transport using the flow over configuration in Fig. 6.1.This discussion of V-defects could not have been more appropriate in the present context of bulk GaN samples grown by oxide vapor transport. The previous study on V-defects (115), and the observation of the same in almost all the samples that were grown by oxide vapor transport make this discussion all the more important. The association of V-defects to that of the oxygen content in the films by Korotkov et al. makes this discussion of paramount importance because apart from these defects, oxide vapor transport is a very good candidate for commercialization of bulk GaN growth technology. The following paragraph summarizes the previous studies on V-defects.

The heteroepitaxial growth of GaN leads to high densities of threading dislocations (TD) in device structures. Also, the interface roughness in group III-nitrides is of considerable importance as it could severely affect the mobility of two-dimensional electron gas in AlGaN/GaN based high electron mobility transistors (14, 15). In addition, several defects such as stacking faults, inversion domain boundaries, and nanopipes are observed in GaN epitaxial layers (16). Threading dislocations observed were reported to be the origin of the so-called V-defects. It has been shown

that the V-defects in InGaN/GaN MQW are sources of leakage current in GaN based LEDs (15). There have been recent studies on nucleation and growth of V-defects in InGaN/GaN system as well as in GaN system (106, 108, 109, 121-130). Liliental-Weber et al. (128) suggested that the impurities may inhibit crystal growth in certain areas leading to the nucleation of V-defects. Northrup et al. (130) attributed V-defects to release of strain energy of a threading screw dislocation. The sustained growth of V-defects was explained from a kinetic perspective by Sharma et al. and Wu et al. (108, 109) in InGaN/GaN system and this concept was extended to GaN by Miraglia et al. (107). In the present study, the effect of the growth time on the size of V-defects in bulk GaN layers grown by vapor transport has been investigated. Single crystal GaN layers were produced at growth rates of ~200 μm /hr. So, this technique is promising for producing bulk GaN. Since the presence of V-defects reduces the effective substrate area, the knowledge of their formation is essential to successfully eliminate them.

9.2 Experimental procedure

The GaN epi seeds on sapphire substrates were obtained from TDI Inc. The GaN epi layer thicknesses were ~3-6 μ and were unintentionally doped to a level of 1 x 10^{16} – 1 x 10^{17} cm^{-3}. Pieces of 8.5 mm x 8.5 mm size were diced from 5 cm wafers. The surfaces of the substrates were cleaned in methanol. GaN layers were grown on the seeds in a vertical resistively heated reactor. This technique and the design of the growth setup were discussed in section 6.1. Commercial GaN powder obtained from Alfa Aesar [99.99% pure metals basis] was used as the source of gallium containing species. A side flow consisted of nitrogen where as the bottom flow contained a

mixture of nitrogen and ammonia. The temperature of the source was varied from 1000^{o}C to 1155^{o}C. The side flow was varied from 320 sccm to 600 sccm. The total bottom flow was 100 sccm, out of which 90 sccm was nitrogen and 10 sccm was ammonia. The distance between the substrate and the source was maintained at ~ 3 mm.

At the beginning of the process, the system was pumped down to < 1 mTorr and back filled to growth pressure [600 Torr] with either nitrogen or argon. Then the temperature of the system was raised slowly to 400^{0}C and maintained there for 30 minutes to account for any outgassing from the powder as well as the system. Once the foreline pressure was down below 10^{-2} Torr, the temperature of the system was ramped up again and stabilized once again at 800^{0} C for 30 additional minutes. At this point, the side nitrogen flow was introduced. This was followed by a final ramping of temperature up to growth temperature [1155^{0}C]. Once the system reached the growth temperature, the bottom flow was introduced. At the end of growth, the power to the heating coils was turned down and the bottom flow was turned off. These growth experiments were performed for 5, 7.5, 15, 30, and 60 minutes.

9.3 Characterization results:

Fig. 9.1(a) shows the surface of the GaN layer grown at a seed temperature of 1185^{0}C and a source temperature of 1155^{0}C. The side flow of nitrogen carrier gas was maintained at 450 sccm. Top view and cross sectional view of a typical V-defect are shown in Fig. 9.1(b) and Fig 9.1(c), respectively. From the cross section in Fig 9.1 (c), the angle between the top surface and the slanted face was measured and the six facets of the V-defect were determined to belong to {1-10-1} family of planes. The size of

the V-defect was defined as the side of the hexagon that is formed. The average size of the V-defect was taken as the median of the numerous V-defect distributions calculated from different areas of the sample. Figures 9.2 & 9.3 show respectively a histogram of the V-defect distribution and the variation of V-defect size with growth time. As can be seen from Fig. 9.2, the distribution of V-defect size peaks for $8\mu < a < 10\mu$, where a is the size of the V-defect. Figure 9.3 shows that the V-defect size increases with thickness of the sample. This is in accord with the observation made by Lin et al. (131) on GaN layers grown by HVPE. They suggested that {1-10-1} facets have more stability as compared to (0001) facets because of the higher number of broken bonds (3) present on (0001) facets compared to that of {1-10-1} that has two broken bonds (131). This implies that the growth rate of {1-10-1} facets is lower in comparison to that of (0001) planes.

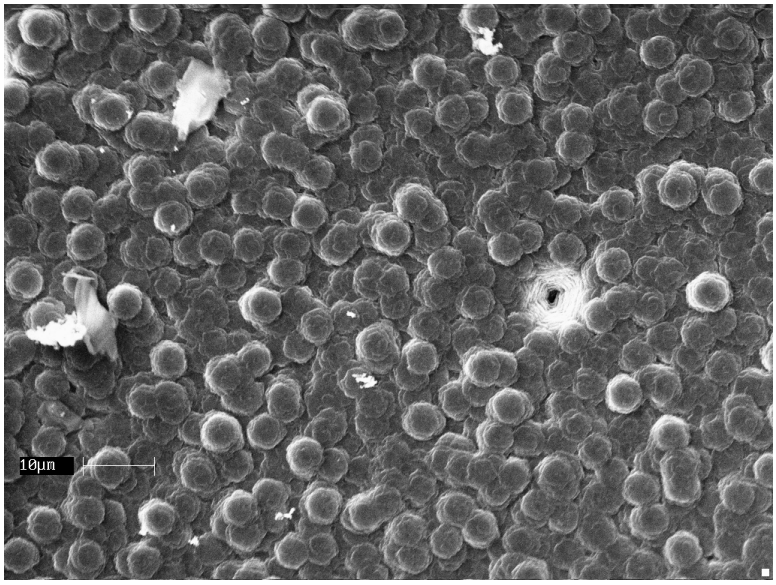

Figure 9.1(a). Surface Morphology

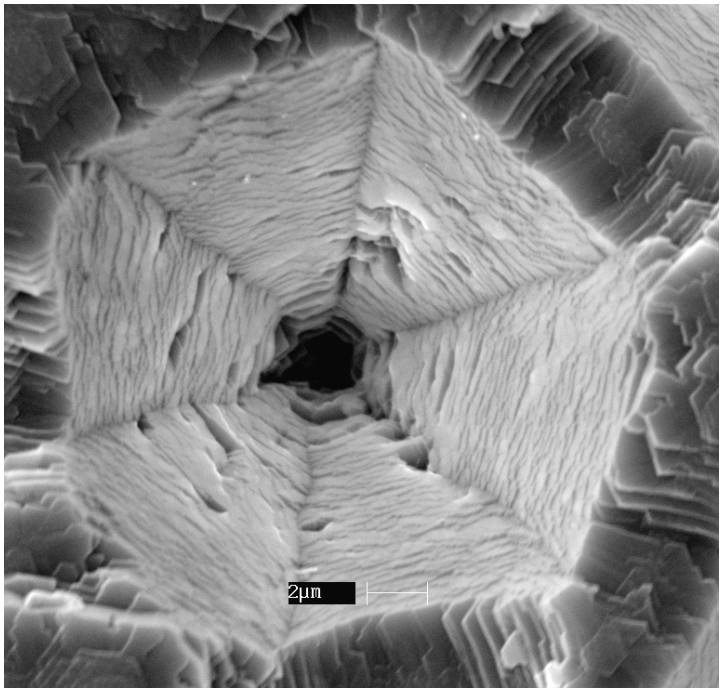

Figure 9.1(b). Top view of the V-defect

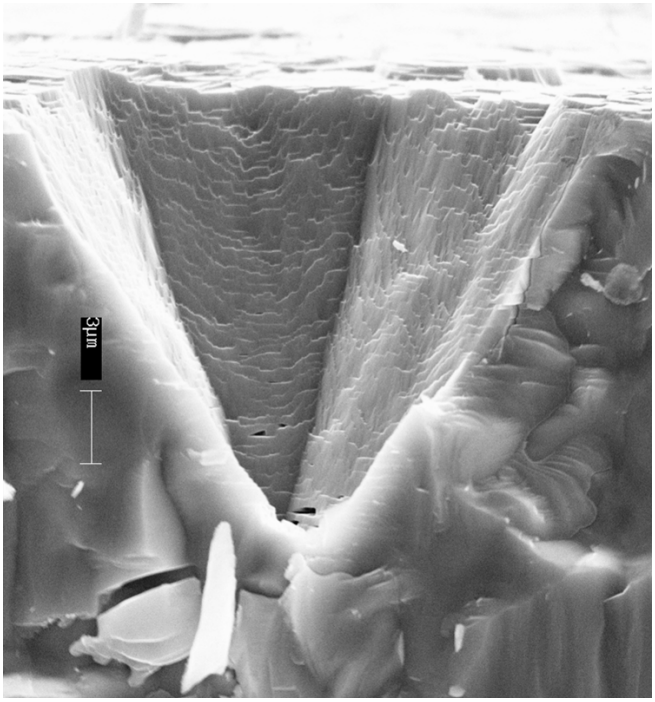

Figure 9.1(c). Cross section of the V-defect

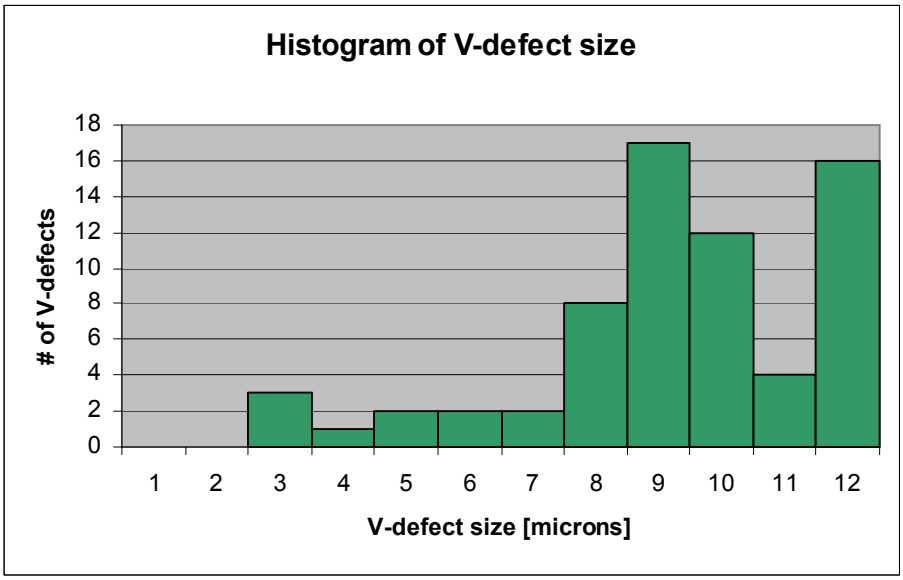

Figure 9.2. Histogram of V-defect size

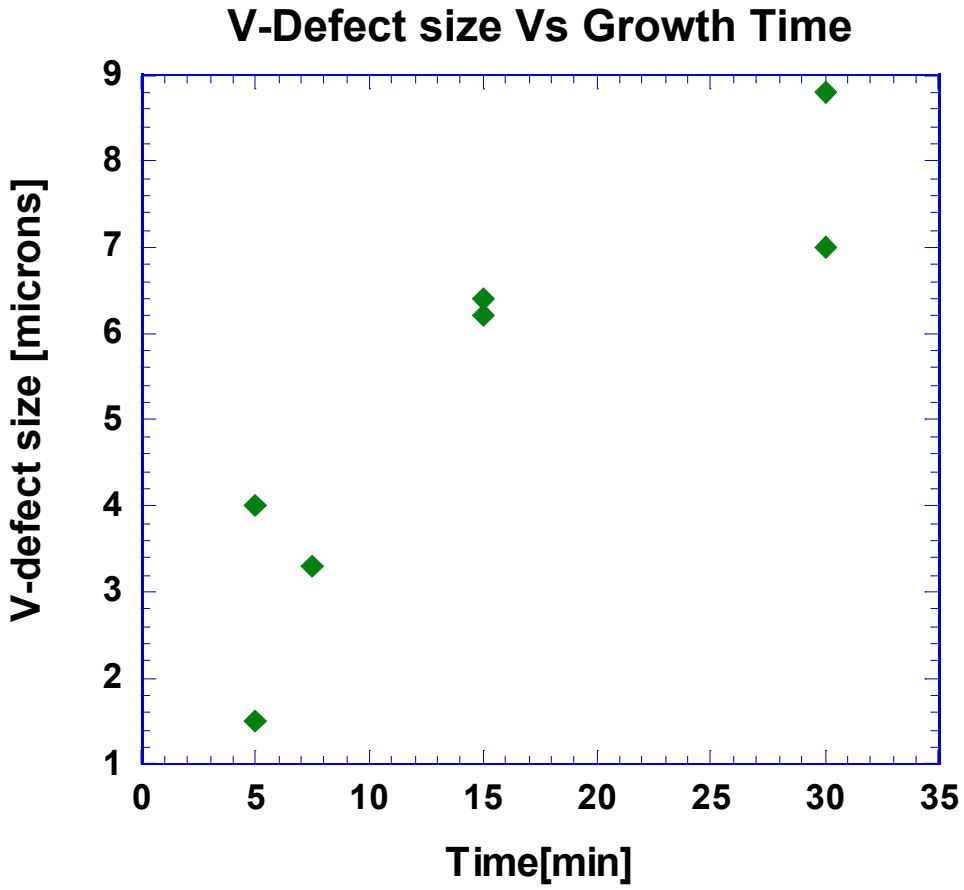

Figure 9.3. Time dependence of V-defect size

Figure 9.4(a) shows the growth mechanism of the V-defect. As can be seen from the figure, the (0001) growth front progresses in vertically upward direction much faster than the {1-10-1} growth front leading to bigger V-defect size as the layer thickens. Since the growth rate involved is very high [~100-200 μm/hr] in our experiments, the surface diffusion rates are not high enough to fill the V-defects. The incorporation efficiency of the growth species is higher on (0001) plane as opposed to the {1-10-1} facets (127, 131). Unlike the InGaN/GaN system where this defect disappears at higher temperatures due to higher surface mobilities of adatoms (108), in our samples, these defects are observed at a growth temperature of 1185^0. Similarly, scanning electron microscopy images of the grown samples were obtained from different locations of the samples and an effective V-defect density was calculated as an average of the V-defect densities from different portions of the sample. The density of V-defects on these samples varied dramatically over the surface and hence a definite dependence of V-defect density on the growth rate could not be drawn. However, the density of these V-defects ranged from 10^4-$10^5/cm^2$.

The observed histogram of V-defect size distribution in Fig. 9.2 and the variation in V-defect size with growth time depicted in Fig. 9.3 may be rationalized referring to a schematic in Fig. 9.4(b). We invoke that V-defects form on **c or c+a** dislocations that produce displacement on the (0001) surface. When growth starts on a GaN seed crystal, V-defects may form on some of these dislocations. As the layer thickens, V-defects get enlarged due to geometrical reasons as illustrated in Fig.4 (b). As argued by Narayanan et al. (132), new threading dislocations (TDs) could form by the condensation of point defects. If a V-defect forms on this new TD, its size will be

small as depicted in Fig. 9.4 (b). Thus, we can qualitatively understand the observations of Figs. 9.2 and 9.3.

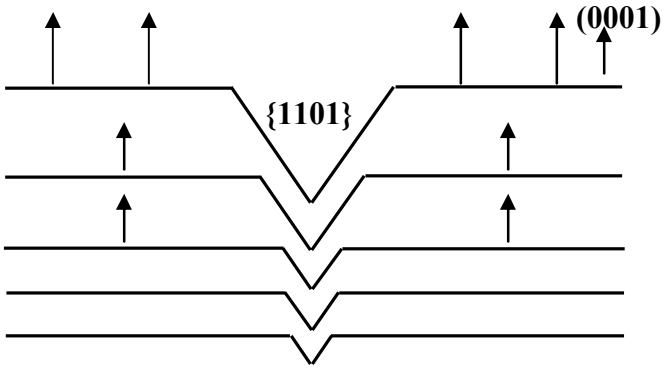

Figure 9.4(a). Growth mechanism of V-defect

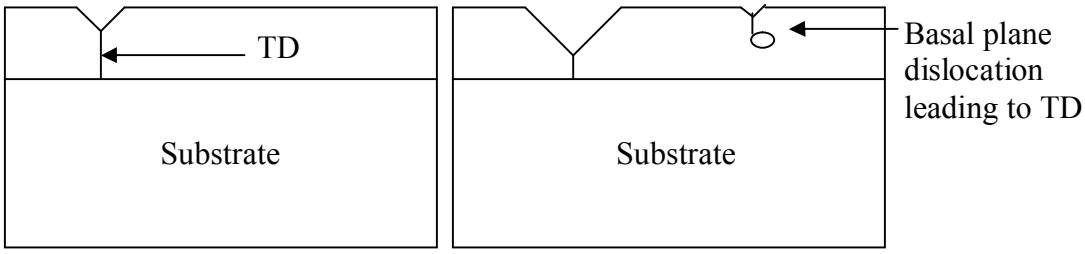

Figure 9.4(b). Condensation of point defects leading to TD that in turn leading to V-defect formation

In summary, the effect of growth time on V-defect size in bulk GaN growth by physical vapor transport has been discussed. It was found that once the V-defect forms, it has a tendency to grow bigger as the growth progresses due to the higher incorporation efficiency of adatoms on (0001) plane rather than {1-10-1} planes. Even though in InGaN/GaN system, V-defects vanish at high growth temperatures [1050^0C] because of higher surface diffusion lengths, in the present discussion, a V-defect

density of ~10^4 - 10^5 / cm^2 was observed even at higher growth temperatures [1185^0C]. This could be attributed to the fact that vapor transport has a very high vertical growth rate as opposed to MOCVD in which sufficient time was allowed for adatoms to diffuse laterally to fill in V-defects.

Chapter 10

Conclusions and Future work.

10.1 Summary

We will summarize the main experimental results that originated from this work and mention the possibile future directions. In the quest to find a commercially viable technology to grow bulk GaN, we have developed a vapor transport technique that is an amalgam of sublimation and vapor transport using a carrier gas trying to exploit the advantages of both the techniques.

Various precursors of gallium for the growth of GaN were experimented. Different configurations, i.e. carrier gas flow through and flow over configurations were also employed to optimize the growth conditions. The conventional sublimation sandwich technique used to grow AlN and SiC sublimation growth was experimented first with commercial GaN powder as the source. However, this resulted in a crust formation problem due to the interaction of ammonia with the commercial GaN powder that was used as the source. This problem was overcome by designing an annular boat growth setup described in section 6.1 that isolated the source material from ammonia. Good quality bulk GaN crystals of 8.5 mm x 8.5 mm were prepared by transporting Gallium containing species [presumably Ga_2O as was found later] obtained from the decomposition of commercial GaN powder with nitrogen as the carrier gas. Growth rates > 200 μm /hr were achieved using this technique. SEM characterization showed that the crosssection of the GaN growth layers to be uniform. The surfaces of the GaN crystals show V-defects and in some cases, particles. AFM scan of the growth layer shows that the growth mode is dislocation mediated spiral

growth. Double crystal X-ray diffraction rocking curve FWHM of the grown layer (~ 5 arc min) was found to be smaller than that of the substrate (~9 arcmin) indicating the higher quality of growth layers compared to the substrate. X ray topography studies performed revealed triple crystal rocking curve widths as small as 36 arcsec. Hall Effect measurements showed carrier concentrations of the order of 6.67 x $10^{18}/cm^3$. SIMS analyses performed on the growth layers showed very high impurity levels of oxygen and silicon that can be attributed to the highly contaminated commercially available source GaN powder. According to the phase diagram, GaN is supposed to undergo incongruent evaporation at typical growth conditions employed in our experiments and result in liquid gallium formation. However, it wasn't the case. An important observation to note from these experiments is that liquid gallium was not observed in the powder after the growth experiments.

In order to decrease the doping densities in the growth layers, the commercial GaN powder was replaced by a lab made high pure GaN powder in the crystal growth experiments. Growth rates dramatically dropped from 200 μm/hr to almost zero when pure GaN was used as the source material. These experiments resulted in liquid gallium formation at temperatures above the triple point. The weight loss of the powder after the experiment is almost one-third of the weight losses observed in experiments with commercial GaN powder as the source. From these experiments it was clear that the oxygen present in commercial powder is influencing the congruent evaporation of GaN under conditions that would normally dictate incongruent evaporation for pure GaN by virtue of thermodynamics. Simulations performed by Dr. Yuri Makarov further supported this argument of formation of volatile oxides of gallium resulting in enhanced transport of gallium. After understanding these experimental results and trying out various other precursors of gallium, it was clear that oxide transport is essential to achieve high growth rates.

This led us to using a mixture of Ga_2O_3 and graphite powder to generate the necessary Ga_2O that acts as a transporting agent of gallium towards the seed. The third generation experimental design employed a flow through configuration as opposed to the flow over configuration used in second generation growth setup. Another source of Ga_2O, commercial GaN powder itself was also used as a precursor in later experiments. It was found that the surface morphologies of the samples grown with commercial GaN powder as the source were better than the ones grown using the mixture of Ga_2O_3 and graphite powder. One sample even exhibited surface morphologies that are free of V-defects. Crystalline quality and growth rates in this design were comparable to the crystals obtained in flow over configuration in design 2. But the surface morphologies of the crystals grown with Ga_2O_3 and graphite powder as the source showed numerous V-defects.

There was an observed trend on the size of these V-defects with time. These defects tend to grow as the growth progresses due to the difference in incorporation efficiencies of adatoms on different crystal planes. In order to increase the area available for device fabrication on the substrate, these V-defects have to be eliminated.

10.2 Future work

Even though high growth rates were achieved using this technique, there are still some challenges that are to be solved: main issue being the possibility of long term growth. From the discussion in chapter 6, it was clear that the source was getting depleted as the growth run progressed. Replenishing the source material during the growth process has to be addressed. Other issues include the oxygen incorporation and V-defects. One has to find a solution to the problem of solving high oxygen incorporation into the grown crystals while still utilizing it for gallium transport. From the results in the experiments performed in flow through configuration, that sufficient ammonia supply

is necessary to successfully suppress the formation of V-defects. Further design changes and process optimization has to be done to increase the uniformity of ammonia profile over the entire surface of the growing crystal. If these issues are solved, this oxide transport technique could potentially become a commercially viable bulk GaN growth technology.

Bibliography

1. S. Strite, H. Morkoc., *J. Vac. Sci. Technol. B* **10**, 1237 (1992).

2. H. Morkoç., *Nitride semiconductors and devices* (Springer, Berlin ; New York, 1999).

3. W. C. Johnson, J. B. Parson, and M. C. Crew., *J. Phys. Chem.* **36**, 2651 (1932).

4. Maruska, H. P., Tietjen, J.J., **15**, 327 (1969).

5. H. Amano, N. Sawaki, I. Akasaki and Y. Toyoda., *Appl. Phys. Lett.* **48**, 353 (1986).

6. H. Amano, M. Kito, K. Hiramatsu and I. Akasaki., *Japanese Journal of Applied Physics, Part 2 (Letters)* **28**, 2112 (1989).

7. S. Nakamura, M. Senoh and T. Mukai., *Japanese Journal of Applied Physics, Part 2 (Letters)* **30**, 1708 (1991).

8. S. Nakamura *et al*., *Appl. Phys. Lett.* **68**, 3269 (1996).

9. S. Nakamura, T. Mukai and M. Senoh., *Appl. Phys. Lett.* **64**, 1687 (1994).

10. M. A. L. Johnson *et al*., *J. Cryst. Growth* **175-176**, 72 (1997).

11. T. S. Cheng *et al*., *J. Cryst. Growth* **166**, 597 (2).

12. W. A. Melton, J. I. Pankove., *J. Cryst. Growth* **178**, 168 (1997).

13. R. D. Dupuis., *J. Cryst. Growth* **178**, 56 (1997).

14. S. Gokden, R. Baran, N. Balkan and S. Mazzucato., *Physica E* **24**, 249 (2004).

15. X. A. Cao, J. A. Teetsov, F. Shahedipour-Sandvik and S. D. Arthur., *J. Cryst. Growth* **264**, 172 (2004).

16. E. Valcheva, T. Paskova and B. Monemar., *Journal of Physics Condensed Matter* **14**, 13269 (2002).

17. Manfra, M. J; Weimann,N.G.; Hsu,J.W.P.; Pfeiffer,L.N.; West,K.W.; Molnar,R.J., 231-2, (IEEE, San Francisco, CA, USA, 2002).

18. D. R. Gaskell, *Introduction to the thermodynamics of materials* (Taylor & Francis, New York, ed. 4th, 2003).

19. N. Newman., *J. Cryst. Growth* **178**, 102 (1997).

20. N. Newman, J. Ross and M. Rubin., *Appl. Phys. Lett.* **62**, 1242 (1993).

21. F. Reif., *Fundamentals of statistical and thermal physics* (McGraw-Hill, New York, 1965).

22. G. J. Van Wylen, R. E. Sonntag., *Fundamentals of classical thermodynamics* (Wiley, New York, ed. 3rd , SI version, 1985).

23. A. W. Searcy, D. W. Ragone, and U. Colombo., *Chemical and Mechanical Behaviour of Inorganic Materials* (Wiley, NewYork, 1970).

24. A. Anders *et al*., *Rev. Sci. Instrum.* **67**, 905 (1996).

25. Bryden,W.A.; Ecelberger,S.A.; Hawley,M.E.; Kistenmacher,T.J., **339,** 497 Proceedings of the 1994 MRS Spring Meeting, Apr 4-8 1994.

26. T. C. Fu *et al*., *J Electron Mater* **24**, 249 (1995).

27. A. Gassmann *et al*., *J. Appl. Phys.* **80**, 2195 (1996).

28. T. Lei, T. D. Moustakas, R. J. Graham, Y. He and S. J. Berkowitz., *J. Appl. Phys.* **71**, 4933 (1992).

29. M. J. Paisley, Z. Sitar, J. B. Posthill and R. F. Davis., *Journal of Vacuum Science & Technology A (Vacuum, Surfaces, and Films)* **7**, 701 (1989).

30. G. Martin, S. Strite, J. Thornton and H. Morkoc., *Appl. Phys. Lett.* **58**, 2375 (1991).

31. Newman,N.; Fu,T.C.; Liu,X.; Liliental-Weber,Z.; Rubin,M.; Chan,J.S.; Jones,E.; Ross,J.T.; Tidswell,I.; Yu,K.M.; Cheung,N.; Weber,E.R., pp 483 (1994) (Mater. Res. Soc, San Francisco, CA, USA, 1994).

32. R. C. Powell, N. E. Lee and J. E. Greene., *Appl. Phys. Lett.* **60**, 2505 (1992).

33. M. Rubin, N. Newman, J. S. Chan, T. C. Fu and J. T. Ross., *Appl. Phys. Lett.* **64**, 64 (1994).

34. H. Sato, T. Sasaki, T. Matsuoka and A. Katsui., *Japanese Journal of Applied Physics, Part 1 (Regular Papers & Short Notes)* **29**, 1654 (1990).

35. J. Unland, B. Onderka, A. Davydov and R. Schmid-Fetzer., *J. Cryst. Growth* **256**, 33 (2003).

36. A. V. Davydov, W. J. Boettinger, U. R. Kattner and T. J. Anderson., *Physica Status Solidi A* **188**, 407 (2001).

37. M. Knudsen., *Ann. Phys.* **47**, 697 (1915).

38. I. Langmuir., *J. Am. Ch. Soc.* **35**, 931 (1913).

39. H. Hertz., *Ann. Phys.* **17**(1882).

40. E. Rutner, P. Goldfinger, J. P. Hirth and United States. Air Force. Systems Command. Aeronautical Systems Division. Directorate of Materials and Processes., *Condensation and evaporation of solids; proceedings* (Gordon and Breach, New York, 1964).

41. A. Somorjai., *Science* **162**, 755 (1968).

42. G. A. Somorjai, and J. E. Lester., ***Progress in Solid State Chemistry,*** (Pergamon, NewYork, 1967).

43. Z. A. Munir, A. W. Searcy., *J. Chem. Phys.* **42**, 4223 (1965).

44. R. Groh, G. Gerey, L. Bartha and J. I. Pankove., *Physica Status Solidi A* **26**, 353 (1974).

45. R. W. Mar, A. W. Searcy., *J. Chem. Phys.* **53**, 3076 (1970).

46. M. V. Averyanova *et al*., *Materials Science & Engineering B (Solid-State Materials for Advanced Technology)* **B43**, 167 (1997).

47. S. Y. Karpov, O. V. Bord, R. A. Talalaev and Y. N. Makarov., *Materials Science & Engineering B (Solid-State Materials for Advanced Technology)* **B82**, 22 (2001).

48. Y. Morimoto., *J. Electrochem. Soc.* **121**, 1383 (1974).

49. C. J. Sun *et al*., *J. Appl. Phys.* **76**, 236 (1994).

50. S. Dushman., *Scientific foundations of vacuum technique* (Wiley, New York, ed. 2d Revised by members of the research staff, General Electric Research Laboratory. J. M. Lafferty, editor, 1962).

51. D. D. Koleske, A. E. Wickenden, R. L. Henry, J. C. Culbertson and M. E. Twigg., *J. Cryst. Growth* **223**, 466 (2001).

52. D. D. Koleske *et al*., *Appl. Phys. Lett.* **73**, 2018 (1998).

53. R. C. Schoonmaker, A. Buhl and J. Lemley., *J. Phys. Chem.* **69**, 3455 (1965).

54. A. Y. Cho., *MRS Bull* **20**, 21 (1995).

55. J. Y. Tsao., *Materials fundamentals of molecular beam epitaxy* (Academic Press, Boston, 1993).

56. D. K. Brice, J. Y. Tsao and S. T. Picraux., *Nucl Instrum Methods Phys Res Sect B* **B44**, 68 (1989).

57. J. L. Vossen, W. Kern., *Thin film processes II* (Academic Press, Boston, 1991).

58. J. L. Vossen, W. Kern., *Thin film processes* (Academic Press, New York, 1978).

59. G. B. Stringfellow., *J. Cryst. Growth* **68**, 111 (1984).

60. V. S. Ban., *J. Electrochem. Soc.* **119**, 761 (1972).

61. S. S. Liu, D. A. Stevenson., **125**, 1161 (1978).

62. D. D. Roccasecca, R. H. Saul and O. G. Lorimor., *J. Electrochem. Soc.* **121**, 962 (1974).

63. C. N. Hinshelwood., *The kinetics of chemical change* (Clarendon Press, Oxford, The, ed. vi, 1 £., 1940).

64. J. I. Pankove, T. D. Moustakas., "Semiconductors and Semimetals ," **50**(1998).

65. C. Y. Yeh, Z. W. Lu, S. Froyen and A. Zunger., *Physical Review B (Condensed Matter)* **46**, 10086 (1992).

66. L. Liu, J. H. Edgar., *Materials Science and Engineering: R: Reports* **37**, 67 (2002).

67. S. D. Lester, F. A. Ponce, M. G. Craford and D. A. Steigerwald., *Appl. Phys. Lett.* **66**, 1249 (1995).

68. R. J. Molnar, W. Gotz, L. T. Romano and N. M. Johnson., *J. Cryst. Growth* **178**, 147 (1997).

69. W. Seifert, R. Franzheld, E. Butter, H. Sobotta and V. Riede., *Crystal Research and Technology* **18**, 383 (1983).

70. A. A. Arendarenko, E. N. Vigdorovich and Y. N. Sveshnikov., *Physica Status Solidi C*, 827 (2003).

71. J. J. Nickl, W. Just and R. Bertinger., *Mater. Res. Bull.* **9**, 1413 (1974).

72. H. Lee, J. S. J. Harris., *J. Cryst. Growth* **169**, 689 (1996).

73. H. Tsuchiya, M. Akamatsu, M. Ishida and F. Hasegawa., *Japanese Journal of Applied Physics, Part 2 (Letters)* **35**, 748 (1996).

74. M. Ilegems., *J. Cryst. Growth* **13-14**, 360 (1972).

75. T. Detchprohm, K. Hiramatsu, H. Amano and I. Akasaki., *Appl. Phys. Lett.* **61**, 2688 (1992).

76. Molnar,R.J.; Nichols,K.B.; Maki,P.; Brown,E.R.; Melngailis,I., **378**, 479 (Materials Research Society, Pittsburgh, PA, USA, San Francisco, CA, USA, 1995).

77. Perkins,N.R.; Horton,M.N.; Bandic,Z.Z.; McGill,T.C.; Kuech,T.F., **395**, 243 (Materials Research Society, Pittsburgh, PA, USA, Boston, MA, USA, 1996).

78. K. Motoki *et al*., *J. Cryst. Growth* **237-239**, 912 (2002).

79. Ivantsov,V.A.; Sukhoveev,V.A.; Dmitriev,V.A., **468**, 143 (Materials Research Society, Pittsburgh, PA, USA, San Francisco, CA, USA, 1997).

80. M. Albrecht, M. Nerding, H.P. Strunk, V.A. Ivantsov, V. Sukhoveev, V.A. Dmitriev, (Materials Research Society, Pittsburgh, PA, USA, Boston, MA, USA, 2000).

81. S. Krukowski, Z. Romanowski, I. Grzegory and S. Porowski., *J. Cryst. Growth* **189-190**, 159 (1998).

82. I. Grzegory., *Journal of Physics: Condensed Matter* **13**, 6875 (2001).

83. I. Grzegory., J. Phys. Chem. Solids 56, 639 (1995).

84. High pressure thermodynamics and solution growth of GaN, (North-Holland, New York, NY, USA, Albany, NY, USA, 1984).

85. I. Grzegory *et al*., *J. Cryst. Growth* **246**, 177 (2002).

86. T. Inoue *et al*., *J. Cryst. Growth* **229**, 35 (2001).

87. H. Yamane, M. Shimada, S. J. Clarke and F. J. DiSalvo., *Chem. Mater* **9**, 413 (1997).

88. F. Kawamura *et al*., *J. Mater. Sci. : Mater. Electron.* **16**, 29 (2005).

89. S. Porowski, I. Grzegory., *J. Cryst. Growth* **178**, 174 (1997).

90. M. Aoki *et al*., *Crystal Growth & Design* **2**, 55 (2002).

91. R. Dwilinski *et al*., *Diamond and Related Materials* **7**, 1348 (1998).

92. D. R. Ketchum, J. W. Kolis., *J. Cryst. Growth* **222**, 431 (2001).

93. R.A. Laudise., *Prog. Inorg. Chem* **3**, 1 (1962).

94. G. A. Slack, T. F. McNelly., *J. Cryst. Growth* **34**, 263 (1976).

95. P. G. Baranov *et al*., *MRS Internet Journal of Nitride Semiconductor Research* **3**(1998).

96. Z. A. Munir, A. W. Searcy., *J. Electrochem. Soc.* **111**, 1170 (1964).

97. C. Wetzel *et al*., *Appl. Phys. Lett.* **65**, 1033 (1994).

98. S. Fischer *et al*., *Appl. Phys. Lett.* **69**, 2716 (1996).

99. G. Kamler, J. Zachara, S. Podsiadlo, L. Adamowicz and W. Gebicki., *J. Cryst. Growth* **212**, 39 (2000).

100. K. Nishino, D. Kikuta and S. Sakai., *J. Cryst. Growth* **237-239**, 922 (2002).

101. I. Mellen Company., *"Assembly and Operating Instructions for High Pressure Furnace System Model CM14-4X18-4Z, Sold To Cornell University."* , 2001).

102. Makarov. Y., *"Final Report on the research work "Analysis of chemical processes involved in the GaN powder charge in sublimation experiments"," Rep. No. 1*, 2002).

103. S. Y. Karpov, V. G. Prokofyev, E. V. Yakovlev, R. A. Talalaev and Y. N. Makarov., *MRS Internet Journal of Nitride Semiconductor Research* **4S1**(1999).

104. S. Y. Karpov, Y. N. Makarov and M. S. Ramm., *MRS Internet Journal of Nitride Semiconductor Research* **2**(1997).

105. M. V. Averyanova *et al*., *MRS Internet Journal of Nitride Semiconductor Research* **1**, 7 (1996).

106. H. K. Cho, J. Y. Lee, G. M. Yang and C. S. Kim., *Appl. Phys. Lett.* **79**, 215 (2001).

107. P. Q. Miraglia, E. A. Preble, A. M. Roskowski, S. Einfeldt and R. F. Davis., *J. Cryst. Growth* **253**, 16 (2003).

108. X. H. Wu *et al*., *Appl. Phys. Lett.* **72**, 692 (1998).

109. N. Sharma, P. Thomas, D. Tricker and C. Humphreys., *Appl. Phys. Lett.* **77**, 1274 (2000).

110. Y. Makarov., *"Modeling analysis of GaN bulk crystal growth using commercial and lab made GaN powder." Rep. No. 4*, 2004).

111. H. Wu *et al*., *J. Cryst. Growth* **279**, 303 (2005).

112. P. Konkapaka, H. Wu, Y. Makarov and M. G. Spencer., *"MURI Reveiw report: Spring 2005: Bulk GaN growth by vapor transport,"* , 2005).

113. Y. Makarov., *"Results on resesarch work: Modeling analysis of GaN bulk crystal growth using commercial and lab made powder," Rep. No. 8*, 2004).

114. G. A. Slack, L. J. Schowalter, D. Morelli and J. A. Freitas Jr., *J. Cryst. Growth* **246**, 287 (2002).

115. R. Y. Korotkov, F. Niu, J. M. Gregie and B. W. Wessels., *Physica B: Condensed Matter* **308-310**, 26 (2001).

116. C. Y. Nam, D. Tham and J. E. Fischer., *Appl. Phys. Lett.* **85**, 5676 (2004).

117. M. Gandouzi, J. C. Bourgoin, J. Mimila-Arroyo, C. Grattepain and C. Grattepain., *J. Cryst. Growth* **218**, 167 (2000).

118. C. J. Frosch., *J. Electrochem. Soc.* **111**, 180 (1964).

119. Y. J. Park, C. S. Oh, T. H. Yeom and Y. M. Yu., *J. Cryst. Growth* **264**, 1 (2004).

120. H. Y. Peng *et al*., *Chemical Physics Letters* **327**, 263 (15).

121. K. Uchida *et al*., *J Electron Mater* **28**, 246 (1999).

122. S. Mahanty *et al*., *Mater Lett* **41**, 67 (1999).

123. B. Jahnen *et al*., *MRS Internet Journal of Nitride Semiconductor Research* **3**, 10 (1998).

124. Y. Kawaguchi *et al*., *J. Cryst. Growth* **189-190**, 24 (1998).

125. I. Kim, H. Park, Y. Park and T. Kim., *Appl. Phys. Lett.* **73**, 1634 (1998).

126. L. T. Romano, B. S. Krusor, M. D. McCluskey, D. P. Bour and K. Nauka., *Appl. Phys. Lett.* **73**, 1757 (1998).

127. N. Duxbury *et al*., *Appl. Phys. Lett.* **76**, 1600 (2000).

128. Z. Liliental-Weber, Y. Chen, S. Ruvimov and J. Washburn., *Phys. Rev. Lett.* **79**, 2835 (1997).

129. S. Keller *et al*., *J. Cryst. Growth* **195**, 258 (1998).

130. J. E. Northrup, J. Neugebauer., *Physical Review B (Condensed Matter)* **60**, 8473 (15).

131. P. -. Lin, Y. C. Sermon Wu., *Mater. Chem. Phys.* **80**, 397 (2003).

132. V. Narayanan, K. Lorenz, Wook Kim and S. Mahajan., *Philosophical Magazine A (Physics of Condensed Matter: Structure, Defects and Mechanical Properties)* **82**, 885 (2002).